BERICHTE
aus dem Fachbereich Geowissenschaften
der Universität Bremen

No. 218

Røy, H.

DYNAMIC STRUCTURE AND FUNCTION OF THE DIFFUSIVE BOUNDARY LAYER AT THE SEAFLOOR

Berichte, Fachbereich Geowissenschaften, Universität Bremen, No. 218,
149 pages, Bremen 2003

ISSN 0931-0800

The "Berichte aus dem Fachbereich Geowissenschaften" are produced at irregular intervals by the Department of Geosciences, Bremen University.

They serve for the publication of experimental works, Ph.D.-theses and scientific contributions made by members of the department.

Reports can be ordered from:

Monika Bachur

Forschungszentrum Ozeanränder, RCOM

Universität Bremen

Postfach 330 440

D 28334 BREMEN

Phone: (49) 421 218-8960

Fax: (49) 421 218-3116

e-mail: MBachur@uni-bremen.de

Citation:

Røy, H.

Dynamic Structure and Function of the Diffusive Boundary Layer at the Seafloor.

Berichte, Fachbereich Geowissenschaften, Universität Bremen, No. 218, 149 pages, Bremen, 2003.

ISSN 0931-0800

Dynamic Structure and Function of the Diffusive Boundary Layer at the Seafloor

Dissertation
zur Erlangung des
Doktorgrades der Naturwissenschaften
am Fachbereich 5
der Universität Bremen

vorgelegt von:
Hans Røy

Bremen 2003

Tag des Kolloquiums:
19 Mai 2003

Gutachter:
Herr Prof. Dr. Bo Barker
Herr Prof. Dr. Kai-Uwe Hinrichs

Prüfer:
Herr Prof. Dr. Prof. Heinrich Villinger
Herr Prof. Dr.Jörn Pechmann

Contents

Thesis abstract

This thesis presents the results of an experimental study of the diffusive boundary layer (DBL) of coastal marine sediments. The focus is on diffusive exchange of O_2 between sediment and water, and the study should be seen in the context of redox cycling in the top layers of the sediment. The aim was to assess the magnitude of the error induced by the common assumption, that the sediment surface is a flat plane with only vertical gradients.

We present a description of the DBL that takes into account topographic structure as well as temporal concentration fluctuations. The erratic behaviour of the O_2 concentration in the DBL is linked to a co-ordinated movement of the entire gradient, which can be explained by molecular diffusion alone.This implies that the average vertical gradient through the DBL reflects the average diffusive flux, as calculated from Fick's first law of diffusion.

The starting point in the description of the topographic structure of the DBL is the ratio between the vertical and horizontal gradients. We show that this ratio is equal to the ratio between the three-dimensional exchange-area and the projected horizontal area. The two ratios together can be used to correct flux-calculations that have been made under the flat plate assumption. Measurements of sediment topography with a spatial resolution of 0.1 mm are presented. These data are combined with two-dimensional O_2 distributions across the sediment-water interface, measured with microsensors. The combined data are used to show that the three-dimensional exchange surface between sediment and water can be quantified from topography alone. This insight is used to calculate the three-dimensional diffusive flux through the DBL from a combination of isolated microprofiles and topographic data. Both measuring principles are effective enough to sample sufficient data for a statistically sound description of actual marine sites. The approach is performed under reproducible conditions in a laboratory flume, as well as on topographic data collected *in situ* at two marine locations. The two studies reveal tight physical and mathematical constraints on the possible discrepancy between the vertical diffusive flux and three-dimensional diffusive flux across the sediment water interface. The flux calculated from vertical microprofiles through the DBL only had to be corrected by a factor 1.12 for a estuarine mud and 1.25 for a near shore sand, even though both sediments had a rich surface topography. We expect that the lower number is the most representative for typical muddy sediments. The improved quantification of diffusive flux allows the fauna-mediated O_2 uptake to be separated from topographical effects, in a study of the seasonal O_2 uptake

dynamics. We also present a novel alternative to the current techniques for determining solute exchange across the sediment water interface. The new method has the advantage of not interfering with hydrodynamic factors that influence the exchange, and not under-representing fauna-mediated exchange. The method was applied successfully *in situ* on three different locations, and compared with *in situ* chamber incubations and microprofile derived fluxes. Lastly, the water motion around a sessile ciliate living within the DBL is investigated. The animal is thought to live in mutualistic symbiosis with sulfide oxidising bacteria, but the pathway supplying the organism with sulfide has been unclear. We show that the organism can live on low concentrations of sulfide, due to the possession of a filter feeding apparatus, and that sufficient amounts of sulfide can de expected to occur in its natural environment.

Thesis introduction

ABSTRACT

This chapter will introduce the diffusive boundary layer (DBL), as it is found over coastal and estuarine sediments. The chapter is not intended as a comprehensive compilation of the newest insight in the DBL, nor does it contain a complete set of references to the work of previous authors who have published on the topic. The aim of the chapter is to give the reader an intuitive understanding of the Diffusive Boundary Layer of marine sediments, and to emphasise the context in which the following specialised manuscripts should be seen.

INTRODUCTION

As microsensors for O_2 became an established tool in aquatic science in the 70's and 80's, they presented the scientists with a counter-intuitive feature. Careful observations revealed that the O_2 concentration started to decrease a short distance *above* O_2 consuming sediments, and not at the sediment surface as first expected. Such a diffusive boundary layer was, however, well known in the science of chemistry (Dworak and Wendt 1977; Shaw and Hanratti. 1977), and its presence in the marine environment could be predicted from basic boundary layer theory. Seeing this layer as a part of the water column, hydrodynamicists referred to the layer as the diffusive sub layer. In microbial ecology, where the microsensors first entered environmental science, the layer was rather seen as a boundary layer around the sediment of interest. Consequently, the phrase diffusive boundary layer (DBL) became established in this field. By 1985, a thorough description of the DBL of aquatic sediments based on direct measurements with microsensors was available (Jørgensen and Revsbech 1985).

The easiest way to understand the DBL is as a film of water that sticks to the solid surface due to viscous forces, and therefore does not participate in the turbulent mixing of the water column. This concept is a simplification, but a very useful analogy. Fig. 1 shows how the concentration gradient above an alabaster plate in clean water looks according to such a model. On the alabaster surface, the concentration of Ca^{2+} and SO_4^{2-} is fixed by the solubility product of $CaSO_4 \cdot 2H_2O$. From the surface, the ions diffuse down a concentration gradient towards the mixed water column. As Ca^{2+} and SO_4^{2-} diffuse away from the surface, they are replaced via dissolution from the solid. The diffusive flux is determined by the

concentration gradient and the coupled diffusion coefficient of Ca^{2+} and SO_4^{2-}, according to Fick's first law:

$$J = -D\frac{\partial C}{\partial z} \quad (1)$$

where D is the effective molecular diffusion coefficient and $\partial C/\partial z$ the concentration gradient. In this simple case, Eq. 1 can be expressed as

$$J = ß(C_w - C_0) \quad (2)$$

where C_0 is the concentration at the alabaster surface, C_w the concentration in bulk water and ß the mass transfer coefficient (Boudreau and Guinasso 1982). ß is thereby the product of the DBL thickness and D. If the alabaster plate was placed in seawater and the dissolution rate measured via weight-loss over time, the only unknown parameter in Eq. 2 would be the DBL thickness. A similar approach has therefore been used to evaluate the thickness of the DBL, primarily at the deep sea floor (e.g. Santschi et al. 1983).

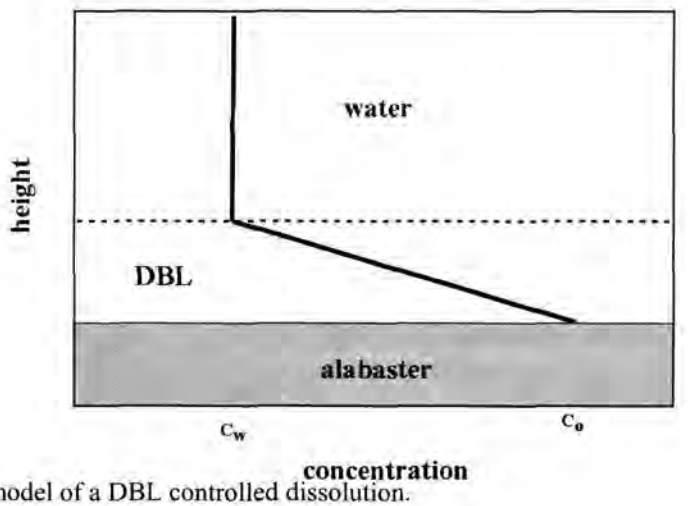

Figure 1. Conceptual model of a DBL controlled dissolution.

The spatial resolution of microsensors allowed the O_2 gradient within the 0.2 – 1 mm thick DBL to be resolved (Jørgensen and Revsbech 1985). This opened the possibility to calculate the diffusive flux of O_2 through the sediment-water interface from the concentration gradient in the DBL directly from Eq. 1. During the following 20 years, diffusive flux calculation from microprofiles in the DBL has become a standard technique. The most widely used approach to calculations of diffusive flux through the DBL is to measure vertical O_2 concentration profiles across the sediment surface. A straight line is then hand-fit to the points that the scientist believes to represent the gradient just above the sediment surface, and the slope of this line is multiplied by the diffusion coefficient for the appropriate temperature and salinity.

One major advantage of calculating flux from the concentration gradient in the DBL is that of a well-defined and constant D. The method is primarily used in coastal and estuarine sediments, biofilms and microbial mats. In the low activity sediments, the concentration decrease through the DBL is too small for an accurate determination of the slope, and modelling of O_2 consumption from the entire profile yields a better estimate (Hulth et al. 1994).

Even though the flux is not calculated from C_0 and C_w, the conceptual model of the DBL as a thin film with exclusively molecular diffusion, separating the sediment from a fully mixed water column is still useful for predictions of how the DBL influences transport related processes. The link between measured gradients and film-theory is the effective DBL (Z_δ), introduced by Jørgensen and Revsbech in 1985. It is defined by extrapolating the linear gradient in the lower DBL to the concentration of the mixed water column. The effective DBL is thereby a functional representation of the actual DBL. Note that the information used to derive the position of the upper limit of the effective DBL is drawn from the bottom of the DBL, where mass transport is purely by diffusion, and not from the transition-region where eddy diffusion and molecular diffusion share the transport.

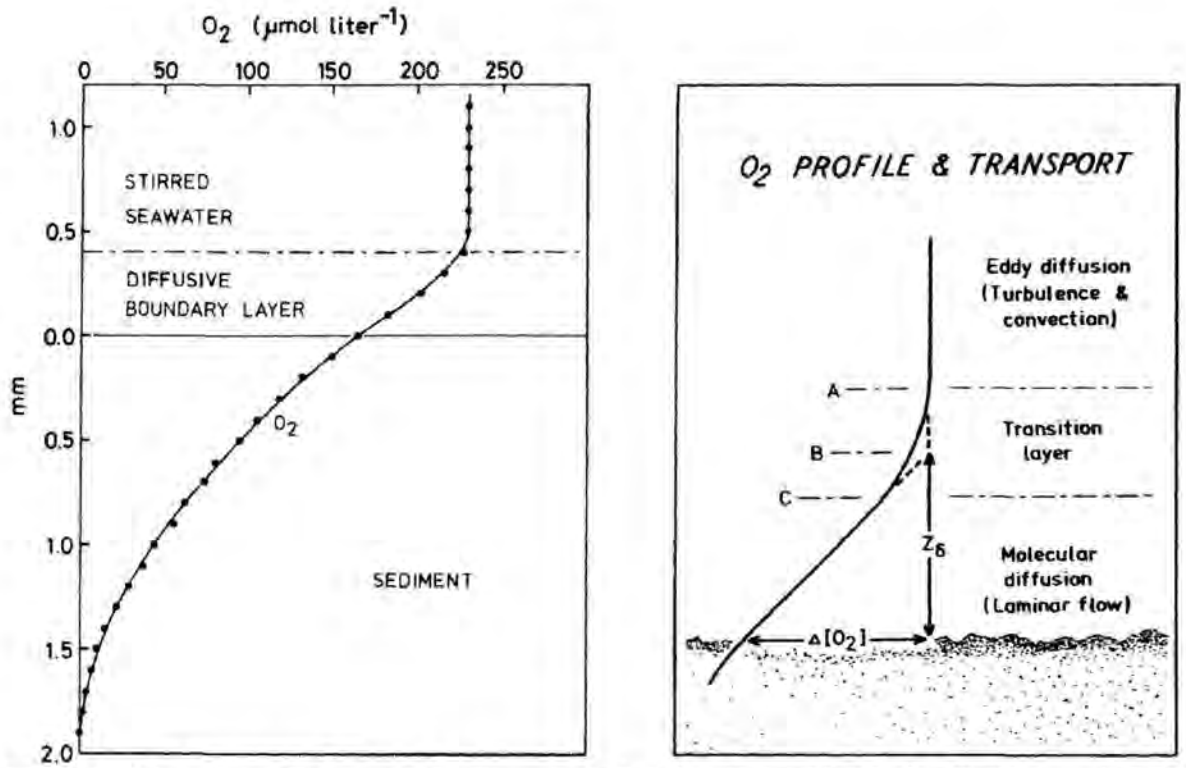

Figure 2. Left. O_2 microprofile across the sediment water interface. A transition (broken line) is seen above the sediment surface between the stirred seawater with homogeneous O_2 distribution and the diffusive boundary layer with a steep O_2 gradient. Right. The boundary layer at the sediment-water interface as determined by chemical transport processes and gradients. The O_2 microgradients are here used to define the outer limit (A) of the diffusive boundary layer as well as the true (C) and the effective boundary layer. From (Jørgensen and Revsbech 1985), Copyright by the American Society of Limnology and Oceanography, Inc.

From the micro profiles, the position of the sediment surface can be determined from a discontinuity in the vertical gradient at the surface. To satisfy conservation of mass, the decreased diffusivity in the sediment will force an increase in gradient right at the interface. This approach often gives a good estimate on the position of the sediment surface, given that the spatial resolution is appropriate. An alternative to the slope-discontinuity method is visual observation through a dissection microscope. Convenient only under laboratory conditions, this method also has the drawback that the electrode tip is thin and seeing it at the sediment-water interface is hard, even under magnification. Recently, a simple technical solution to the problem has been presented, where a fibre-optic sensor glued to the chemical sensor determines the position of the sediment surface from backscatter of near-infrared light (Klimant et al. 1997).

So far, it has been described how this point we have demonstrated how the linear gradients in the DBL can be exploited to calculate diffusive fluxes. It has also been shown that the gradient can be used to describe the actual DBL with a stagnant-film analogue, the effective DBL. The descriptive approach has, however, not explained why the DBL is present or what controls its thickness. For this, we must turn our attention to the turbulent water column.

THE TURBULENT WATER COLUMN

The water masses of the sea are turbulent and exhibit an ability to transport and mix momentum, kinetic energy and solutes at a rate that is far in excess of that associated with molecular movements alone. The process behind this mixing is that the apparent randomness of turbulent motion will stretch and distort any given fluid parcel into fine structures, after which random molecular motions take over and homogenises the inter-tangled parcels (Dade et al. 2001).

Even though turbulent mixing is associated with discrete structures in the flow, it can be modelled as a continuous diffusive transport process (e.g. Dade 1993). The magnitude of the turbulent diffusive flux is determined by the concentration gradient, the area over which the exchange takes place and a coefficient of proportionality. We can name the coefficient of proportionality D_e for eddy diffusivity. The magnitude of D_e depends on the eddy structure of a given flow, and also on the distance over which the transport is observed. Eddies that are much smaller or much bigger than the transport distance are not effective in dispersing water and solutes, compared to those eddies whose dimensions are more comparable to the transport distance. (Lerman 1979). Even in calm regions of the deep

sea, eddy diffusivity in the boundary layer is about 6 orders of magnitude larger than the molecular diffusion coefficient. Due to shear-induced turbulence, D_e increases down through the BBL, when viewed on a scale of meters (Boudreau 2001).

THE BENTHIC BOUNDARY LAYER

At the interface between a stationary solid and a moving fluid, the velocity of the fluid is zero. As water in nature is rarely stagnant, the corollary of this "no-slip" condition is that there is a gradient in the speed of flow near every sediment surface. Speed changes from zero at the surface to what we will call the „free stream" velocity some distance away. In the case of the ocean floor, this region of velocity gradient is known as the benthic boundary layer (BBL).

The classical example of a developing boundary layer is when a flow encounters a plate with a leading edge. A short distance downstream from the leading edge, only a small part of the flow has been affected by the presence of the plate. In this layer the velocity must go from zero at the surface to free stream velocity through a thin layer of strong shear. Because kinetic energy is exchanged between the lowest free stream fluid and the boundary layer by turbulent mixing and viscous friction, the boundary layer develops upwards down the flow. The rate at which it grows depends on the turbulence present in the flow and the roughness of the plate. But generally, the angle between the surface of the plate and the average position of the outer edge of the boundary layer is in the order of a few degrees, gradually decreasing towards zero downstream. At some point the growing boundary layer will reach some outer limit, like the water surface, and the flow is all boundary layer. From now on, the velocity profile does not change any more and the boundary layer is fully developed. A more detailed introduction to developing boundary layers can be found in the first chapters of most basic textbooks dealing with fluids (e.g. Denny 1993; Vogel 1994).

The forces that act to retard the water near the sediment surface also dampen fluctuations in the velocity components. At some point near the sediment surface the turbulence will be suppressed to such an extent that momentum transfer changes from being turbulent to becoming viscous. These two regions of different momentum transfer mechanisms divide the BBL into sub layers that are recognisable in time-averaged vertical velocity profiles. Nearest the sediment, where momentum transfer is dominated by the constant viscosity, the velocity profile is linear (Cladwell and Chriss 1979). Above, the increasing turbulent mixing gives the velocity profile a logarithmic shape. They can be named linear and logarithmic layer respectively, but the lower part is most often referred to

as the viscous sublayer (VSL). Other sublayers of the flow can be distinguished, but will not be presented here.

The upper edge of benthic boundary layer in the sea is not generally restricted by the water surface. Defining the practical thickness of the benthic boundary layer brings up the risk of imposing a discrete nature its limits that is not necessarily the case in nature. In the upper part of the log layer the velocity slowly approaches the free stream velocity, and our preference to draw the limit at 90 or 99% is more a feature of our anatomy than of the BBL (Denny 1993). As a rule of thumb, it takes about 1 m to practically reach free flow velocity, even though the presence of the sea floor affects the water column much higher than this (Dade et al. 2001).

The limit of the viscous sublayer is easier to define. One approach is to restrict the viscous sublayer to the strictly linear part of the vertical velocity profile. But most often the boundary between VSL and log-layer is taken to be the intersection between a linear fit to a lower part and a log fit to points further away from the sediment. The lower limit is the sediment surface. Defined this way, the VSL ranges somewhere between 1 mm and 1 cm. Even though the VSL is only a small part of the entire BBL, it is usually here that most change in velocity takes place.

THE DIFFUSIVE BOUNDARY LAYER

Even though turbulence can be disregarded in momentum transfer within a viscous sublayer, it is still present. Such a turbulent flow with predominantly viscous momentum transfer is called linear, saving the term laminar to a flow totally free of turbulent mixing between adjacent layers. According to this definition, we can not expect to find strictly laminar flow over a sediment surface except maybe under very special circumstances. One implication of this is that the transport of small dissolved molecules across the VSL is not restricted to molecular diffusion. Only in the lower ~10 % of the VSL has turbulent mixing been suppressed to such an extent that molecular diffusion become significant (Boudreau and Guinasso 1982). Because the turbulent mixing drops rapidly towards the sediment surface, the transition from eddy diffusion to molecular diffusion is short. Below this transition zone the transport is by molecular diffusion alone and concentration gradients are linear. According to a formal definition, the DBL is the zone where molecular diffusion is the most important mass transport process. The upper limit of this DBL would then be the plane above the sediment surface where molecular diffusion equals eddy diffusion. In contrast to the effective DBL defined earlier, the formal definition of the DBL is not a

functional description. It is possible to have two boundary layers with the same thickness, according to the formal definition, that supply different resistance to diffusive transport. This definition is therefore rarely used except for very general discussions.

Assuming eddy diffusion coefficients to be equal for all molecules in a given flow, the different molecular diffusion coefficients of different molecules would cause equal molecular and eddy diffusion to be reached at different distances from the sediment surface for the different chemicals. The molecular diffusion coefficients for most biogeochemically important gases, ions and molecules is within one order of magnitude. As the eddy diffusivity is proportional to the 3rd to 4th power of the distance to the surface, the theoretical distances of equal molecular and eddy diffusion for these compounds fall within an order of two (Jørgensen 2001). Still, it is obvious that the DBL is not a feature of the flow alone. We cannot find a general DBL as a layer that sticks differently to the surface than the water generally, as we could with the viscous sublayer. The DBL is as much a feature of the particular diffusing molecules of interest as it is of the flow.

O_2 FLUX TO COASTAL AND ESTUARINE SEDIMENTS

Molecular oxygen is transported into fine-grained sediments via two fundamentally different mechanisms: Molecular diffusion through the sediment surface, and via fauna irrigation. For coastal marine sediments, the balance between the two processes is roughly 50-50% (Jahnke 2001). Although the final delivery of oxygen through burrow walls also occurs via molecular diffusion, the burrows can not be considered as a simple extension of the sediment surface. The most important reason is the behaviour of the responsible animal. Burrowing animals ventilate their burrows for a multitude of reasons. The most common examples are to acquire oxygen and food particles from the water column, and flushing toxic reduced substances from the burrow (Kristensen 1988; Kristensen 2000; Aller 2001). Often the burrows are only flushed periodically, which cause temporally unstable redox conditions (Kristensen 1985). A typical scenario is that a burrow will go anoxic, after which ammonia, Fe^{2+} and Mn^{2+} will diffuse into the lumen. Such diffusive loss to the burrow water is often facilitated by steeper redox zonation at the burrow walls than at the sediment surface, due to migration of the burrow through the sediment, high surface to volume ratio due to the cylindrical architecture, and defecation within the burrow. When the animal resumes ventilation, the accumulated reduced solutes are flushed into the water column, without passing through an oxidised sediment layer that could have retained them. The

details of the processes in the burrow walls can therefore not be explained without considering the behaviour of the burrow inhabitants.

In comparison to the conditions in the animal burrows, the thin oxic zone at the visible sediment surface is stable and homogeneous. In the present work we will concentrate on this thin oxic skin, and on its coupling to the water column. Not because the diffusive O_2 flux it is more important than the than the fauna-mediated O_2 transport, but to achieve focus on a part of the marine environment with its one distinct characteristics.

DIFFUSIVE CONTROL OF O_2 FLUX AND CONSUMPTION

In the simple example of alabaster dissolution, the concentration of the solutes of interest at the surface of the "sediment" was known and constant. A similar simple assumption can not be made for the O_2 concentration at the sediment-water interface (C_0). If we consider a steady state situation with a given flux, the concentration at the sediment-water interface will be dictated by the concentration change across the effective DBL that is necessary to achieve the gradient corresponding to the flux (Eq. 1). If the thickness of the DBL is then doubled, the gradient would be half and the initial diffusive flux would thereby be halved as well. But the lower O_2 flux into the sediment would cause decreasing O_2 concentration at the sediment surface (C_0), and thereby partly re-establish the flux. To properly understand this mechanism, we must understand the dynamics of O_2 consumption within the sediment.

In contrast to most chemicals of the solid phase, the distribution of O_2 in the oxic skin is surprisingly well ordered, and under tight control of molecular diffusion. The turnover time of the entire pool is typically in the order of a few minutes, and the supply via diffusion is therefore generally close to steady state with consumption. From the surface and downwards, the diffusive flux can be described via Fick's first law (Eq. 1), just as the flux in the DBL could. The mineral grains of the sediment do, however, not allow diffusion of gasses or ions at any appreciable rate. For any cross section of sediment, only the pore space fraction is therefore available to diffusion. Further, the effective diffusion coefficient inside the sediment is lower than in the free water, as molecules must take longer paths in and out between the sediment grains. To account for these constraints, Fick's first law must be modified to account for diffusion within the sediment:

$$J = -\varphi D_s \frac{\partial C}{\partial z} \qquad (2)$$

where φ is the porosity and D_s is the effective diffusion coefficient in the porewater. The relation between φ and D_s can be found in the literature (e.g. Iversen and Jørgensen 1993; Ullman 1982; Boudreau 1996).

The important point at this time is that the flux is proportional to the slope of the profile. If we now consider the gradient a short distance into the sediment, the gradient must have decreased as the flux has been decreased by the amount of O_2 consumed in the sediment above. For each step we go further into the sediment, the gradient is further decreased. A constant volume-specific consumption rate will give a constant decrease in slope with depth, the characteristics of a second-degree polynomial. During steady state the slope at zero O_2 must be zero, i.e. the O_2 distribution form a parabola with its extremum tangenting the axis describing depth. Bouldin (1968) supplied a description of the concentration distribution (C) as a function of D_s, C_0 and the volume specific O_2 consumption rate (R):

$$C = (R/2D_s)z^2 - (2C_0R/Ds)^{0.5}\, z + C_0 \qquad (3)$$

Since the introduction of microsensors to marine science (Revsbech et al. 1979), direct measurements of the O_2 micro-distribution has been possible. These sensors measure the concentration at a resolution of down to about 50 µm, with the maximum resolution controlled by the diffusion sphere around the O_2 consuming sensor tip. Rasmussen and Jørgensen (1992) showed that measured O_2 distributions could be described with the analytical solution (Eq. 3) with an astonishing accuracy. Some profiles could be described by a single constant rate, while others were best described when the profile was divided into regimes of different rates (see also Berg et al. 1998). The subdivision can usually be attributed to different availability of electron donors between the top and the bottom of the oxic zone.

As the flux could be calculated from the change in concentration over depth, so can the rate be calculated from the change in flux with depth. To measure a reliable concentration gradient, we need two points with well-separated concentrations. Two to three concentration measurements distributed over 100 to 300 µm are usually well suited for coastal and estuarine sediments. If we wish to calculate the change in gradient over distance by another numerical differentiation, the resolution is obviously less than the resolution of the slope measurements. So, we will need a large part of the profile to get a good estimate of the rate. Due to the low resolution in the determination of the rate, relative to the resolution

of the concentration measurements, R usually appears as a step-function when plotted together with the concentration profile.

A perfect fit to one or two parabolas implies that, for practical considerations, oxygen is consumed according to zero-order kinetics. This means that every unit of oxic sediment consumes a constant amount of oxygen per unit time, independent of oxygen concentration. In spite of the zero order kinetics, the momentary oxygen consumption of the sediment as a whole reacts to a change in the oxygen concentration of the water column. The main mechanism behind this coupling is that higher O_2 concentrations at the sediment surface leads to a deeper O_2 penetration and thereby a larger O_2 consuming oxic sediment volume. As long as the volume specific O_2 consumption rate is constant, the relation between steady-state O_2 flux and penetration dept will be linear. But the relation between C_0 and O_2 penetration is not linear. The concentration increase necessary to shift the profile one fixed distance into the sediment will become larger and larger, because the slope of the profile increases together with the concentration. The O_2 penetration depth is therefore proportional to the square root of C_0.

The expressed steady state flux to the sediment is a balance between the impedance of the DBL and the dynamics of O_2 consumption within the sediment. As shown, both phenomena can be described mathematically, and we can exploit this to investigate how the O_2 consumption of the sediment is influenced by changes in the DBL thickness. Diffusive O_2 uptake in coastal and estuarine sediments range between 3.9 and 82 mmol m^{-2} d^{-1} (Canfield and Teske 1996). With a DBL thickness of 0.5 mm, 3.9 mmol m^{-2} d^{-1} correspond to a concentration change across the DBL of 11μM. Therefore, a water column O_2 concentration of 260 μM would imply a O_2 concentration at the sediment water interface of 249 μM. The theoretical O_2 penetration is 12 mm (see Rasmussen and Jørgensen 1992 for details). If we could strip away the entire DBL, the O_2 concentration at the sediment surface would increase to the water column value of 260 μM. The resulting increase in O_2 penetration and flux is only about 2%. The insensitivity of the flux to the presence of the DBL in this case is because the DBL constitute an insignificant part of the total distance that O_2 must diffuse between the water column and the sites of consumption.

A more typical O_2 flux to an estuarine sediment is 15 mmol m^{-2} d^{-1} (Chapter 5). In this case, the concentration decrease across the DBL is 42 μM and the O_2 penetration is reduced to about 3 mm. Removing the DBL in this case would cause an increase in flux and O_2 penetration of 11%. A hypothetical removal of the entire DBL is only interesting to achieve a feeling for the influence that the DBL can have on processes in the sediment. For

practical considerations it is more relevant to evaluate the influence of realistic changes in DBL thickness. In the later example, fluctuations in DBL thickness between 0.25 and 1 mm will be reflected in flux fluctuations in the range of ± 5%.

The theoretical change in flux as a response to changes in the DBL can be reproduced experimentally (e.g. Steinberger and Hondzo 1999). The response-time is in the range of minutes to a few hours for O_2 penetrations in the range of coastal and estuarine sediments. Details of how the dynamics of the change can be calculated are found in Chapter 2. It must, however, be emphasised that these changes in fluxes are short-term effects. Consumption of O_2 in aquatic sediments is attributed to two types of reactions: aerobic decomposition of organic matter and oxidation of reduced products of anaerobic decay, including NH_4^+, Mn^{2+}, Fe^{2+}, H_2S, FeS, and FeS_2. The oxidation of these compounds can not be expected to be in steady state with their production (e.g. Jørgensen 1996). The reduced products of anaerobic decay are produced throughout the bioturbated sediment horizon, and their reoxidation is de-coupled from the production in both time and space. The coupling between production and reoxidation happens through a large buffer, primarily connected to the iron cycle. A change of the pool of reactive iron in the top cm of marine sediments from its reduced to its oxidised form typically requires an amount of O_2 equivalent to the O_2 flux during an entire month (e.g. Jørgensen 1996; Jørgensen 1977). In temperate regions a distinct seasonal cycle exists, in which the reducing equivalents from organic matter oxidised during late summer are first caught in the pool of iron sulfides, and not represented in the O_2 flux before this pool is reoxidised during winter and spring. Short-term changes in O_2 flux connected to changes in the DBL thickness are first of all a changes in the elastic redox system of the sediment. Whether impedance in the DBL plays a role in determining the average O_2 consumption, depends on whether the volume of oxic sediment is a controlling factor for the balance between oxidation and burial of reducing equivalents. This question can not be answered from model calculations along the lines presented here.

In one special case, diffusive limitation can not be disregarded. As Jørgensen (2001) pointed out, there is an upper limit to the diffusive flux through a DBL of given effective thickness and overlying O_2 concentration. This limit is reached when the concentration at the surface is zero, and the gradient therefore can not become any steeper. Typical values for effective DBL and bulk water concentration is 0.5 mm and 260 µM. This gradient of 520 µM/mm corresponds to a flux of 94 mmol O_2 m^{-2} d^{-1} when using 2.1×10^{-5} as D. This high flux is seldom approached in modern marine sediments. But the limit is directly proportional to the O_2 concentration in the water column. Atmospheric O_2 concentrations

similar to the current was first reached by the end of the Proterozoic or later (Klein et al. 1992). If we assume that the Proterozoic oceans had a similar O_2 demand as the modern oceans (Canfield and Teske 1996), we can predict that the low atmospheric O_2 levels during most of the Proterozoic have been reflected in diffusion limitation of the benthic microbial communities. The observed O_2 uptake rates in modern coastal sediments are generally 10-30 mmol O_2 m^{-2} d^{-1} (Jørgensen 2001). This corresponds to diffusive limitation in the DBL at a O_2 concentration in the water column of 27-81 µM. 27-81 µM corresponds to saturation with an atmosphere with 10 - 30 % of the present O_2 level.

It should be clear from this introduction, that it is not possible to separate processes in the DBL from processes in the sediment and still make general conclusions on the influence of the DBL on processes in the sediment. So even though a study of the DBL above decomposing chicken-food can give important insight in the control of the thickness of the DBL (Steinberger and Hondzo 1999), the direct measurements of the influence of flow on O_2 utilisation can only be applied on sediments with a similar O_2 flux.

AIM AND OUTLINE OF THE THESIS

This introduction has described the DBL as a static phenomenon along one axis. In this respect, the conceptual model of the DBL has changed very little since the systematic description by Jørgensen and Revsbech in 1985. The static description has been adequate to explain a large number of phenomena, such as the dependency of the O_2 consumption rate in coherent sediments, and the diffusive constraints of microbial mats. There been a latent concern, that the one-dimensional description of sediments with sculptured surfaces contained an error of unknown magnitude. The difference between total O_2 uptake and vertical diffusion through the DBL has, for example, most often been commented on with weak statements like "*...fauna irrigation and three-dimensional effects*". Temporal concentration-fluctuations in the DBL have also been of concern. Besides being the preferred sampling device, transparent core-liners have also been used as experimental vessel for most studies that used microsensors. The small volume of water contained in a core-liner had the convenient side effect to impose a stability on the DBL that was known not to reflect *in situ* conditions. As the nature of the concentration fluctuations was not known, it was also not known how well the static DBL in the experimental systems represented the dynamic DBL *in situ*. The experimental efforts to clarify the influence of surface topography and temporal fluctuations has primarily supplied examples to illustrate

the possibility of an influence, rather than systematic studies to understand phenomena and quantify effects.

The following 6 chapters are the results of 4 years of work centred on the DBL of coastal and estuarine sediments. The reader will find a description of the DBL that takes temporal concentration fluctuations as well as surface topography into account.

Chapter 2 will explain how the gradients in the DBL behave under fluctuating conditions. The aim of this study was to identify the mechanism behind concentration fluctuations, and clarify if and how such fluctuations could be incorporated in the static conceptual model of the DBL. Its conclusions will allow us to disregard imposed stability as an artefact in the following manuscripts.

Chapter 3 presents a method for measuring surface topography, which can resolve features of the same scale as the thickness of the DBL. The topographic data is combined with two-dimensional O_2 distributions across the sediment-water interface, measured with microsensors. The combined data are used to show how topography of the DBL follows topography of the sediment-water interface. It is shown that the structure of the DBL can be predicted from the topographic data alone. This insight is exploited to calculate the influence of surface enlargement and horizontal gradients, which are both not accounted for by the one-dimensional model of the DBL. This, and the preceding study, was performed under reproducible conditions in a laboratory flume.

Chapter 4 builds largely on the methods and argumentation of Chapter 3, but applies the methods *in situ*. This chapter contains a discussion of the constraints on horizontal gradients in the DBL and proposes a range of the error induced by neglecting topography when considering diffusive fluxes.

The core of Chapter 5 is a comprehensive dataset describing the seasonal dynamics of one dimensional diffusive O_2 uptake measured with microsensors and total O_2 uptake measured with closed-core incubations. This dataset was supplemented with measurements of the difference between vertical diffusive flux and the total diffusive flux. This made it possible to separate "topographical effects" from fauna mediated O_2 uptake. An observed discrepancy between laboratory and *in situ* closed-core incubations could thereby be attributed to under-representation of large macrofauna in the laboratory incubations.

Apart form illustrating the seasonal dynamics of diffusive and fauna mediated O_2 uptake, Chapter 5 also illustrate several weaknesses in the current techniques for determining the O_2 flux across the sediment-water interface. Chapter 6 presents a new method that eliminates the most important artefacts associated with the current methods.

The new method is non-invasive, and fundamentally different from any other technique commonly used to measure solute flux today.

In the last chapter, the knowledge about advective transport and diffusive constraints gained during the work with the DBL is used to gain insight in the function of a symbiotic association between a benthic ciliate and sulfide oxidising bacteria.

REFERENCES

Aller, R. C. 2001. Transport and reaction in the bioirrigated zone, p. 269-301. *In* B. P. Boudreau and B. B. Jørgenesen [eds.], The benthic boundary layer: Transport processes and biogeochemistry. Oxford University Press.

Berg, P., N. Risgaard-Petersen and S. Rysgaard. 1998. Interpretation of measured concentration profiles in sediment pore water. Limnol. Oceanogr. 43: 1500-1510.

Boudreau, B. P. 1996. The diffusive tortuosity of fine-grained unlithified sediments. Geochim. Cosmochim. Acta. 60: 3139-3142.

Boudreau, B. P. 2001. Solute transport above the sediment-water interface., p. 104-126. *In* B. P. Boudreau and B. B. Jørgenesen [eds.], The benthic boundary layer: Transport processes and biogeochemistry. Oxford University Press.

Boudreau, B. P. and N. L. Guinasso. 1982. The influence of a diffusive sublayer on accretion, dissolution, and diagenesis at the sea floor, p. 115-145. *In* K. A. Fanning and F. T. Manheim [eds.], The dynamic environment at the ocean floor. Lexington.

Bouldin, D. R. 1968. Models for describing the diffusion of oxygen and other mobile constituents across the mud-water interface. J. Ecol. 56: 77-87.

Canfield, D. E. and A. Teske. 1996. Late proterozoic rise in atmospheric oxygen concentration inferred from phylogenetic and sulphur-isotope studies. Nature. 382: 127-132.

Cladwell, D. R. and T. M. Chriss. 1979. The Viscous Sublayer at the Sea Floor. Science. 205: 1131-1132.

Dade, B. W. 1993. Near-bed turbulence and hydrodynamical control of diffusional mass transfer at the sea floor. Limnol. Oceanogr. 38: 52-69.

Dade, B. W., A. J. Hogg and B. P. Boudreau. 2001. Physics of flow above the sediment-water interface, p. 4-43. *In* B. P. Boudreau and B. B. Jørgenesen [eds.], The benthic boundary layer: Transport processes and biogeochemistry. Oxford University Press.

Denny, M. V. 1993. Air and water. The Biology and physics of life's media. Princeton University Press.

Dworak, R. and H. Wendt. 1977. Stochastic fluctuations of mass transport through turbulent boundary layers. Berichte der Bunsen-Gesellschaft Phyk. Chem. 81: 864-869.

Hulth, S., T. H. Blackburn and P. O. J. Hall. 1994. Arctic sediments (Svalbard): consumption and microdistribution of oxygen. Mar. Chem. 46: 293-316.

Iversen, N. and B. B. Jørgensen. 1993. Diffusion Coefficients of Sulfate and Methane in Marine Sediments Influence of Porosity. Geochim. Cosmochim. Acta. 57: 571-578.

Jahnke, R. A. 2001. Constraining organic matter cycling with benthic fluxes, p. 302-319. *In* B. P. Boudreau and B. B. Jørgenesen [eds.], The benthic boundary layer: Transport processes and biogeochemistry. Oxford University Press.

Jørgensen, B. B. 1977. The sulfur cycle of a coastal marine sediment (Limfjorden, Denmark). Limnol. Oceanogr. 22: 814-832.

Jørgensen, B. B. 1996. Case study - Aarhus Bay, p. *In* [eds.], Eutrophication in Coastal Marine Ecosystems.

Jørgensen, B. B. 2001. Life in the diffusive boundary layer, p. 348-373. *In* B. P. Boudreau and B. B. Jørgenesen [eds.], The benthic boundary layer: Transport processes and biogeochemistry. Oxford University Press.

Jørgensen, B. B. and N. P. Revsbech. 1985. Diffusive boundary layers and the oxygen uptake of sediments and detritus. Limnol. Oceanogr. 30: 111-122.

Klein, C., N. J. Beukes, H. D. Holland, J. F. Kasting, L. R. Kump and D. R. Lowe. 1992. Proterozoic atmosphere and ocean, p. *In* J. W. Schopf and K. Cornelis [eds.], The Proterozoic biosphere. Cambridge University Press.

Klimant, I., G. Holst and M. Kühl. 1997. A simple fiberoptic sensor to detect the penetration of microsensors into sediments and other biogeochemical systems. Limnol. Oceanogr. 42: 1638-1643.

Kristensen, E. 1988. Benthic fauna and biogeochemical processes in marine sediments: Microbial activities and fluxes, p. 275-299. *In* T. H. Blackburn and J. Soerensen [eds.], Nitrogen cycling in coastal marine environments. John Wiley & Sons Ltd.

Kristensen, E. 2000. Organic matter diagenesis at the oxic/anoxic interface in coastal marine sediments, with emphasis on the role of burrowing animals. Hydrobiologia. 426: 1-24.

Kristensen, E., M. Jensen and T. Andersen. 1985. The Impact of Polychaete (*Nereis-Virens* Sars) Burrows On Nitrification and Nitrate Reduction in Estuarine Sediments. J. Exp. Mar. Biol. Ecol. 85: 75-91.

Lerman, A. 1979. Geochemical processes water and sediment environments. John Wiley & Sons.

Rasmussen, H. and B. B. Jørgensen. 1992. Microelectrode studies of seasonal oxygen uptake in a costal sediment: role of molecular diffusion. Mar. Ecol. Prog. Ser. 81: 289-303.

Revsbech, N. P., B. B. Jørgensen and T. H. Blackburn. 1979. Oxygen in the sea bottom measured with a microelectrode. Science. 207: 1355-1356.

Santschi, P. H., U. P. Nyffeler, W. S. Azevedo and W. S. Broecker. 1983. Estimates of the resistance to chemical transport posed by the deep-sea boundary layer. Limnol. Oceanogr. 28: 899-912.

Shaw, D. A. and T. J. Hanratti. 1977. Turbulent mass transfer rates to a wall for large Schmidt numbers. Amer. Inst. Chem. Eng. Jour. 23: 28-37.

Steinberger, N. and M. Hondzo. 1999. Diffusional mass transfer at sediment-water interface. J. Environ. Eng.-ASCE. 125: 192-200.

Ullman, W. and R. Aller. 1982. Diffusion-Coefficients in Nearshore Marine-Sediments. Limnol. Oceanogr. 27: 552-556.

Vogel S. 1994. Life in moving fluids - the physical biology of flow. Princeton University Press.

Overview of manuscripts

Transmission of oxygen concentration fluctuations through the diffusive boundary layer of a marine sediment (2)

Hans Røy, Markus Hüttel and Bo Barker Jørgensen

(Submitted to Limnology & Oceanography)

The role of small-scale sediment topography for oxygen flux across the diffusive boundary layer (3)

Hans Røy, Markus Hüttel and Bo Barker Jørgensen

(Published in Limnology & Oceanography)

The influence of topography on the functional exchange-surface of soft sediments, assessed from *in situ* measured sediment topography (4)

Hans Røy, Markus Hüttel and Bo Barker Jørgensen

(Submitted to Limnology & Oceanography)

Seasonal dynamics of benthic O_2 uptake in a semi enclosed bay: Importance of diffusion and fauna activity (5)

Ronnie N. Glud, Jens K. Gundersen, Hans Røy, and Bo Barker Jørgensen

(Published in Limnology & Oceanography)

Oxygen uptake by aquatic sediments measured with a new non-invasive eddy correlation technique (6)

Peter Berg, Hans Røy, Felix Janssen, Volker Meyer,

Bo Barker Jørgensen, Markus Hüttel, and Dirk de Beer

(In press in Marine Ecology Progress Series)

Transport of water and solutes around the symbiont bearing sessile ciliate, *Zoothamnizm niveum* (7)

Hans Røy, Kay C. Vopel, Markus Hüttel, Bo Barker Jørgensen, and Jörg Ott

(For puplication in Aquatic Microbial Ecology)

Page left blank intentionally

Transmission of oxygen concentration fluctuations through the diffusive boundary layer of a marine sediment.

Hans Røy, Markus Hüttel and Bo Barker Jørgensen

ABSTRACT

Even though the O_2 concentration in the diffusive boundary layer overlying natural marine sediments usually varies over time, microprofiles with little or no error bars on the single measurements are abundant in the literature. With the temporal concentration-fluctuations not accounted for in the conceptual models used to describe the DBL, it is unclear which implications their presence or absence has on phenomena investigated with microprofiles. We therefore analysed the concentration fluctuations in the diffusive boundary layer above a marine sediment. One microsensor was introduced into a laboratory flume from below, and positioned with the sensing tip precisely at the sediment surface. A second microelectrode was introduced from above through the flowing water column and positioned within the DBL, directly above the tip of the lower sensor. The two sensors were used to measure time-series of the fluctuating O_2 concentration at the two points simultaneously, which demonstrated a tight coupling of concentration-fluctuations across the DBL. We then applied a dynamic model accounting only for molecular diffusion plus zero order consumption within the sediment, which alone could explain the observed coupling through the DBL. The approach enabled calculation of entire instantaneous O_2 profiles from the top of the true DBL to depth of O_2 penetration. Such profiles confirmed that concentration-fluctuations were linked from the top of the true DBL down to about 0.5 mm sediment depth. The profiles simply appeared to bend back and forth, without loosing the general shape known from the averaged steady state O_2 distribution.

INTRODUCTION

The diffusive boundary layer (DBL) is the 0.2 to 1.2 mm thick film of water coating non-permeable sediments and through which molecular diffusion is the dominant transport mechanism for solutes (Boudreau and Jørgensen 2001). Viscous forces reduce turbulent mixing in the lowest part of the benthic boundary layer. At a distance of about one mm from the sediment surface, turbulent mixing becomes insignificant for the transport of dissolved substances relative to molecular diffusion.

The lowest part of the DBL in which transport is solely by molecular diffusion exhibits linear concentration profiles, and is here referred to as the true DBL (Fig 1). If the gradient in this layer is extrapolated to the concentration in the water column, we obtain the so-called effective DBL (Jørgensen and Revsbech 1985). The effective DBL represents an idealised layer with a linear gradient throughout, that yield the same flux as the actual DBL (Fig 1).

Although the combined thickness of DBL and oxic sediment layer can be less than a millimetre, highly resolved measurements of oxygen concentration gradients are possible. The diffusive flux (J) through the DBL and across the sediment-water interface can be calculated using Fick's first law of diffusion:

$$J = - D \, dC/dz \qquad (1)$$

where D is the molecular diffusion coefficient in water and dC/dz the vertical concentration gradient.

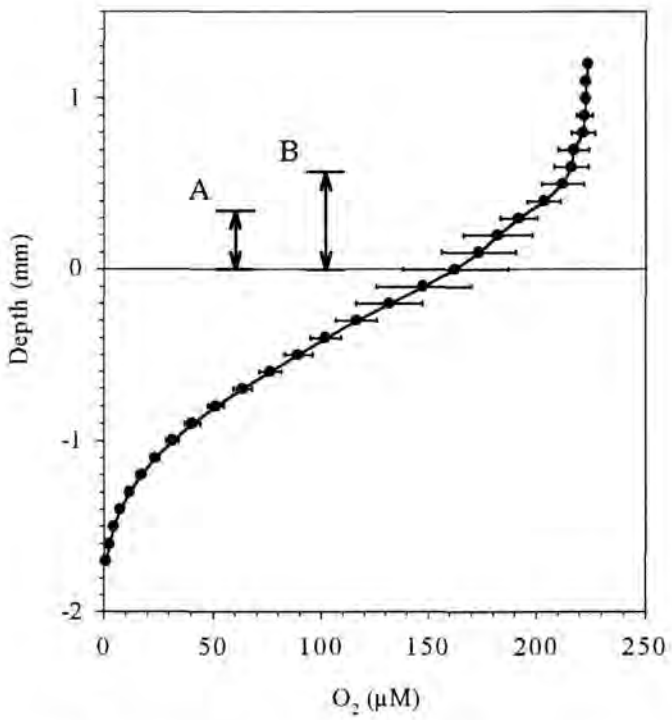

Figure 1. Example of a time-averaged O_2 microprofile through the sediment-water interface. The strictly linear part from the sediment surface and 0.6 mm up is the true DBL (A). By extrapolating this linear part of the profile to the O_2 concentration of the water column, the effective DBL is found (B). The error bars indicate 2 × standard deviation.

The mineral grains of the sediment do not allow diffusion of gasses or ions at any appreciable rate. For any cross section of sediment, only the pore space fraction is therefore available to diffusion. Further, the effective diffusion coefficient inside the sediment is lower than in water, as molecules must take a longer path around the sediment grains. To account for this, Fick's first law must be modified to be valid for diffusion within the sediment:

$$J = - \varphi D \, dC/dz \tag{2}$$

where φ is the porosity and D_s is the effective diffusion coefficient in the sediment. Several empirical relation between φ and D_s exists (e.g. Boudreau 1996). For clay-silt sediment, (Iversen and Jørgensen 1993) give:

$$D_s = \frac{D}{1+3(1-\varphi)} \tag{3}$$

To satisfy conservation of mass, the flux on both sides of the sediment-water interface must be equal. The restricted diffusion inside the sediment thereby forces the slope of the microprofile to become steeper, forming a slope-discontinuity in oxygen microprofiles at the sediment-water interface. This feature is often observed in experimental data. By combining Eq. 1, 2 and 3, we can derive the relation between φ and the ratio between the slopes right above and right below the sediment surface:

$$\varphi = 4\left(\frac{dC/dz_{sediment}}{dC/dz_{water}} + 3\right)^{-1} \tag{4}$$

Various O_2-consuming processes co-exist in marine sediments and each process is controlled by its own kinetics. The combined kinetics work in a way that, *in situ*, the amount of O_2 consumed per unit of oxic sediment per unit time can not be correlated to the O_2 concentration. Instead, the steady state oxygen microprofiles can most often be explained very accurately by analytical modelling according to zero order kinetics (i.e. no dependence of concentration). Due to different substrate pools, the best fit is often achieved when the profiles are divided into zones of different rates (e.g. Berg et al. 1998). Within each zone, O_2 is still consumed at a constant rate. In spite of the zero order kinetics, the momentary oxygen consumption of the sediment as a whole reacts to a change in the oxygen concentration of the water column. The main mechanism behind this coupling is that higher O_2 concentrations at the sediment surface leads to a deeper O_2 penetration and thereby a larger O_2 consuming oxic sediment volume.

The application of the simple Fick's first law implies a static DBL. However, it is known from experimental work that concentrations of reactive solutes in the DBL are often very variable (Dworak and Wendt 1977; Jørgensen and Des Marais 1990). Measurements with fast reacting microelectrodes reveal pronounced variability for O_2 in the DBL in natural environment and set-ups that are designed to mimic the flow environment at the seafloor, such as sediment incubations in flumes. In confined systems, like sediment cores, concentration fluctuations are less pronounced or not present. With the concentration fluctuations not accounted for in the conceptual models used to describe the DBL, it is unclear which implications imposed stability could have on phenomena investigated with microprofiles. It has, for example, been proposed that fluctuations in the DBL reflect turbulence within the layer, which would imply that flux-calculations based on the linear concentration gradient at the sediment-water interface underestimate the actual diffusive flux (Gundersen and Jørgensen 1990).

This paper analyses the impact of temporal concentration-fluctuations in the DBL, in a system where the instability was pronounced. We apply a dynamic model accounting only for molecular diffusion plus zero order consumption within the sediment, which alone can explain an observed coupling of concentration fluctuations through the DBL. We did not try to identify the hydrodynamic forces responsible for initiating the oscillations, but focused on a better conceptual understanding of the processes governing reactive solute flux through the DBL. We present a dynamic description of the DBL that will allow a case to case judgement on whether the fluctuations must be considered, or if the static view will suffice. The description is also used to discuss sound experimental procedures when measuring microprofiles, especially with respect to calculations of the diffusive flux through the DBL.

METHODS

We used a flume with an internal base area of 30 × 300 cm^2. Flow was driven by re-circulating the water through an external centrifugal pump. Before flowing over the sediment, the water passed through 5 cm of filter sponge and two 5 cm long straw collimators to reduce inflow turbulence. One centimetre after the last collimator a 2 mm thick wire was placed across the bottom of the flow to start development of a turbulent boundary layer. Downstream from this point there was 250 cm of free surface flow over naturally sculptured sediment. The bulk flow velocity of ~7 cm s^{-1}, resulted in a Reynolds number of 5700. Shear velocity (u_*) after 200 cm of free flow, estimated from the velocity gradient in the viscous sublayer was 0.15 cm s^{-1}.

Sediment was collected from an intertidal mudflat near Dangast, Germany. One m^2 of surface sediment, 5 cm deep, was brought to the laboratory and placed with intact stratification in the flume. A 5 cm layer of North Sea water, diluted to match the porewater salinity of 25 ‰, was added and unidirectional flow established. The sediment was allowed to equilibrate in the flume for 6 months after which the fauna composition, water column O_2 concentration, diffusive O_2 uptake, and visual appearance were constant over a time scale of weeks.

The sediment topography was mostly composed of 0.5 - 2 mm high mounds with a density of 5,000 m^{-2}, produced by numerous oligochaetes of the Tubifex family. Faecal mounds produced by the polychaete *Heteromastus filiformis* were equally conspicuous. These mounds were 5 to 10 mm high and occurred at 110 m^{-2}. The surface structure was kept dynamic by constant reworking by shrimps, present from the time of sampling. The median grain size was 6.3 µm. Porosity was 77 % (± 2.5, n = 5) in the upper 15 mm, determined by drying samples at 60 °C until constant weight. Permeability in the top 18 mm was 1.52×10^{-13} (SE 0.29×10^{-13}, n = 3) m^2, measured with a constant head of 500 Pa (Klute and Dirksen 1986). The organic carbon content was 2.9 (SE 0.2 n = 10) % dry weight, determined with a CNS analyser.

Clark-type O_2 microelectrodes (Revsbech 1989) with a tip diameter of ~15 µm were used for the experiments. The electrode shafts were made especially long and slender, reaching only 1 mm in diameter at 50 mm from the sensing tip. The 90 % response time to a sudden, large change in O_2 concentration was approximately two seconds and stirring sensitivity was not measurable within the range of flow velocities encountered in the study. The electrodes were calibrated between the O_2 concentration in the mixed water column, determined by Winkler titration (Strickland and Parson 1972), and the anoxic sediment.

Two sensors were introduced vertically into the DBL from opposite directions, 200 cm downstream of the wire-trip. The lower sensor was introduced through the sediment from below. This was possible through flexible silicone-rubber (Dow Conning 734) ports cast into holes in the flume bottom. Although extremely sensitive to bending, electrode tip will most often survive penetration through up to 10 mm of this material (Ziebis et al. 1996). The two sensors were initially aligned tip to tip while observing through a stereo microscope. Pre-defined vertical distances were then fixed using micromanipulators. To explore the temporal structure of the DBL, O_2–concentration time-series were recorded simultaneously with both sensors. The signal was sampled through a 1 Hz low-pass filter at 2 Hz.

RESULTS

O_2 microprofiles measured from above showed conventional looking profiles with a ~ 0.3 mm - thick true DBL and ~ 0.6 mm thick effective DBL (Fig. 1). Periodic deviations from bulk water O_2 concentration appeared up to 2.5 mm above the sediment surface, causing time-averaged profiles to curve up to this height. In the sediment, the profiles were parabolas, indicative of molecular diffusion and zero order kinetics (Rasmussen and Jørgensen 1992). The ratio between the slope of the microprofiles below and above the sediment-water interface was 1.4. According to Eq. 4, this implies a porosity in the surface sediment of 0.9.

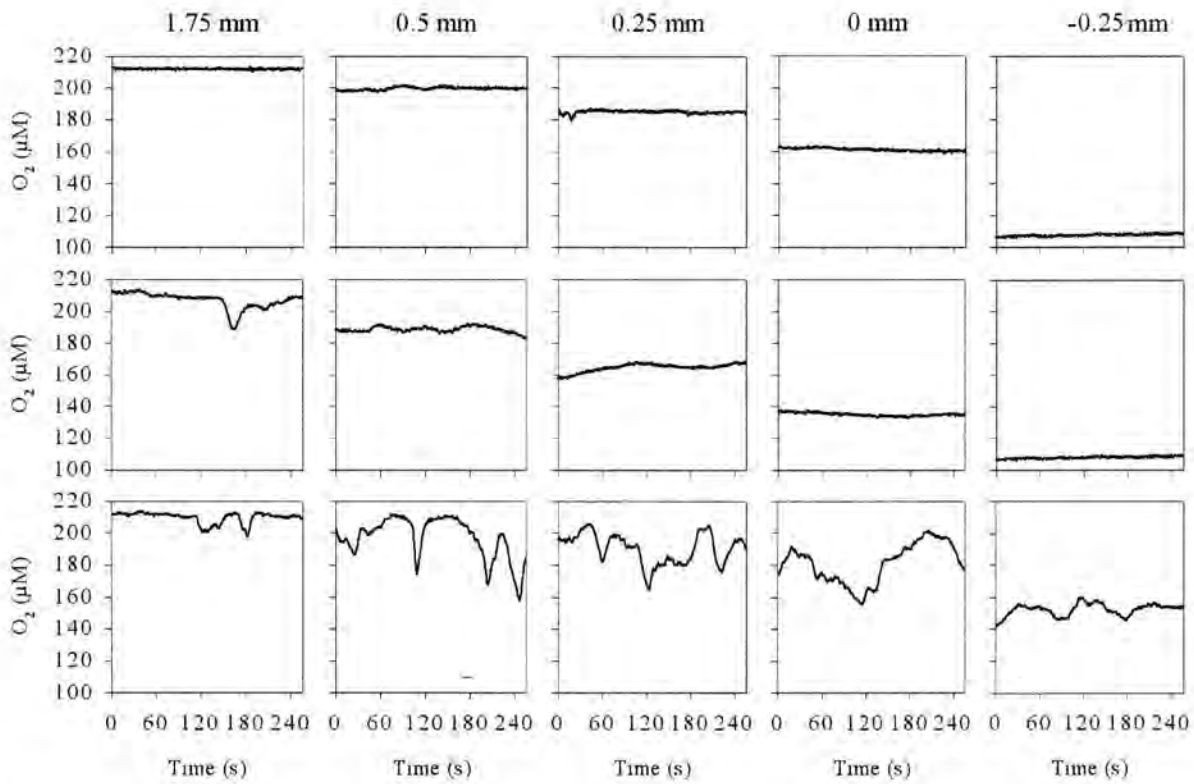

Figure 2. O_2 concentration time-series close to the sediment surface 15 cm (top row), 100 cm (middle row) and 150 cm (bottom row) downstream from the leading edge of the sediment. The approximate heights of the sensing tip relative to the sediment surface were 1.75 mm, 0.5 mm, 0.25 mm, 0.0 mm and –0.25 mm.

When measured from below, the DBL was somewhat thicker, in accordance with earlier observations (Glud et al. 1994; Lorenzen et al. 1995). To avoid disturbing the sites where the microelectrodes had successfully penetrated the silicon ports and sediment, whole profiles were not measured from below.

O_2 fluctuations in the DBL were found to vary strongly with the downstream position in the flume. The combination of porous material and straw-collimators in the inflow effectively removed all large-scale turbulence, causing O_2 distribution in the DBL to be stable close to the flow entrance. Further downstream, the development of a turbulent flow caused strong fluctuations in O_2 concentrations in the DBL (Fig. 2).

When one electrode was placed precisely at the sediment surface and the second directly above in the DBL, the signals appeared closely coupled (Fig. 3, solid curves). The vertical distance between the two electrodes while acquiring the data in Fig. 3 was 125 µm and the average concentration difference was 15.6 µM. This gives a diffusive flux of 22 mmol O_2 m^{-2} day^{-1}, according to and Eq. 1. Extrapolating the gradient to the bulk water O_2 concentration gives a 614 µm thick effective DBL. Oxygen penetration into the sediment in the close surroundings was 1.7 mm, which agree well with calculation assuming according to zero order kinetics and steady state (Rasmussen and Jørgensen 1992).

The concentration difference between the two positions (ΔC) was not constant but was coupled to the concentration fluctuations. The shaded areas in Fig. 3 show the rate at which the concentration difference changed (dΔC/dt). Positive values appear where the

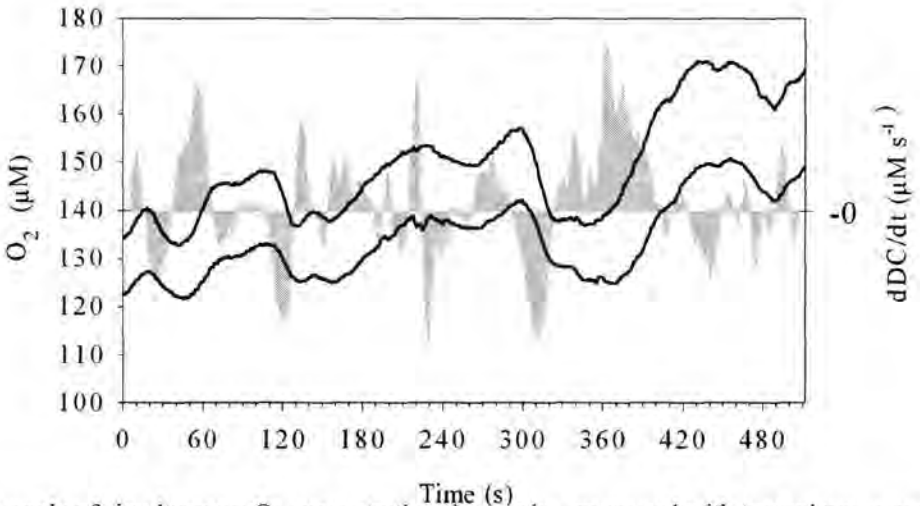

Figure 3. Example of simultaneous O_2 concentration time series, measured with two microsensors. The upper solid line is derived from the upper sensor within the true DBL, while the lower line was recorded at the sediment surface from below. The shaded area indicates the change in concentration difference between the two electrode signals in µM s^{-1}. Positive values show situations where the two signals are drifting apart, whereas negative values show that the signals are approaching each other. The sudden transient drop in O_2 concentration at the sediment-water interface at 225 seconds were cause by a passing harpacticoid copepod.

signals are drifting apart and negative values when the signals are nearing each other. Note that decreasing O_2 concentration is typically accompanied by decreasing concentration difference (negative $\partial\Delta C/\partial t$) and vice versa, so that the fluctuations are slightly dampened at the lowest position. Note also that the response of the lower sensor is slightly delayed relative to the signal of the upper sensor. In Fig. 3, this can be seen best around peaks of the upper sensor. The delay is, however, seen more clearly when the rate of concentration-change at the sediment surface is plotted as a function of the rate of change further up in the DBL (Fig. 4, filled symbols). The coupling of the two signals causes the plot to move between simultaneously increasing concentrations in quadrant I, and simultaneously decreasing concentrations in quadrant III. However, the delay at the sediment-water interface causes the rate at the lower sensor to increase still a short time after the rate has started decreasing at the upper sensor. As a result, the plot describes a counter-clockwise semicircle. How wide the circle is opened is a sensitive measure of the delay of the response on the lower sensor.

The delayed and depressed signal at the sediment-water interface shows that concentration fluctuations must be controlled from above. If the concept of a "true DBL" as a zone of exclusively diffusive transport is valid, the coupling of fluctuations across the DBL must be via molecular diffusion too. By applying a dynamic model accounting only

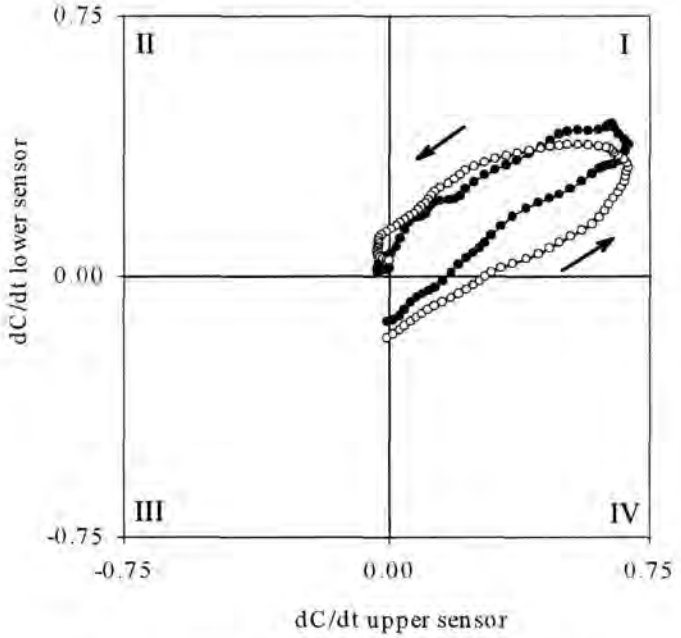

Figure 4. Short sequence of rate of change in O_2 concentration (dC/dt) at the sediment surface, as a function of the rate of change 125µm higher up in the DBL. The rates of change have been calculated from the concentration measurements seen from 40 to 83 seconds in Fig. 3. The closed symbols represent data measured with two sensors Open symbols represent the same values of the upper sensor, but the data of the lower sensor were replaced by modeled values

for molecular diffusion plus zero order consumption within the sediment, we can identify to which extent the observed coupling of the concentration fluctuations can be explained by diffusion rather than by turbulence.

The applied numerical model is a vertical array of cells, each representing a 25 µm thick zone (Fig 4). The top cell represents the position of the upper sensor, and the array extends downwards across the sediment-water interface to well below the expected penetration depth of O_2. Between the cells, O_2 is transported by molecular diffusion according to Eq. 1 or Eq. 2. In the cells representing sediment, O_2 is consumed according to zero order kinetics. The model was evaluated in 0.125 second steps, by applying a measured O_2 concentration in the top cell and calculating the O_2 distribution in the remaining cells. The maximum divergence when model runs were reproduced with 10 times higher temporal resolution was 0.02 µM. To mach the temporal resolution between measured concentrations and model runs, the measured time series were interpolated accordingly.

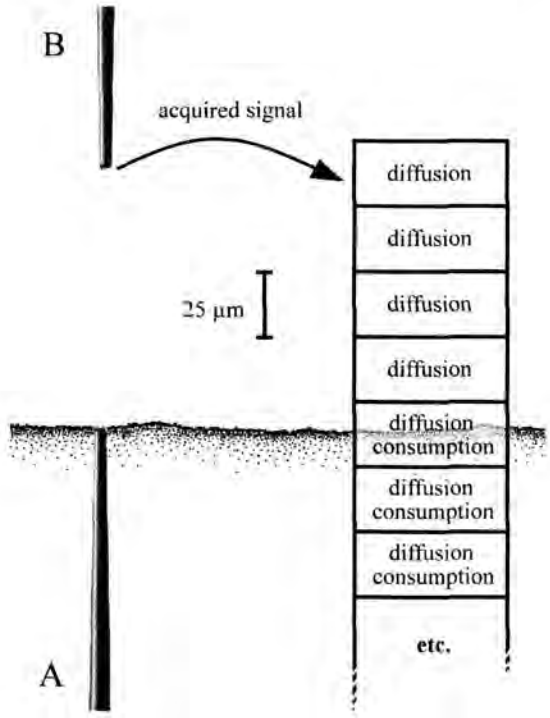

Figure 5. Experimental set-up and model structure. The two sensors (A and B) were introduced from opposite directions and aligned horizontally tip to tip. The lower sensor was fixed with the tip exactly at the sediment-water interface and the upper sensor placed above in the true DBL. The model consists of cells each representing a 25 µm thick zone. The top cell is located at the height of the upper sensor, and the concentrations measured by this sensor were used to force the model. Transport between adjacent cells was calculated from the concentration difference according to Fick's first law, taking into account the finite porosity when the border between the cells in question was within the sediment. Consumption in the sediment cells was independent of depth and concentration, provided that enough O_2 was present in the cell. This requirement was only expressed in the last cell containing O_2. The model was extended so far downwards that zero oxygen was always reached. The cell at the sediment-water interface was modelled as half sediment, half water column.

All parameters used to set up the model are available as physical constants or from interpretation of the microelectrode data: D at appropriate temperature and salinity was taken from (Li and Gregory 1974). Porosity was calculated from the slope discontinuity as discussed above. D_s was calculated from D and porosity according to Eq. 3. The average concentration difference between the two sensors, together with the distance between the sensors and D, provide the diffusive flux according to Eq. 1. The concentration at the sediment-water interface (C_0) is taken from the average concentration at the lower sensor. The depth-independent consumption rate of O_2 per unit volume of porewater (R) was found by dividing the flux by O_2 penetration-depth and porosity.

When forced with a constant value in the top cell and allowed to run to steady state, the model gives a linear gradient above the interface, a slope discontinuity at the interface and a parabolic decrease to zero O_2 in the sediment. The same result can be derived analytically (Rasmussen and Jørgensen 1992), and the two procedures are in perfect agreement. The top cell can now be forced with the fluctuating time series of O_2. Time series from any layer can then be calculated (Fig. 6), as can entire instantaneous O_2 profiles all the way to the penetration depth of O_2 (Fig. 7). As the history of the O_2 concentration was not known, the model was initialised with a steady state profile modelled from the average O_2 concentration in the top cell. The first approximately 60 s should therefore be disregarded. Apart from this initial phase, a close match between modelled and measured O_2 concentration at the sediment-water interface can be seen (Fig. 6). As seen in Fig 4, even the magnitude and delay in the rate of change could be accurately simulated.

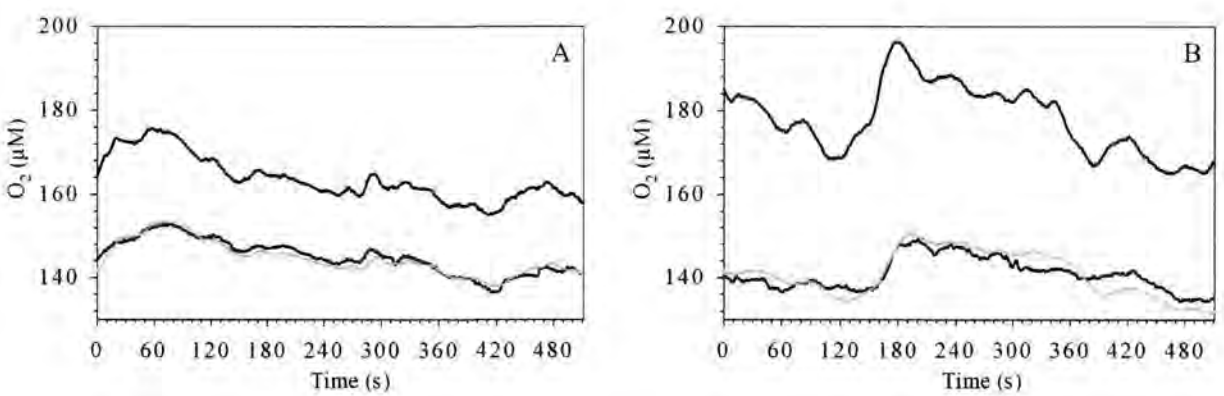

Figure 6. Comparison of modelled and measured O_2 concentrations at the sediment-water interface. The upper heavy line was measured within in the DBL, and the lower heavy line precisely at the sediment surface. The grey line represents the modeled concentration at the sediment surface, after using the values measured in the DBL as model input. The distances between the sensors were 100 µm in 5A and 200µm in 5B.

DISCUSSION

While the sequentially measured time series in Fig. 2 give a chaotic impression of the gradient in the DBL, the modelled instantaneous profiles in Fig. 7 show a much more orderly system. During this sustained concentration increase over 50 seconds, also represented from 374 s to 424 s in Fig. 3, the O_2 profile bent towards higher concentrations. When viewed over longer time, the profile appears to be gently rocking back and forth without a breakdown of the general profile shape. We should therefore realise that the error bars in Fig 1, at least for the linear part of the DBL and downwards, represent such co-ordinated concentration fluctuations.

The decreasing amplitude with depth is in part due to the decreasing O_2 concentration, but mostly caused by the strong influence of distance on diffusive transport. This can be demonstrated by modelling the propagation of a 20µM step-down in O_2 concentration, imposed 300 µm above the sediment surface. In our example, concentrations at the sediment-water interface will have reached halfway to the new steady state after 33 seconds. After these 33 seconds, a point 300µm within the sediment has only covered 13% of the way to its new steady state, and the change one mm into the sediment is absolutely

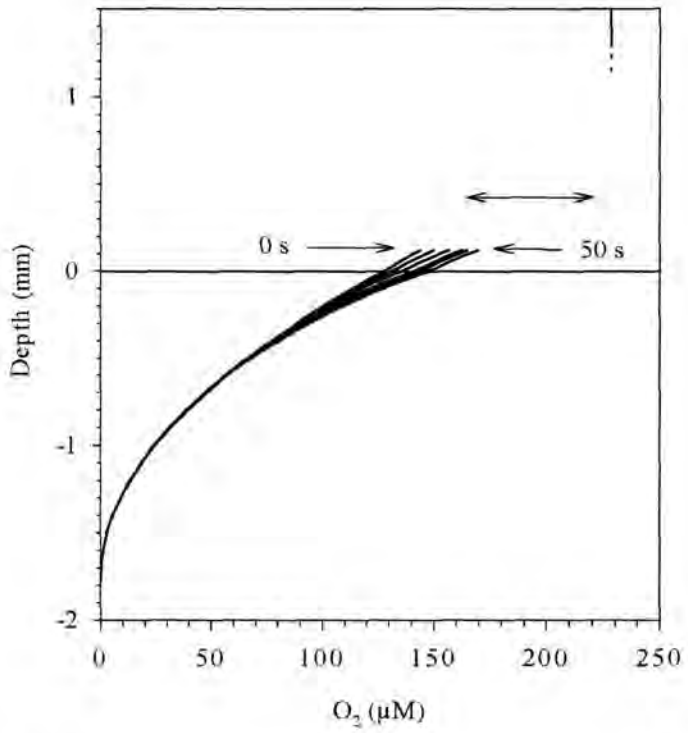

Figure 7. Example of modeled instantaneous O_2 profiles over 50 seconds of naturally increasing O_2 concentrations. The time between the profiles is 10 seconds. The concentration at the top of the profile was measured, and the modelled concentration at the sediment surface verified with the lower sensor as in Fig. 6. This interval with extreme fluctuation, seen also from 374 to 424 seconds in Fig. 3, was chosen for clear illustration. Most other 50 s intervals showed a smaller amplitude and more than one fluctuation.

insignificant. The 120 seconds needed to bring about 50% of the full change 300μm into the sediment would barely cause a 1 μM change at one mm depth. Thus, with a time-scale of the fluctuations in the range of 20 to 120 seconds, the sediment at 300μm depth experience the fluctuations from the much DBL depressed, and the sediment one mm from the surface see a stable O_2 concentration. To get the entire 1.7 mm deep profile to within 1 μM of the new steady state after a 20 μM change at the top of the DBL requires about 10 minutes.

The concentration fluctuations generate temporal heterogeneity around the sediment-water interface with a period of about 20 to 120 seconds. As the single points in microprofiles are usually integrated over just a few seconds, the result is often irregular profiles. Averaging over several fluctuations is an obvious solution to this problem. But with a period of up to several minutes, this might require impractical long measuring time for a profile. An alternative is measuring fast, thus trying to outrun the fluctuations. This approach can yield sound looking profiles, even under fluctuating conditions as shown in Fig. 2. Yet, the method should be avoided as the profiles might easily be measured during changing concentrations in the DBL, thus causing artifacts in the profiles. It can be assumed that the fluctuations constitute a roughly constant fraction of the concentration difference between the sediment surface and the water column. If this assumption is true, the fluctuations contribute a constant relative noise to flux-calculations from DBL-profiles. It therefore makes sense to integrate O_2 measurements in the DBL over several minutes, even though the small fluctuations in a shallow gradient appear to be negligible. Long integration time especially make sense *in situ*, where the constant temperature and isolation from electric and magnetic noise make differential measurements of even small changes highly accurate.

In laboratory situations when only processes within the sediment are of interest, the most practical solution is to avoid hydrodynamic conditions that cause fluctuations. This can be done by avoiding well-developed turbulent flows, by for example measuring in sediment cores and stirring the shallow water column only by a gentle air-jet. Small flow-cells perform equally well, given that unstable turbulence in the inflow is dissipated. However, these approaches require that the flow velocity is adjusted to provide a realistic thickness of the DBL.

If the objective for acquiring the microprofiles goes beyond flux calculations, the fluctuations should not be considered as simple measurement noise. The fluctuations are a natural property of the DBL, as the turbulence controlling its upper limit is not uniform. So whereas the error bars in Fig. 1 are still the best description in the curving part of the DBL,

the profile in the linear part and downwards can be much better understood from the representation in Fig. 7. The significance of presence or absence of concentration fluctuations should be considered from case to case. Generally, the major influence of oxygen on aspects like kinetics and chemotaxis occurs at concentrations below 10 μM. To have these low concentrations influenced by the fluctuations require such a shallow O_2 penetration that an effect is not likely to be present in except in sulfureta. When dealing with such diffusion limited systems, considerations about concentration driven phenomena, such as the ability of *Thiovulum majus* to swim along the 10 μM isopleth (Thar 2001), should take into account that the gradient in the DBL under at least some conditions is migrating up and down.

This far, we have traced the propagation of the concentration fluctuations from a given point in the DBL and away from the point of origin. Although the origin of the fluctuations was not the objective of this study, it is interesting to compare the time scale of the observed fluctuations with temporal structures in the turbulent flow. Turbulence is not strictly random, but to some extent organised in large-scale structures, known as coherent motions. Dade et al. (2001) gives the time-scale to be $10^2\ u_*^2/\nu$, when observed from a fixed point. In our case, this would imply a time-scale of 46 seconds. ($\nu = 1.04\times10^2$ cm^2 s^{-1}, $u_* =$ 0.15 cm s^{-1}). So, whereas the time-scales of the O_2 fluctuations are far to long to be explained by impact of single eddies, the frequencies lie within the range that could be explained by coherent motions.

REFERENCES

Berg, P., Risgaard-Petersen, N. Rysgaard, S. 1998. Interpretation of measured concentration profiles in sediment pore water. Limnol. Oceanogr. 43: 1500-1510.

Boudreau, B. P. 1996. The diffusive tortuosity of fine-grained unlithified sediments. Geochim. Cosmochim. Acta. 60: 3139-3142.

Boudreau, B. P. and B. B. Jørgensen. 2001. The Benthic Boundary Layer: Transport processes and biogeochemistry. Oxford University Press.

Dade, B. W., A. J. Hogg and B. P. Boudreau. 2001. Physics of flow above the sediment-water interface, p. 4-43. *In* B. P. Boudreau and B. B. Jørgenesen [eds.], The benthic boundary layer: Transport processes and biogeochemistry. Oxford University Press.

Dworak, R. and H. Wendt. 1977. Stochastic fluctuations of mass transport through turbulent boundary layers. Berichte der Bunsen-Gesellschaft Phyk. Chem. 81: 864-869.

Glud, R. N., J. K. Gundersen, N. P. Revsbech and B. B. Jørgensen. 1994. Effects on the benthic diffusive boundary layer imposed by microelectrodes. Limnol. Oceanogr. 39: 462-467.

Gundersen, J. K. and B. B. Jørgensen. 1990. Microstructure of diffusive boundary layers and the oxygen uptake of the sea floor. Nature. 345: 604-607.

Iversen, N. and B. B. Jørgensen. 1993. Diffusion Coefficients of Sulfate and Methane in Marine Sediments Influence of Porosity. 57: 571-578.

Jørgensen, B. B. and D. J. Des Marais. 1990. The diffusive boundary layer of sediments: Oxygen microgradients over a microbial mat. Limnol. Oceanogr. 35: 1343-1355.

Jørgensen, B. B. and N. P. Revsbech. 1985. Diffusive boundary layers and the oxygen uptake of sediments and detritus. Limnol. Oceanogr. 30: 111-122.

Klute, A. and C. Dirksen. 1986. Hydraulic conductivity and diffusivity: laboratory methods, p. 687-734. In A. Klute [ed.], Methods of soil analysis - part 1 - physical and mineralogical methods. American Society of Agronomy.

Li, Y. H. and S. Gregory. 1974. Diffusion of Ions in Sea-Water and in Deep-Sea Sediments. Geochim. Cosmochim. Acta. 38: 703-714.

Lorenzen, J., R. N. Glud and N. P. Revsbech. 1995. Impact of microsensor-caused changes in diffusive boundary layer thickness on O_2 profiles and photosynthetic rates in benthic communities of microorganisms. Mar. Ecol. Prog. Ser. 19: 237-241.

Rasmussen, H. and B. B. Jørgensen. 1992. Microelectrode studies of seasonal oxygen uptake in a coastal sediment: role of molecular diffusion. Mar. Ecol. Prog. Ser. 81: 289-303.

Revsbech, N. P. 1989. An oxygen microsensor with a guard cathode. Limnol. Oceanogr. 34: 472-276.

Strickland, J. D. and T. R. Parson. 1972. A practical handbook of seawater analysis. Pergamon Press.

Thar, R. F. T. 2001. True chemotaxis in oxygen gradients of the sulfur-oxidizing bacterium *Thiovulum majus*. Appl. Environ. Microbiol. 67: 3299-3303.

Ziebis, W., S. Forster, M. Huettel and B. B. Jørgensen. 1996. Complex burrows of the mud shrimp *Callianassa truncata* and their geochemical impact in the sea-bed. Nature. 382: 619-622.

The role of small-scale sediment topography for oxygen flux across the diffusive boundary layer

Hans Røy, Markus Hüttel and Bo Barker Jørgensen

ABSTRACT

At the scale of centimetres or millimetres, marine sediment surfaces are sculptured into complex three-dimensional landscapes. A detailed study of fluxes through the diffusive boundary layer (DBL) therefore requires concurrent information on the surface structure. Using natural sediment in a laboratory flume, we investigated the impact of small-scale sediment-topography on diffusive oxygen flux through the DBL. Topographic maps of the sediment surface with 0.1 mm horizontal resolution were acquired with a custom-made optical technique, and immediately afterwards the oxygen diffusion field across the sediment-water interface was measured with microsensors in known orientation within the described topography. A method was developed to calculate the three-dimensional diffusive flux through the DBL, based on the combination of vertical O_2 microprofiles and the high-resolution topographic data. Even though the sediment surface investigated was elaborately sculptured by fauna, the combined influence of increased surface area and horizontal concentration gradients within the DBL induced less than 10% difference between one-dimensional and three-dimensional diffusive flux calculations. The relatively low impact of surface topography is explained by the geometry of the diffusion field, as well as effects of the rapid diffusion of O_2 at small scales.

INTRODUCTION

The diffusive boundary layer (DBL) is the thin film of water covering fine-grained sediments, through which molecular diffusion is the dominant transport mechanism for dissolved material. Viscous forces reduce turbulent mixing in the lowest part of the benthic boundary layer. At a distance of a few tenths of a mm from the sediment surface, turbulent mixing becomes insignificant for the transport of dissolved substances relative to molecular diffusion (Boudreau and Jørgensen 2001). The lowest part of the DBL is therefore characterised by linear concentration profiles.

As with the velocity boundary layer, the upper limit of the DBL is not well defined. Here, the concentrations of dissolved substances approach the free-stream concentration

asymptotically. Jørgensen and Revsbech (1985) introduced the effective DBL (Z_δ) as a practical definition of the DBL thickness. According to this definition, the upper DBL limit is found by extrapolating the gradient at the sediment surface to the free-stream concentration. Defined this way, the effective DBL is functionally equal to the actual DBL with respect to transport via molecular diffusion across the layer.

Although the thickness of the DBL in marine environments is only 0.2 – 1.2 mm (Jørgensen 2001), the DBL can play an important role for reactions for which the rate or spatial distribution is controlled by transport resistance (Boudreau and Guinasso 1982). Examples are dissolution or precipitation reactions such as the accretion of ferromanganese nodules (Boudreau 1988), or the rapid exchange of nutrients and gases between surface sediments and water column (Jørgensen and Revsbech 1985; Blackburn et al. 1994; Canfield and Teske 1996).

Oxygen plays a key role for the respiration of benthic microbial communities. As oxygen is relatively easy to measure, it has been the preferred model substance for diffusive boundary layer studies. Due to its low solubility in seawater and high rate of consumption, oxygen generally penetrates only a few mm into fine-grained coastal sediments (Revsbech et al. 1979; Cai and Sayles 1996). Therefore, the DBL can constitute a significant transport resistance for oxygen flux between water and these sediments. With microsensors, direct measurements of oxygen concentration gradients in the DBL are possible. The diffusive flux (J) through the DBL and across the sediment-water interface can be calculated using Fick's first law of diffusion:

$$J = - D \, dC/dz \qquad (1)$$

where D is the molecular diffusion coefficient and dC/dz the vertical concentration gradient. Such calculations of diffusive fluxes based on measured microprofiles of gases and ions are common in aquatic science e.g. (Jørgensen and Revsbech 1985; Rasmussen and Jørgensen 1992; Steinberger and Hondzo 1999; Boudreau 2001).

Our current conceptual understanding of the DBL, as well as the application of the simple Fick's first law of diffusion, treats the sediment-water interface as an infinite flat plane crossed by one-dimensional chemical gradients. However, sediment surfaces are sculptured into elaborate landscapes when viewed at the scale of the DBL (Paul et al. 1978; Swift et al. 1985; Briggs 1989; Gundersen and Jørgensen 1990; Jørgensen and Des Marais 1990; Wheatcroft 1994; Fenchel 1996; Ziebis et al. 1996a; Ziebis et al. 1996b), and this

surface topography also affects the structure of the DBL. For example, on the upstream side of obstacles the DBL is compressed, whereas on the lee side it is expanded. Surface structures with a characteristic dimension smaller than half the thickness of the DBL, however, are not reflected in the oxygen gradients within the DBL (Jørgensen and Des Marais 1990).

When compact topographical structures protrude through the viscous sublayer, they induce turbulence. Thereby the interaction between topography and flow influences the thickness of the DBL, not only locally but also far downstream of the structures themselves. (Boudreau and Guinasso 1982; Weissburg and Zimmer-Faust 1994). The hydrodynamic mechanisms that regulate the thickness of the DBL are, however, out of the scope of this study.

Due to surface topography, horizontal as well as vertical gradients are present in the DBL. In addition, the effective exchange-area is larger than the projected horizontal area suggesting that the microbial community can exchange solutes with the overlying water more effectively than predicted from one-dimensional models and measurements.

Two-dimensional O_2 distributions at the sediment-water interface have been presented from decaying detritus (Jørgensen and Revsbech 1983), mats of colourless sulphur bacteria (Fenchel and Bernard 1995; Jørgensen and Revsbech 1983) and biofilms (de Beer et al. 1994; de Beer and Stoodley 1995). Across this range of communities, with laminar to turbulent flows, isolines of oxygen concentration are smooth lines loosely following the relief of the sediment-water interface. Even a sediment relief elaborately structured by polychaete tubes (Jørgensen and Revsbech 1985) shows no large deviation from this picture. Electrode-independent methods with a resolution better than 30 μm show the same smoothed out isolines compared to the sediment surface (Glud et al. 1996). The reason for the smoothness is that, at the small scale, molecular diffusion levels out any heterogeneity in solute distribution that is not maintained by effective sinks and sources. It is the same diffusion effect that causes microprofiles to be smooth and continuous in one-dimensional representations. Irregular microprofiles are mostly caused by temporal variation or instrument noise. Isolines contain important information about diffusive fluxes. Since concentrations are constant along these lines, no net diffusion occurs along them and the direction of diffusive transport is at right angles to the isolines. The slope of an isoline touching the sediment surface at a specific point will, therefore, define the angle at which net diffusion across the sediment-water interface occurs at that point.

For most surfaces, the isolines clearly do not describe an infinite flat plane. To account for complex three-dimensional diffusion in biofilms, de Beer and Stoodley (1995) analysed horizontal gradients around vertical surfaces of cell clusters, as well as vertical gradients across horizontal surfaces. By estimating the coverage of the various surface-structures with a confocal scanning laser microscope, they calculated diffusive fluxes taking into account all spatial dimensions. Given that the DBL was kept thin (high flow velocity) relative to the biofilm landscape of ~300 μm diameter cell clusters and 100 μm wide voids, the total mass transport exceeded the calculated one-dimensional flux by 100-150%. During less extreme flows however, the topographic effect was almost completely smoothed out.

Jørgensen and Des Marais (1990) applied a different approach to calculate the flux across a mapped complex topography: By assuming that the path of diffusion was normal to the sediment surface and that the exchange-area was defined by the upper DBL limit, they calculated a correction-factor for the average vertical flux which accounted for both underestimated gradients and underestimated exchange-area. By using their so called double cosine correction on the oxygen flux across the sediment-water interface of a hypersaline microbial mat, they calculated that surface topography increased the flux by 49% relative to a one-dimensional diffusive flux calculated from the vertical oxygen microgradients.

The aim of the present study was to analyse the relation between surface roughness and three-dimensional diffusive fluxes through the DBL of marine sediments. For this purpose, a laser-based light striper method was developed for mapping surface topography with a horizontal resolution better than 100 μm. The relationship between diffusive flux and topography then was investigated by acquiring spatially structured microsensor data within the mapped topography. As an alternative to sampling a natural location, a sediment block was brought to the laboratory and allowed to develop a stable community. With respect to the relationship between diffusive flux and topography, the artificial community was considered representative for coastal sediments, where surface structures, solute fluxes and chemical zonations are governed by microbial metabolism, redox reactions, diffusion and bioturbation.

MATERIALS AND METHODS

Flume and Sediment.

The experimental work was conducted under unidirectional flow in a laboratory flume, 300 cm long, 30 cm wide and 25 cm high. Subtracting a total of 40 cm from the channel length for flow conditioning, the flume accommodates a 260 cm free-flow section. Undisturbed layers of silty surface sediment (60 cm long, 30 cm wide and 5 cm thick) were collected at low tide from an intertidal mudflat of the German Wadden Sea. These sediment blocks were placed with intact stratification in the flume, covering the entire length of the free-flow section. The flume was then filled with filtered North Sea water to produce a water depth of 10 cm above the sediment.

The developing flow along the free-flow section lead to different structure of the DBL in different parts of the flume. Most notably, O_2 profiles measured only a few cm downstream from the inflow show a much more abrupt transition from free-flow O_2 concentration to the linear gradient in the DBL than what is observed from *in situ* profiles (e.g. Gundersen and Jørgensen 1990). Also the temporal dynamics of the DBL within the flume change with the developing flow structure. Dependencies of concentration fluctuations on flow parameters have been described from other experimental systems (Gundersen and Jørgensen 1990; Jørgensen and Des Marais 1990; Guss 1998) but the mechanisms behind are poorly understood. With the flume dimensions and sediment roughness used in this study, an increasing instability of the DBL was observed with increasing distance from the water inlet. A similar effect was observed when the flow velocity was increased, which is in contrast to the observations of Gundersen and Jørgensen (1990). This discrepancy is most likely due to the larger size of the flow channel used in this study.

In order to maintain a stable sediment respiration, temperature was kept constant at 19°C and organic material was supplied to the sediment surface in the form of homogenised algae once every month. Accumulation of nutrients in the flume was prevented by occasionally exchanging the entire water volume of 91 L. Before the experiments were started, the sediment had been maintained in the laboratory for two years.

At the time of the experiments, the infauna was dominated by oligochaetes of the Tubificidae family, which did not produce visible burrows. The worms deposited black faecal material on the surface in small circular mounds. Within one hour the mounds collapsed, leaving slightly raised black spots of 1-2 mm diameter. After another 4-5 hours the spots gradually vanished, unless the worms supplied new material. Repeated defecation

at the same positions formed sediment mounds of up to 5 mm in diameter, similar in colour to the undisturbed surfaces. The abundance of oligochaetes was more than 5000 per m^2 and, consequently, their mounds were dominating features on the sediment surface.

Another conspicuous feature were faecal mounds produced by the polychaete *Heteromastus filiformis*. These mounds were 5 to 10 mm high and occurred at a density of 110 m^{-2}. These mounds were cone shaped and consisted of ~ 0.5 mm long, uniformly egg-shaped pellets.

The macrofauna included a few juvenile individuals of the common shrimp, *Crangon crangon*. The life expectancy of these crustaceans was 6 to 12 months, and they were the only animals in the flume restocked. The physical activity of the shrimps had a strong influence on the surface structure, as the sediment surface without physical disturbance would completely turn into overlapping faecal mounds. Inspection of the sediment with a dissection microscope revealed that the surface microstructure consisted entirely of faecal material in different stages of disintegration. The sub-surface sediment, however, did not appear to be formed by discrete pellets.

Median grain size of the sediment was 6.3μm. Porosity, as determined by drying samples at 60 °C until constant weight, was 77 % in the upper 15 mm (s.e. 2.5, n=5). Permeability in the top 18 mm was 1.52×10^{-13} m^2 (s.e. 2.85×10^{-14} m^2, n=3), measured with a constant head of 500 Pa (Klute and Dirksen 1986). The organic carbon content was 2.9 % dry weight (s.e. 0.2, n=10), determined with a CNS analyser.

Topographic mapping.

For optical measurements of topography, a laser line was projected vertically down on the sediment surface from a diode laser (Lasiris LAS-670-5 laser with LAS-1 Line-20° TS line generator). A glass plate suspended in the air-water interface assured that refraction was constant and well defined (Fig 1). The cross-section of the 0.2 mm wide laser line had a gaussian intensity distribution. Along the central 55 mm of the line used for measurements, light intensity and line width varied insignificantly. An image of the projected laser line was recorded by a digital camera (1280 x 1024 pixel PCO SensiCam with a 35 mm objective). The camera was pointed at the laser line at an angle of 45°. Due to refraction in the air-glass-water interface, the resulting angle between the camera axis and vertical was approximately 30°.

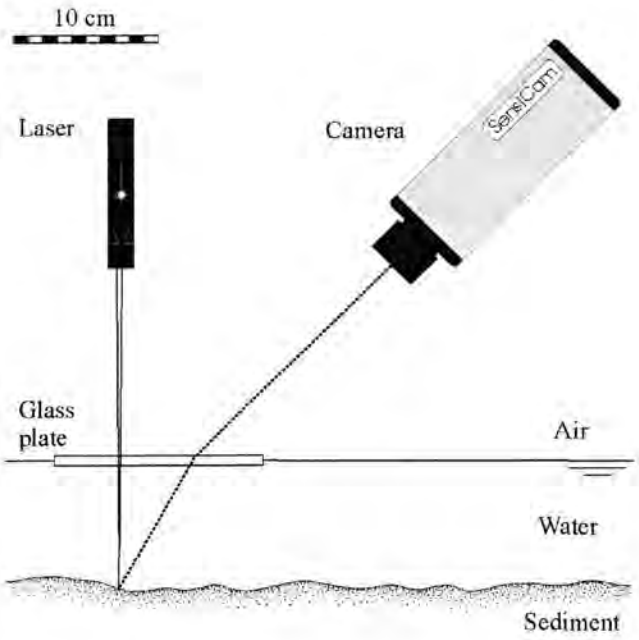

Figure 1. Set-up used to measure sediment topography. The digital camera, the laser and the glass plate were combined in one rigid mechanical unit.

For each vertical column of pixels in the digital image, the position of the laser line was determined. Sub-pixel accuracy was achieved by the use of a three point estimator and the known gaussian intensity distribution across the line (Raffel et al. 1998). In this way, the image was transformed to an array of surface elevations, expressed in pixel co-ordinates (Fig 2A).

To calculate the scale between the pixel co-ordinates and real distances (Fig. 2B), a 1 mm line grid was imaged in the plane of the laser sheet. Separate vertical scales for each pixel column were found by linear regression on the known calibration points. Given a distance of 300 mm between camera and the 60 mm wide projected laser line, the perspective distortion induced by the central projection of the imaging system was insignificant. Therefore, the vertical scale did not vary measurably within the images, and the linear regressions consistently gave r^2 values better than 99.9%. The mean scale of all 1280 pixel columns was used to transform the vertical pixel scale into millimetres.

Likewise, the horizontal scale was determined for each horizontal row of pixels in the image. Due to the 60 degrees tilt of the image plane of the camera relative to the laser beam, the horizontal scale was a function of the vertical position in the image. Therefore, the scaling factor from the pixel row best representing the average position of the laser line was used for horizontal calibration. Within the band of pixel rows ever containing the sediment surface, the difference in scale between the highest elevations and the deepest depressions was less than 1.4 %.

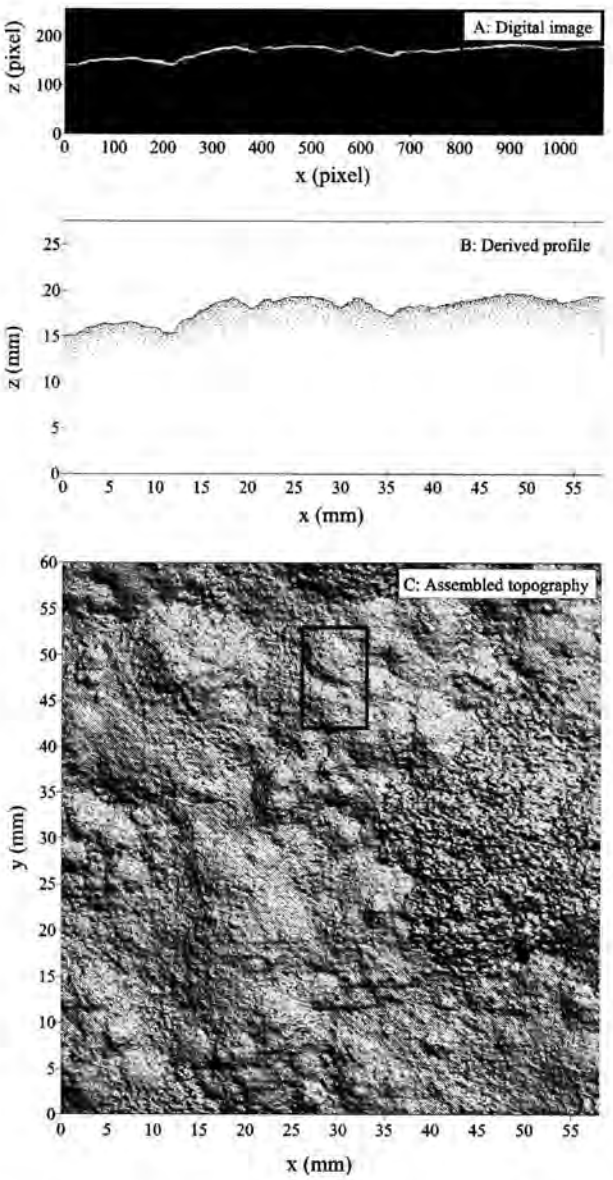

Figure 2. (A) Digital image of the intersection between a laser sheet and the sediment surface, generated with the set-up shown in Fig 1. (B) The topographic profile derived from (A) consisting of 1088 data points, one for each pixel column in the digital image. (C) Topography of a 60 x 55 mm sediment surface area depicted as a computer generated shaded relief. The data were assembled from the topographic profile shown in (B), together with another 600 similar profiles. The direction of scanning was from left to right. A more detailed map of the framed area can be seen in Fig. 6.

To extend the data to three dimensions, the laser-camera assembly was moved horizontally in 100 µm steps perpendicular to the laser line. Assembling data from 601 images, the sediment area covered in each mapping procedure was 55 x 60 mm (Fig. 2C). The horizontal resolution was 100 µm in the direction of translation and approximately 50 µm along the laser line. As data points were evenly distributed along both horizontal axes, the data could be written into the matrix format of the software package Surfer 6 (Golden Inc.) without transformation.

In general, more than 99% of the measured points had an elevation within 100 µm of the average elevation of their immediate neighbours. However, due to occasional oligochaete worms or plant fibres protruding from the sediment, ~1 % were often found as isolated points several mm up into the water column. Such outlying points, that were not part of the sediment-surface, were removed from the dataset and a new point was interpolated.

On topographic slopes steeper than 60° and facing away from the camera, the sediment would obstruct the camera's view of the laser line. The mapping algorithm finds the position of the laser line based on the position of the maximum light intensity within each column of pixels. It will, therefore, propose a position even when the laser line is not visible to the camera. In these cases the maximum intensity found is low compared to what is found when the laser line is visible and it is easily identified as invalid. Such steep surface elements were rare and covered << 1% of the surfaces measured.

Image recording and motion-control, as well as data extraction and processing, were performed by routines written in Labview with IMAQ vision extension (National Instruments). The routines for data extraction are available as MS Windows executable files from the first author.

Microsensor analysis.

In order to assess spatial oxygen variability, temporal concentration variation had to be minimised. As a compromise between downstream flow-development and DBL stability, the microelectrode data presented were recorded at the flume centreline 50 cm downstream from the leading edge of the sediment block. The O_2 sensors used were Clarke type microelectrodes with internal reference and guard cathode (Revsbech 1989). Tip diameters were 15 µm, stirring sensitivity less than 1 % and response time about 1 s. The electrodes were calibrated between the O_2 concentration in the mixed water column determined by Winkler titration, and anoxic sediment, assuming a linear current response. The electrode

signal was recorded on an IBM compatible PC using a LAB-PC 1200 AI analog-to-digital converter (National Instruments). The microsensors were positioned using a computer-controlled motorised translation-table (Physik Instrumente M-150.20) for each of the 3 axes. By recording evenly spaced vertical microprofiles, two-dimensional grids of O_2 distributions were acquired. Horizontal and vertical resolutions were 100 µm.

Optical fibres with light-scattering titanium dioxide coated tips were introduced through silicone-rubber ports built into the flume bottom. When placed exactly at the sediment surface and illuminated from below, the tips provided luminescent fix-points that were used to align microsensor and laser scanning measurements horizontally. Vertical alignment between oxygen microprofiles and topographic maps were based on the change in oxygen gradient at the sediment water interface (Rasmussen and Jørgensen 1992). The use of aligned profiles assured ample numbers of profiles with sufficiently distinct changes in gradients to make an accurate determination with this technique.

RESULTS

Flow structure.

Fig. 3 shows the vertical velocity-profile in the region of the flume where microsensors were deployed. Shear velocity (u_*), determined from the velocity gradient in the linear part of the profile, was 0.09 cm s^{-1}. Assuming the free-stream velocity above the logarithmic layer to be approximately 20 u_* (Denny 1993), the corresponding free-stream velocity would be 1.8 cm s^{-1}. This flow velocity is in the low range for coastal marine environments. But a well-developed transition between DBL and turbulent mixed water column showed that the conditions were still far from stagnant (Fig. 4B). Shape and gradient of our microprofiles compared well with those measured in similar sediments in the field (e.g. Gundersen and Jørgensen 1990). According to our experience, a shorter free-flow distance would have produced a more stable DBL resulting in smoother isolines, but would have compromised the desire for a realistic microprofile shape.

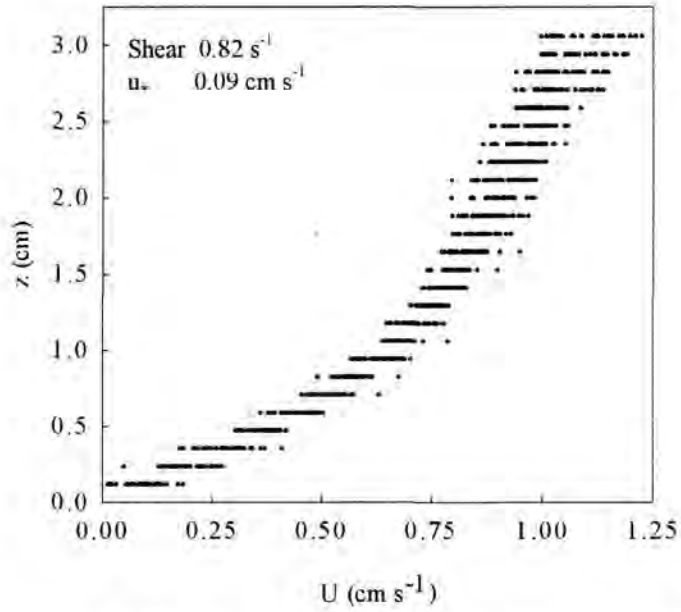

Figure 3. Vertical flow velocity profile above the sediment surface measured with digital particle image velocimetry (PIV). The points are single measurements. The position of the sediment surface was determined from the images used for the PIV. The shear is found by linear regression of the lowest 10 mm of the profile. Shear stress (τ_b) is calculated as shear multiplied with dynamic viscosity (v) at the appropriate temperature and salinity. Shear velocity (u_*) is calculated according to the equation $u_* = (\tau_b/\text{density})^{1/2}$. For a description of PIV, see Raffel et al. (1998).

Topography and microsensor measurements.

Selected areas of sediment surface were mapped twice with the described line striping method (Fig. 2C). Between the scannings, transects of vertical O_2 distribution through the sediment-water interface was recorded within the mapped areas (Fig. 4A). The 3 to 5 mm long oxygen transects were placed so that the macroscopic topography was symmetrical around the transect. The oxygen gradient perpendicular to the plane could therefore be assumed to be minimal. Due to the long measuring procedure of several hours per transect, the dense population of oligochaetes would occasionally modify the topography within the areas where O_2 microprofiles were being recorded. In such instances, the topographic data as well as the [O_2] transect were discarded. Flat areas not recently disturbed by macrofauna had a uniform O_2 penetration of about 2.9 mm while the disturbed areas displayed considerable variation.

Single-point three-dimensional flux calculations.

From the two-dimensional O_2 data, isolated vertical microprofiles can be extracted (Fig. 4B). The gradient (dC/dz), describing the vertical diffusive flux (J_z) down to the sediment surface, can be found by linear regression of the data in the lowest 300 μm of the DBL. Similarly, the horizontal gradient at the same point of the surface can be found by selecting O_2 data from the same depth of neighbouring profiles. Analogous to the vertical flux, the horizontal flux (J_x) is calculated based on the gradient from the horizontal row of points stretching from the sediment surface into the water column (Fig. 4C).

To calculate the magnitude and direction of the resulting diffusive flux, we consider J_x and J_z as vectors (Fig. 4D). If there is no horizontal gradient perpendicular to the measured vertical plane, the measured vertical and horizontal flux vectors can be used to calculate the resultant vector, J_n. The magnitude of J_n and the angle (α) between J_n and vertical are found by simple trigonometry:

$$J_n = (J_x^2 + J_z^2)^{1/2} \tag{2}$$

$$\cos \alpha = J_z / J_n \tag{3}$$

Rearranging Equation 3, we get an expression for J_n as function of the angle (α) and the vertical flux:

$$J_n = J_z \times 1/\cos \alpha \tag{4}$$

A flux is defined as the transport per unit area and time. The exchange-area (A') should be measured perpendicular to the direction of diffusion (Fig. 4D). Similar to the relation between J_n and J_z, the relation between A' and the projected horizontal area (A) can be described by the angle (α) between horizontal and A':

$$A'/A = 1/\cos \alpha \tag{5}$$

The plane defined by A' in Fig. 4D is perpendicular to J_n. The concentration gradient along this plane is therefore zero, i.e. this is locally an isoline of constant concentration.

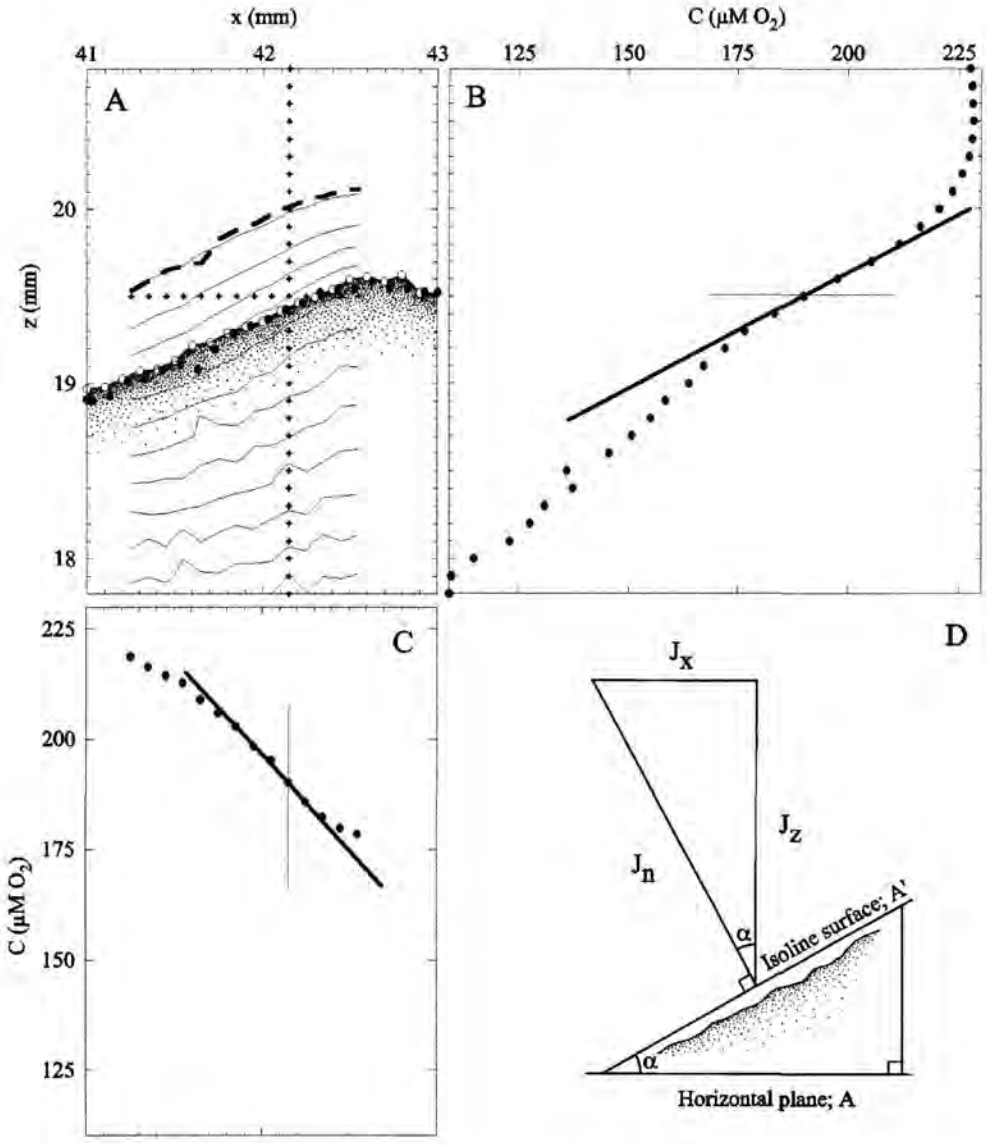

Figure.4 (A) Vertical section of the sediment water-interface. The circles indicate points determined on the sediment surface by two successive scanning procedures. Filled circles are from the first pass, while open circles are from the second. In the vertical plane, the O_2 concentration was measured with 100 by 100 µm grid spacing. Isolines of equal O_2 concentration are shown as thin black lines, while the upper limit of the effective DBL (Jørgensen and Revsbech, 1985) is drawn as a thicker dashed line. The vertical column of crosses indicates the position where the O_2 profile shown in panel (B) was recorded. Likewise, the horizontal row of crosses indicates where the profile shown in panel (C) was recorded. (B) Vertical O_2 microprofile extracted from the two-dimensional distribution in (A). The vertical flux (Jz) can be calculated from the slope of the profile (thick line) above the sediment surface. (C) Horizontal O_2 microprofile extracted from the two-dimensional O_2 distribution in panel (A). Analogous to the vertical flux, the horizontal flux (J_x) can be calculated from the slope of the profile (thick line) leading from the water column towards the sediment surface. (D) Geometric representation of the two-dimensional flux calculation (see text for details).

Accordingly, the local magnitude of $1/\cos \alpha$ can be calculated from the area of the isoplanes, where these intersect the sediment surface, and the projected horizontal area underneath them.

Fig. 4D shows that the α used for exchange-area calculation and α used to calculate J_n from J_z are identical. The parameter $1/\cos \alpha$ is the relation between total exchange-area and projected horizontal area as well as the ratio J_n/J_z. It is generally convenient to express a measured flux between water column and sediment based on the projected horizontal area rather than based on the actual exchange-area. Following the nomenclature of Jørgensen and des Marais (1990), we will call this flux J'. Combining Equation 4 and 5, a relation between J', J_z and α can be written:

$$J' = J_z \times (1/\cos \alpha)^2 \quad (6)$$

Area-based three-dimensional flux calculations

When dealing with areas rather than single points, the relationship between A' and A will be more readily available than the distribution of α. As we will focus on the difference between J' and J, we rearrange Equation 6 and base it on A'/A to get the expression:

$$J'/J_z = (A'/A)^2 \quad (7)$$

To apply Equation 7 directly, we would have to map an isoplane over extensive areas. For bioturbated sediments, the required area coverage is not possible via conventional single point microsensor measurements. Alternatively, equivalent information can be found from high-resolution topographic data. As seen in Fig. 5, the O_2 isolines do not follow the smallest details of the sediment topography. They rather resemble a smoothed sediment surface, lacking features that are much smaller than the thickness of the DBL. The same smoothing effect can be imposed mathematically on the measured sediment topography by replacing each measured height with the average of all heights within a distance corresponding to the thickness of the effective DBL (Z_δ). By smoothing that way, a virtual sediment surface that is nearly parallel to the isolines can be obtained (Fig.s 5 & 6). By using A'/A from these approximated isolines, the ratio between vertical and horizontal fluxes can be calculated for the entire topographical map.

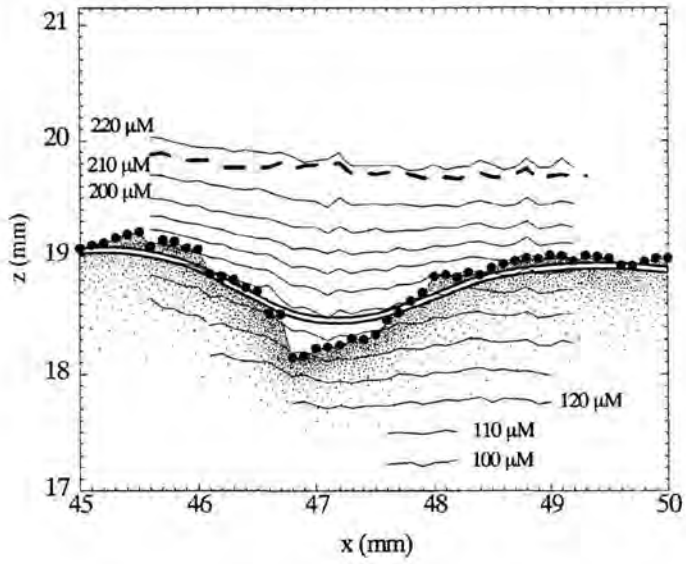

Figur 5. O_2 distribution at sediment surface topography. The O_2 isolines are represented by thin lines, while the upper limit of the effective DBL (Jørgensen and Revsbech, 1985) is drawn as a thicker dashed line. Filled circles are points determined as the sediment surface by optical line striping. By smoothing the sediment surface with a matrix with the same size as the thickness of the DBL (1.4 mm), a surface that is nearly parallel to the isolines is generated (double line). Not every profile has been extended to the full oxygen penetration depth. The areas where isolines are seen represent the areas where data are present in full resolution.

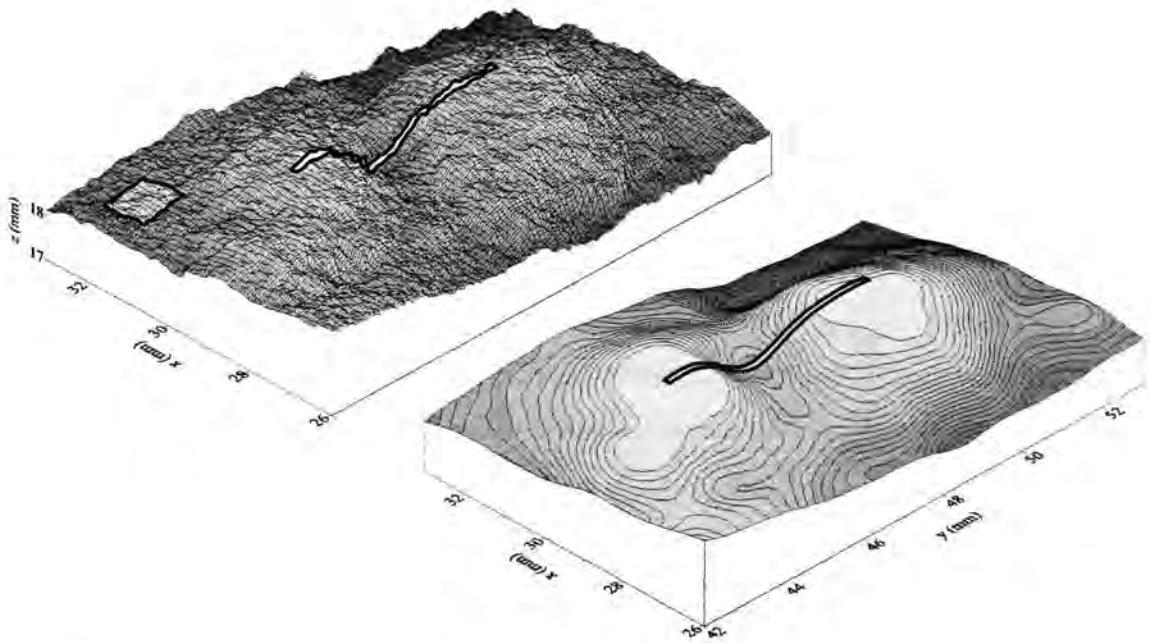

Figure 6. Small section of a topographic map before and after data smoothing. The square insert in the non-smoothed surface indicates the size of the smoothing-matrix. The smooth surface mimics the distribution of an arbitrary O_2 isoline, and can be used to calculate A'/A and thereby J'/J_z (see text for details). The cut-out was taken from the map shown in Fig 3C. The double-line marks the position where the transect shown in Fig. 5 was recorded.

By varying the size of the smoothing-kernel, different thicknesses of DBL's can be simulated independent of the actual DBL thickness during measurements. In addition to the scannings made in connection with the O_2 measurements, 5 random areas along the centreline of the flume were mapped. For each map, J'/J_z was estimated from topography based on a range of smoothing-kernel sizes (Fig. 7). The interpolated line of J'/J_z plotted against the applied smoothing-kernel size, shows the dependency of J'/J_z on DBL thickness and will be characteristic for a given sediment (Fig. 7). From the vertical axis of Fig. 7, we can now read the factor J'/J_z, for a range of DBL thicknesses. This factor must be multiplied to a flux calculated from a vertical micro profile to get the total diffusive flux (J').

Vertical DBL thicknesses in the flume, measured from above, ranged between 0.4 and 1.4 mm with an estimated average of 0.6 mm. When a 0.6 mm smoothing-kernel is used for the estimation of J'/J_z, a 10% difference is found between one-dimensional vertical flux calculation and the calculation taking topography into account ($J'/J_z = 1.1$ in Fig. 7).

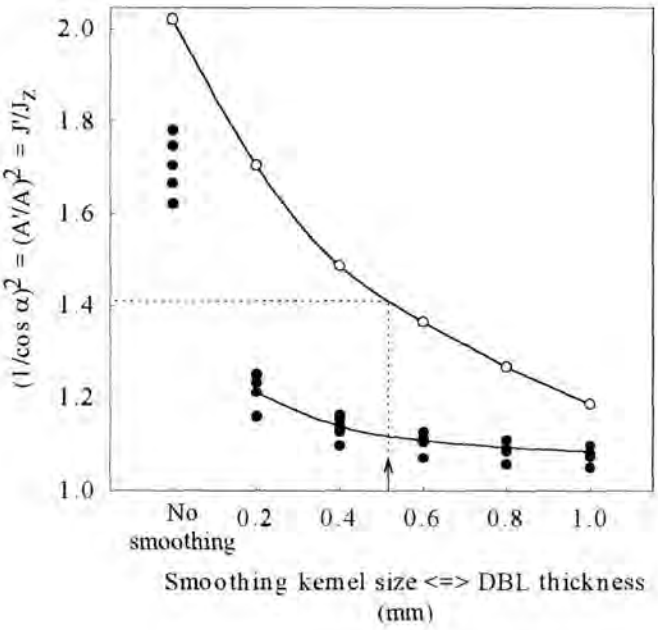

Figure 7. Estimated ratio between total three-dimensional diffusive O_2 flux and one-dimensional vertical diffusive O_2 flux, calculated from topography with different degrees of smoothing. Filled circles originate from this study. Open circles are derived by smoothing the 3.4 x 3.8 mm of microbial mat surface mapped by Jørgensen and Des Marais (1990). The dotted line relates the mean Z_δ of 0.52 mm that was measured by Jørgensen and Des Marais (1990) to a correction factor slightly above 1.4. The estimates based on no smoothing correspond to isolines that strictly follow the measured topography.

The DBL thicknesses quoted here were, however, measured from above and thereby underestimated due to compression of the DBL during measurement (Glud et al 1994). Lorenzen et al. (1995) described the effect of the DBL compression as equivalent to an increase in flow velocity. Accordingly, the thinning of the DBL should cause the O_2 isolines to follow the sediment surface more closely than in the absence of the sensor (Jørgensen and Des Marais 1990; Gundersen and Jørgensen 1990; de Beer et al. 1996). A topography smoothing matrix that successfully reproduces isolines measured from above will, therefore, leave topographic features that would be smoothed out by the thicker DBL when the sensor is not present and A'/A will be overestimated. The 10% difference between J_z and J' calculated from a 0.6 mm matrix is thereby a maximum estimate.

DISCUSSION

Jørgensen and Des Marais revisited.

In order to compare our method and results to that of Jørgensen and Des Marais (1990), we recalculated their raw data. As these authors acquired both oxygen isolines and topography, a comparison between cosine correction based on smoothed topography and cosine correction based directly on isolines can be made: By smoothing the topographic data with a range of kernel sizes, estimates of J'/J_z for different thicknesses of DBLs were calculated. Fig 7 shows that such a calculation would relate the mean Z_δ of 0.52 mm that was measured by these authors to a correction factor slightly above 1.4. Jørgensen and Des Marais (1990) defined the upper DBL limit as the 90% O_2 saturation isoplane, and reported A'/A for this isoplane to be 1.14. Following Equation 7, J'/J_z based on the isoplane alone is 1.3.

Although O_2 isolines are mostly parallel down through the DBL, they are somewhat smoother in the upper part of the DBL than at the sediment water interface. The J'/J_z of 1.30 calculated based on the 90 % isoplane should, therefore, be considered a minimum estimate. On the contrary, the J'/J_z of 1.49 reported in the original manuscript may be considered as a overestimation as their assumption that the flux is normal to the sediment topography, is incompatible with the discrepancy between sediment surface and isoline topography. Apart from the fact that the correction method based on smoothed topography gives a value between minimum and maximum estimate, one should note that topographic data are not included in the correction calculated to be 1.3, and chemical data are not included in the calculation of the factor 1.4.

The different dependencies of J'/J_z on DBL thickness between the data from the current study, and the data from Jørgensen and Des Marais (1990), are linked to differences

in surface morphology. The surface of the microbial mat was structured by tufts and clusters of cyanobacteria and diatoms, with dimensions of the same scale as the DBL. The degree of smoothing imposed by the DBL is therefore critical. In the case of the bioturbated sediment, the surface roughness was dominated by structures that were either below or above the range of potential DBL thicknesses. The DBL thickness, and thereby flow velocity, was in the latter case much less critical for the influence of topography on the ratio J'/J_z.

A similarly direct comparison to method and results of de Beer and Stoodley (1995) is not possible, as topographical maps were not acquired. However, these authors also observed that the effect of 100 -300 μm scale topography was dependent on the DBL thickness: With a <50 μm thick DBL the isolines and DBL would follow the complex surface structure and a large topographic effect could be observed, whereas a 100-200 μm thick DBL excluded topographic effects. A similar result would have been produced from a smoothed topography approach, because a smoothing-kernel of 50μm square would change the depicted topography only slightly, while a 150 μm kernel would effectively fill in the 100 μm voids.

Applicability of the method.

Fig 4D and Equation 7 show that the shape of the isolines in the DBL determines exchange-area as well as the direction of net diffusion. It would therefore be obvious to base calculations of horizontal influence directly on chemical measurements rather than estimating from sediment topography as proposed in this paper. Heterogeneity in oxygen uptake of sediments should cause the oxygen isolines to cross even a perfectly flat surface at angles that are not predictable from the topography. Yet, the appearance of all previously published isoline data indicate that mathematically smoothed topography data will in most cases generate a virtual sediment surface that is nearly parallel to the isolines. The feasibility is further supported by the good agreement between the independent calculations based on topography and on isolines for the data from of Jørgensen and Des Marais (1990).

If strong local hotspots of flux have a scale comparable to that of the DBL, such heterogeneity will bend the isolines sufficiently to cause significant horizontal gradients in the DBL in addition to gradients caused by surface topography. As the relation between α and J'/J_z is not linear, the combination of topography and flux hotspots may produce effects even larger than expected from independent measurements of both phenomena. The method presented here should, therefore, be used with caution in environments where extreme heterogeneity can be expected. Examples are bioturbated, photosynthetically active,

communities, where reduced sediment can be exposed on the sediment surface in direct contact with diatoms and cyanobacteria performing oxygenic photosynthesis (Fenchel 1996).

Applications of the $(1/\cos \alpha)^2$ parameter.

Sediment and DBL topography cause one-dimensional measurements to underestimate the diffusive flux. Still, one-dimensional microprofile measurements are widely used for investigations of sediment communities. From topography-derived $(1/\cos \alpha)^2$, we are able to estimate the topography-related error caused by the one-dimensional assumption. Furthermore, $(1/\cos \alpha)^2$ provides an index of the smoothness of a sediment with respect to diffusive solute exchange across the DBL. A value of one signifies a sediment that is perfectly flat with respect to diffusive flux, while higher values indicate the influence of topography. The index is independent of the spatial resolution of the topographic data due to the well-defined smoothing procedure involved, given that the resolution is high enough to resolve features of a size similar to the thickness of the DBL.

The sediment studied had been maintained in the laboratory for two years, and only few parameters were thereby representative for the original sampling site. But with respect to microbial respiration and biogenic sculpturing, the system was comparable to typical fine-grained coastal sediments. The following general conclusions about constraints on the magnitude of J'/J_z are therefore valid, even though the exact values should not be extrapolated to any given marine location.

As seen in Fig 2, the sediment surface was far from being a flat plate, and the moderate effects of topography on the flux may appear surprising. By examining the constraints on $1/\cos \alpha$, however, one realises that even distinct topography does not necessarily create a large topographical influence on the diffusive flux: The relation between the slope of the isolines and J'/J_z is not linear. This can be realised directly from Equation 2. As the two partial fluxes are squared before adding, the larger one will dominate the result if the difference is large. For instance, in the example in Fig 4, the ratio J_n/J_z is only 1.14, even though the J_x is more than 50 % of J_z. The faecal mounds, that shaped the topography formed small islands where local horizontal fluxes were significant, superimposed on a much larger background of flat surface for which J'/J_z was practically one. Even if the faecal mounds had been spaced more closely, the correction would still have been negligible on the tops and in the bottom of the valleys. Additionally, the DBL smoothes the topographic structures such that peaks are flattened and depressions filled in.

Only steep features of a size easily visible induce significant topographic effects in the DBL. In conclusion, even though a sediment surface is structured into elaborate landscapes, diffusion through the DBL may still be sufficiently well modelled based on one-dimensional microprofiles and a flat plate assumption.

ACKNOWLEDGEMENT

We thank Gabriele Eickert and Anja Eggers for construction of the microsensors, and Volker Meyer for assistance with the electronics. Ronnie Glud and Dirk de Beer supplied examples of two-dimensional O2 distributions for inspiration and mathematical method development before data were available from our own efforts. Many ideas presented in this paper originate from work co-supervised by Niels Peter Revsbech, who is thanked for his continued interest and support. Careful reviews from Dr. Lauren Mullineaux and two anonymous reviewers were much appreciated. The project was supported by the Max Planck Society, and Hans Røy was supported by a stipend from the Danish Research Agency.

REFERENCES

Blackburn, T. H., N. D. Blackburn, K. Jensen and N. Risgaard-Petersen. 1994. Simulation-model of the coupling between nitrification and denitrification in a fresh-water sediment. Appl. Environ. Microbiol. 60: 3089-3095.

Boudreau, B. P. and N. L. Guinasso. 1982. The influence of a diffusive sublayer on accretion, dissolution, and diagenesis at the sea floor, p. 115-145. In K. A. Fanning and F. T. Manheim [eds.], The dynamic environment at the ocean floor. Lexington.

Boudreau, B. P. 1988. Mass-transport constraints on the growth of discoidal ferromanganese nodules. Am. J. Sci. 288: 777-797.

Boudreau, B. P. and B. B. Jørgensen. 2001. The Benthic Boundary Layer: Transport processes and biogeochemistry. Oxford University Press.

Boudreau, B. P. 2001. Solute transport above the sediment-water interface, pp 104-126. In B. P. Boudreau and B. B. Jørgensen (eds.), The Benthic Boundary Layer: Transport Processes and Biogeochemistry. Oxford University Press.

Briggs, K. B. 1989. Microtopographical roughness of shallow-water continental shelves. IEEE J. Oceanic Eng. 14: 360-367.

Cai, W. J. and F. L. Sayles. 1996. Oxygen penetration depths and fluxes in marine sediments. Mar. Chem. 52: 123-131.

Canfield, D. E. and A. Teske. 1996. Late proterozoic rise in atmospheric oxygen concentration inferred from phylogenetic and sulphur-isotope studies. Nature. 382: 127-132.

De Beer, D., P. Stoodley, F. Roe and Z. Lewandowski. 1994. Effects of biofilm structure on oxygen distribution and mass transport. Biotechnol. Bioeng. 43: 1131-1138.

De Beer, D. and P. Stoodley. 1995. Relation between the structure of an aerobic biofilm and transport phenomena. Water Sci. Technol. 32: 11-18.

De Beer, D., P. Stoodley and Z. Lewandowski. 1996. Liquid flow and mass transport in heterogeneous biofilms. Water Res. 30: 2761-2765.

Denny, M. W. 1993. Air and water. Princeton University Press.

Fenchel, T. and C. Bernard. 1995. Mats of colourless sulphur bacteria. I. Major microbial processes. Mar. Ecol. Prog. Ser. 128: 161-170.

Fenchel, T. 1996. Worm burrows and oxic microniches in marine sediments. I. Spatial and temporal scales. Mar. Biol. 127: 289-295.

Glud, R. N., J. K. Gundersen, N. P. Revsbech and B. B. Jørgensen. 1994. Effects on the benthic diffusive boundary layer imposed by microelectrodes. Limnol. Oceanogr. 39: 462-467.

Glud, R. N., N. B. Ramsing, J. K. Gundersen and I. Klimant. 1996. Planar optrodes - a new tool for fine scale measurements of two-dimensional O_2 distribution in benthic communities. Mar. Ecol. Prog. Ser. 140: 217-226.

Glud, R. N., C. M. Santegoeds, D. de Beer, O. Kohls and N. B. Ramsing. 1998. Oxygen dynamics at the base of a biofilm studied with planar optodes. Aquat. Microb. Ecol. 14: 223-233.

Gundersen, J. K. and B. B. Jørgensen. 1990. Microstructure of diffusive boundary layers and the oxygen uptake of the sea floor. Nature. 345: 604-607.

Güss, S. 1998. Oxygen uptake at the sediment-water interface simultaneously measured using a flux chamber method and microelectrodes - Must a diffusive boundary layer exist ? Estuar. Coast. Shelf Sci. 46: 143-156.

Jørgensen, B. B. 2001. Life in the diffusive boundary layer, p. 348-373. In B. P. Boudreau and B. B. Jørgenesen [eds.], The benthic boundary layer: Transport processes and biogeochemistry. Oxford University Press.

Jørgensen, B. B. and D. J. Des Marais. 1990. The diffusive boundary layer of sediments: Oxygen microgradients over a microbial mat. Limnol. Oceanogr. 35: 1343-1355.

Jørgensen, B. B. and N. P. Revsbech. 1985. Diffusive boundary layers and the oxygen uptake of sediments and detritus. Limnol. Oceanogr. 30: 111-122.

Jørgensen, B. B. and N. P. Revsbech. 1983. Colorless sulfur bacteria, Beggiatoa spp and Thiovulum spp in O_2 and H_2S microgradients. Appl. Environ. Microbiol. 45: 1261-1270.

Klute, A. and C. Dirksen. 1986. Hydraulic conductivity and diffusivity: laboratory methods, p. 687-734. In A. Klute [ed.], Methods of soil analysis - part 1 - physical and mineralogical methods. American Society of Agronomy.

Lorenzen, J., R. N. Glud and N. P. Revsbech. 1995. Impact of microsensor-caused changes in diffusive boundary layer thickness on O_2 profiles and photosynthetic rates in benthic communities of microorganisms. Mar. Ecol. Prog. Ser. 19: 237-241.

Paul, A. Z., E. M. Thorndike, L. G. Sullivan, B. C. Heezen and R. D. Gerard. 1978. Observations of the deep-sea floor from 202 days of time-lapse photography. Nature 272: 812-814.

Raffel, M., C. Willert and J. Kompenhans. 1998. Particle image velocimetry. Springer.

Rasmussen, H. and B. B. Jørgensen. 1992. Microelectrode studies of seasonal oxygen uptake in a coastal sediment: role of molecular diffusion. Mar. Ecol. Prog. Ser. 81: 289-303.

Revsbech, N. P., B. B. Jørgensen and T. H. Blackburn. 1979. Oxygen in the sea bottom measured with a microelectrode. Science 207: 1355-1356.

Revsbech, N. P. 1989. An oxygen microsensor with a guard cathode. Limnol. Oceanogr. 34: 472-276.

Steinberger, N. and M. Hondzo. 1999. Diffusional mass transfer at sediment-water interface. J. Environ. Eng.-ASCE. 125: 192-200.

Swift, S. A., C. D. Hollister and R. S. Chandler. 1985. Close-up stereo photographs of abyssal bedforms on the Nova Scotian continental rise. Mar. Geology. 66: 303-322.

Weissburg, M. J. and R. K. Zimmer-Faust. 1994. Odor plumes and how blue crabs use them in finding prey. J. Exp. Biol. 197: 349-375.

Wheatcroft, R. A. 1994. Temporal variation in bed configuration and one-dimensional bottom roughness at the mid-shelf stress site. Cont. Shelf Res. 14: 1167-1190.

Ziebis, W., S. Forster, M. Huettel and B. B. Jørgensen. 1996a. Complex burrows of the mud shrimp Callianassa truncata and their geochemical impact in the sea-bed. Nature. 382: 619-622.

Ziebis, W., M. Huettel and S. Forster. 1996b. Impact of biogenic sediment topography on oxygen fluxes in permeable seabeds. Mar. Ecol. Prog. Ser. 140: 227-237.

The influence of topography on the functional exchange-surface of soft sediments, assessed from *in situ* measured sediment topography

Hans Røy, Markus Hüttel and Bo Barker Jørgensen

ABSTRACT

The influence of small-scale topography on the exchange surface between sediment and water was investigated in two coastal marine sediments. One site was a fine near-shore sand at Giglio Island, Italy. This sediment was rich in organic material, had a very active fauna, and a rich surface topography. The other site was a typical estuarine mud in Aarhus Bay, Denmark. The topography at both sites was measured *in situ*, with a horizontal resolution of about 0.1 mm. The topographic data were used to calculate the area of the three-dimensional exchange surface, which was 12% larger than the projected base area in the near-shore sand and 7% larger in the muddy sediment. In addition to the enlarging of the surface area, topography also caused horizontal gradients that were not included in the vertical O_2 flux calculated from the concentration gradient in the diffusive boundary layer. To account for both effects, fluxes calculated from the gradient in the DBL should be corrected by a factor 1.14 for the estuarine mud, and 1.25 for the near-shore sand. Due to longer diffusive distance, topography had a smaller impact on the area of the oxic-anoxic interface than on the exchange surface between sediment and water. For the near-shore sand the oxic-anoxic interface was a factor 1.06 larger than the projected horizontal area and for the estuarine mud, the enlargement was by a factor 1.03. By considering the constraints on exchange surface enlargement, and by comparing with previous studies, we argue that the range of topographic influence is representative for most marine sediments.

INTRODUCTION

Although electron acceptors in marine sediments are utilised according to an ordered sequence with depth, it is recognised that the seabed is a complex and heterogeneous environment (e.g. Fenchel 1996). A large part of the heterogeneity in the top 10 cm of the sediment is derived from the pool of iron and reduced sulfur in the solid phase (Thamdrup et al. 1994). Transport of these minerals within the sediment is mainly by particle transport due to various activities of the benthic fauna, collectively referred to as bioturbation. Though the effect of bioturbation can sometimes be described as a diffusive process (Thamdrup et al. 1994), the mechanism is through the discrete movement of sediment packages by discrete animals. As the turnover time of iron oxides and iron-sulfides is relatively long, disruptions of the sediment lamination can persist over a long time. Without spatial or temporal averaging, the solid phase is therefore better described as a mosaic of hotspots (Harper et al. 1999) or as a geometric analogue to a generalised burrow structure (Aller 1980), than by an ordered lamination.

In contrast to iron oxides and iron-sulfides, the turnover time of O_2 in coastal sediments is less than one hour. The O_2 diffusion through the sediment-water interface is therefore generally in steady state with the momentary O_2 consumption in the thin oxic surface layer. Processes in this oxic zone, and on its boundaries, therefore occur in a laminated structure that coats the sediment.

In addition to the O_2 diffusing through the sediment surface, a large amount of O_2 is transported into coastal sediments by the benthic fauna. To separate these processes from the diffusive processes in focus, it is necessary to distinguish between fauna-mediated oxygen consumption (FOU) and diffusive oxygen uptake (DOU). The FOU comprises all O_2 consumption that is directly associated with the activities of the benthic macrofauna. This includes the respiratory oxygen consumption of the animals themselves, the oxygen uptake of burrow walls with associated flora and fauna, as well as the oxygen consumed by oxidation of reduced solutes released from the burrows. Pooling of these very different oxygen-consuming processes is done due to practical considerations, as it is often impossible to separate one process experimentally without changing others irreversibly. According to Jahnke (2001), FOU is generally insignificant in areas with fluxes below 2.73 mmol m^2 day^{-1}. This is primarily the deep sea floor. In coastal and estuarine areas where the fluxes are an order of magnitude higher, FOU typically contributes ~50% of TOU.

The DOU, which is in focus here, is the flux of oxygen diffusing across the sediment surface. In fine grained sediments, this oxygen flux must pass the diffusive boundary layer

(DBL), a 0.2 – 1.2 mm thick film of water through which molecular diffusion is the dominant transport mechanism for dissolved material (Boudreau and Jørgensen 2001). Due to the diffusive transport, the DBL is characterised by linear concentration profiles. The gradients of these profiles can be measured with microelectrodes, and the vertical diffusive flux (J_z) calculated using Fick's first law of diffusion:

$$J_z = -D\, dC/dz \qquad (1)$$

where D is the molecular diffusion coefficient and dC/dz the vertical concentration gradient.

The classical laminar concept of the redox layering, and the application of the simple Fick's first law of diffusion (Eq. 1), treats the sediment-water interface as an infinite flat plane with only vertical chemical gradients. However, sediment surfaces are sculptured into elaborate landscapes across a range of scales (Paul et al. 1978; Swift et al. 1985; Briggs 1989; Gundersen and Jørgensen 1990). As pointed out by Wheatcroft (1994), the topography at a given site is dynamic, and temporal variations in topography at a single site might be just as large as variations from site to site.

A number of studies have evaluated the discrepancy between observed topography and the infinite flat plane (Jørgensen and Des Marais 1990; Gundersen and Jørgensen 1990; de Beer et al. 1994; de Beer and Stoodley 1995, Røy et al 2002, see comparison in the last reference). Common for all investigations is the visualisation of oxygen concentration fields as isolines or isoplanes. Apart from visualising the O_2 distribution, the isolines also contain information about the direction of the diffusive flux. Since concentration is constant along these lines, no net diffusion occurs along them and the direction of diffusive transport is at right angles to the isolines. In other words, an isoline touching the sediment surface at a specific point will define the local exchange surface between sediment and water. Jørgensen and Des Marais (1990) observed that surface structures with a characteristic dimension smaller than half the thickness of the DBL are not reflected in the oxygen isolines within the DBL. Thus, isolines of oxygen concentration are smooth lines loosely following the relief of the sediment-water interface (Glud et al. 1996; Fenchel and Bernard 1995; Jørgensen and Revsbech 1983; de Beer et al. 1994; de Beer and Stoodley 1995). The reason for the smoothness is that, at small scales, molecular diffusion levels out any heterogeneity in solute distribution that is not maintained by effective sinks and sources. It is the same diffusion effect that causes microprofiles to be smooth and continuous in one-dimensional representations.

The fact that O_2 isolines resemble a smoothed sediment surface was exploited by Røy et al. (2002) to generate approximated isolines from high-resolution topographic data. They showed that smoothing the topographic data with a matrix corresponding to the thickness of the effective DBL (δ), generated a virtual sediment surface that was practically parallel to the isolines in the DBL. At each point on the mapped surfaces, the area of this exchange surface (A') relative to the projected horizontal surface (A) could then be calculated. The enlarged surface could then be accounted for by simply multiplying a calculated vertical diffusive flux by A'/A.

In addition to enlarging the surface area, topography also cause horizontal gradients that are not represented in vertical profiles. The error is related to the angle, α, between the exchange surface and horizontal. Simple geometry implies that the error can be corrected by multiplying the gradient by ($1/\cos \alpha$) (Jørgensen and Des Marais 1990). Røy et al. (2002) showed that A'/A is equal to ($1/\cos \alpha$). Glud et al. (2003) chose to view the missing representation of horizontal gradients as an underestimation of the diffusive distance through the DBL. They therefore multiplied the gradient by (δ/δ'), which is the ratio between the measured DBL thickness the actual DBL thickness perpendicular to the slanted sediment surface. Again, this is just another view of the same geometric problem, and (δ/δ') is equal to A'/A. It follows, that a diffusive flux must be multiplied by A'/A twice to account for topographic effects. Once to account for increased surface area, and once to account for missing representation of the horizontal gradients. Denoting the 3-dimensional diffusive flux J', the relation between vertical diffusive flux (J_z) and 3-dimensional diffusive flux become:

$$J' = J_z \times (A'/A)^2 \quad (2)$$

Mapping isolines directly with microsensors is a tedious and slow procedure. It is therefore only suited for generating illustrative examples. The topographic data necessary to generate the approximated isolines, however, can cover large enough areas to adequately represent the average A'/A.

The current study builds largely on the argumentation and methods presented by Røy et al. (2002). But where the former used a laboratory-contained model-system to illustrate that correction of J_z based on topographic data was possible, the current study applies this principle on topographic data acquired *in situ*. The topographic data acquired to do this, surpass previously published topography measurements of marine sediments by

about an order of magnitude. The aim was to quantify the momentary influence of topography in one-dimensional calculations of diffusive oxygen uptake for actual marine locations, and to evaluate how far a one-dimensional view on the oxic zone is from reality.

METHODS AND STUDY SITES

Bay of Campese, Isola del Giglio, Italy. Isola del Giglio is a small island in the Mediterranean Sea, 150 km Northwest of Rome (42°20'N 10°52'E). The study site was on the southern side of a small open bay, locally known as the Bay of Campese. Mapping and coring was performed at 25 m water depth, 200 m seawards from the rocky shore. The sediment was a sandy silt, with a median grain size of 31 µm. Porosity was 62% (SE = 1, n = 4) and permeability 2.95 10^{-13} m^2 (SE = 0.53 10^{-13} m^2, n = 4). Autumn senescence of *Posidonia* meadows in the shallow regions of the bay, and the recent passage of a severe storm, had caused accumulation of seagrass-debris on the sediment. Consequently, the organic content was relatively high with 2.24% (SE = 0.13, n = 4).

A diverse and active fauna was observed at the study site. Most conspicuous for their impact on surface topography were hermit crabs (*Pagurus prideauxi* and *Paguristes oculatus/eremita*), whose tiny footprints densely dotted the sediment surface. Digging activity of the hermit crabs, together with spider crabs (*Inachus dorsettensis)*, added topographic variation one order of magnitude larger than the footprints. Large permanently burrowing animals like the polychaete *Aphrodita aculeata*, and brittlestars of the *Ophiouridae* family were abundant and contributed to sediment sculpturing as well. Large numbers of fish were observed to disturb the sediment-water interface during foraging at or below the sediment surface. The most important species, judging from size, abundance and feeding mode, was Red Mullet (*Mullus surmuletus)*, but various gobis were also numerous. The mud shrimps *Callianassa truncata*, which forms conspicuous landscapes of cones and funnels in the shallower regions of the bay (Ziebis et al. 1996) was not observed at the study site. When Giglio was visited in October 2001, the water column was unstratified down to at least 30 m with a temperature of 22 °C.

Aarhus Bay, Denmark. Aarhus Bay is a semi-enclosed bay on the Baltic Sea – North Sea transition. The bay covers 320 km^2 and has an average depth of 15m. The central regions of the bay, containing the study site at 56°09.1' N 10°19.2' E, consist of a ~50 km^2 plane with only minor water depth variations. The study site is identical to "station 170006" designated by the local county, who has monitored benthic fauna and water chemistry there since 1979. The site is generally known as "station 6", and has been used intensively for scientific

studies of early diagenesis (for an overview, see Jørgensen 1996). The county monitoring program (www.aaa.dk) classifies the fauna as a typical Abra-community, dominated by *Abra alba*, *Mysella bindentata*, *Corbula gibba*, *Pectinaria koreni* and *Nephtys* sp. The biomass is dominated by the large molluscs icelandic cyprine (*Arctica islandica*), sand gaper (*Mya arenaria*) and pelican's foot (*Aporrhais pespelecani*). The sediment consists of sandy clay. The sediment was not inspected by divers when the measurements were performed, but during dives in March 2001, the visible fauna consisted mainly of the brittle star *Ophiura albida*. During measurements, in December 2001, the water column was unstratified with a temperature of 5.7 °C.

Microsensor analysis.

Sediment cores from each study site were recovered in polycarbonate tubes with 50 mm inner diameter. The cores were brought to the laboratory and pre-incubated for 2 to 3 days under gentle stirring and dim light. Temperature and water-column oxygen concentration was held at *in situ* conditions throughout. Oxygen microprofiles were measured in the cores using Clark type O_2 microelectrodes with internal reference and guard-chatode (Revsbech 1989). Tip diameters were 15 µm to 25 µm, stirring sensitivity less than 1 % and response time about 1 s. The electrodes were calibrated between the O_2 concentration in the mixed water column determined by Winkler titration, and anoxic sediment. The electrode signal was recorded on an IBM compatible PC using a LAB-PC 1200 AI analogue-to-digital converter (National Instruments). Vertical diffusive oxygen flux was calculated from the slope of the concentration gradient in the DBL, according to Eq.1.

Topographic mapping

The micro-topography at the study sites was determined optically using an *in situ* version of the instrument described by Røy et al. (2002). A line generating laser-diode module (Lasiris LAS 670 5 with LAS 20 line) was positioned on a moving sledge at ~ 15 cm distance to the seafloor. A digital video camera (SONY DX-1000 in Amphibico UW housing) was fixed relative to the laser, imaging the vertically projected laser line from an angle of 45°. The translation mechanism of the sledge was fitted with a magnetic position sensor with optical output that changed state for every 0.1 mm of translation. The output of the position sensor was made visible to the camera by coupling the signal into the field of view through an optical fibre. On Giglio, the instrument was placed and operated by SCUBA divers, whereas

in Aarhus Bay the instrument was lowered from the ship and remotely operated (Glud et al. 2003).

One frame was extracted from the continuous video recording for each 0.1 mm of translation based on the state of the position sensor. The images of the projected line were then used to determine the relative height of the sediment surface. Resolution in the direction of translation is given by the distance translated between the extracted images, i.e. 0.10 mm. Along the laser line, the resolution depended on the magnification factor of the camera, and therefore on range-, zoom-, and focus settings. For the settings used, the horizontal resolution was 0.10×0.10 mm^2 for the Giglio data and 0.13 x 0.10 mm^2 for the data recorded in Aarhus Bay.

The image quality produced by extraction from the digital video did not match the quality that can be obtained by digital still-image camera (Røy et al. 2002). Pixel to pixel noise in the images translates directly to point to point noise in determination of the surface heights from the images. Surface-areas calculated without smoothing will therefore be enhanced by area increase caused by random peaks and valleys as well as real topography, resulting in an overestimation. After application of the 0.6×0.6 mm^2 smoothing kernel from which the exchange surface can be derived (Røy et al. 2002), however, each point on the surface contain of ~30 single determinations. This procedure effectively filters out point to point noise. So even though the topographic data contain a random variation on the individual datapoints at full resolution, the noise is insignificant at the resolution at which the information about A' is derived.

Each topographical map was smoothed by convoluting with flat matrices of a range of sizes. For each map and matrix size, the ratio between total surface area (A') and projected horizontal area (A) was calculated following the procedure of Røy et al. (2002).

Finally, artificial sediment images for representation were generated by the simulation of a distant light source illuminating an isometric topographic model from a 40° angle (Surfer 6, Golden).

RESULTS

For both sites, the oxygen distribution within the sediment followed the parabolic profile typical for impermeable sediments (Fig. 1). Diffusive oxygen flux along the vertical axis (J_z) was 34 mmol (SE 1.9, n = 5) m^{-2} day^{-1} in the Giglio sediment and 12 (SE 3.5, n = 6) mmol m^{-2} day^{-1} in Aarhus Bay.

The micro-topography of the Giglio sediment was a mosaic of overlapping sediment mounds (Fig. 2A). *Posidonia* leaf fragments lying on top of the actual sediment, as seen at 10, 40 in Fig. 2A, added further topographic variation. According to Røy et al. (2002), the surface calculated by smoothing the topography with a 0.6 × 0.6 mm^2 kernel closely resembles the DBL (Fig 3).

Whereas Fig. 3 only represents a small subsection of one map, Fig. 4A shows the ratio between the smoothed surface area (A') and the projected area (A) for all measured maps, after application of a range of smoothing kernels. Multiplying $(A'/A)^2 = 1.25$ derived by smoothing with the 0.6 × 0.6 mm^2 kernel to the vertical diffusive flux results in a total diffusive flux of 38 mmol m^{-2} day^{-1}.

Compared to Giglio, the sediment mapped in Aarhus Bay appeared as a smoothly rolling landscape, containing discrete biogenic structures such as tracks and faecal mounds (Fig. 2B). Following the same procedure as above, $(A'/A)^2$ is 1.14 resulting in a total diffusive flux of 14 mmol m^{-2} day^{-1}.

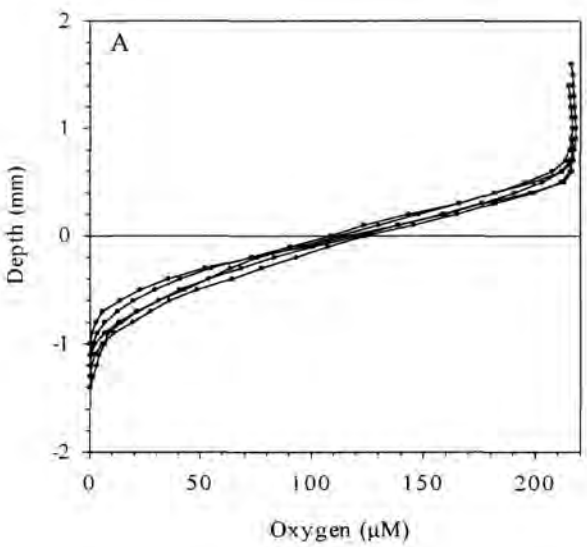

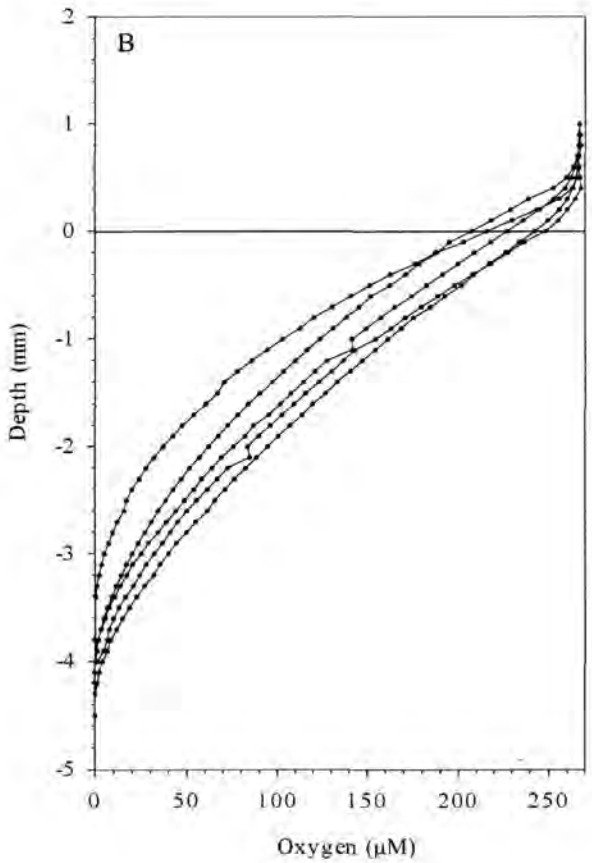

Figure 1: O_2 micro-profiles across the sediment water interface, measured ex situ in cores. Fig. 1A from Giglio and Fig. 1B from Aarhus Bay.

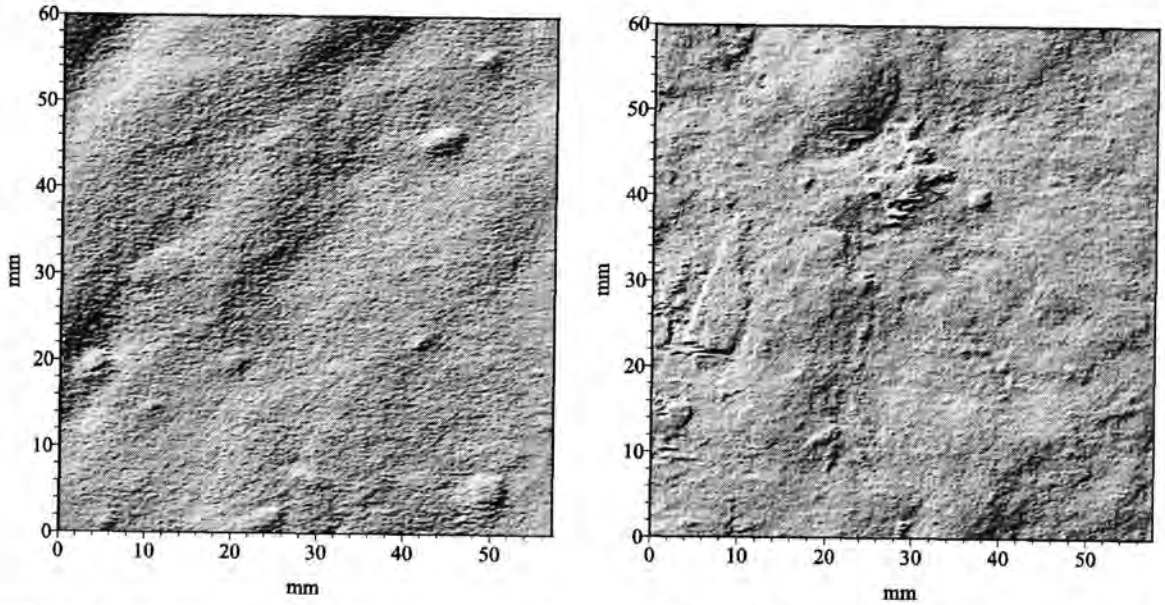

Figure 2. Topography measured *in situ*, presented as shaded relief. The images are generated with a simulation of distant light source illuminating the topography from a 35° angle. Left. An example measured in the Bay of Campese, Giglio, and Fig. Right. Example measured in Aarhus Bay.

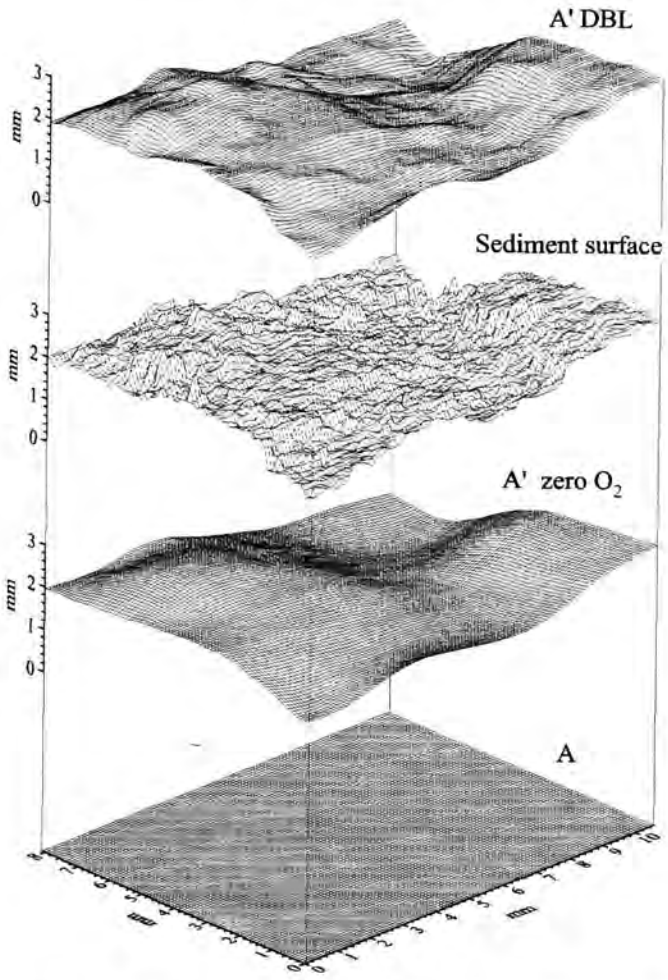

Figure 3. Example of the topography of 3 interfaces around the sediment surface. The sediment surface has been measured. The DBL is the interface between sediment and water. It has been approximated as smoothing the measured sediment surface with a matrix with the same size as the thickness of DBL (0.6 mm). Likewise, the zero isoline is approximated smoothing with a kernel with the same dimension as the distance from the top of the DBL to the penetration depth of O_2 (see text for details).

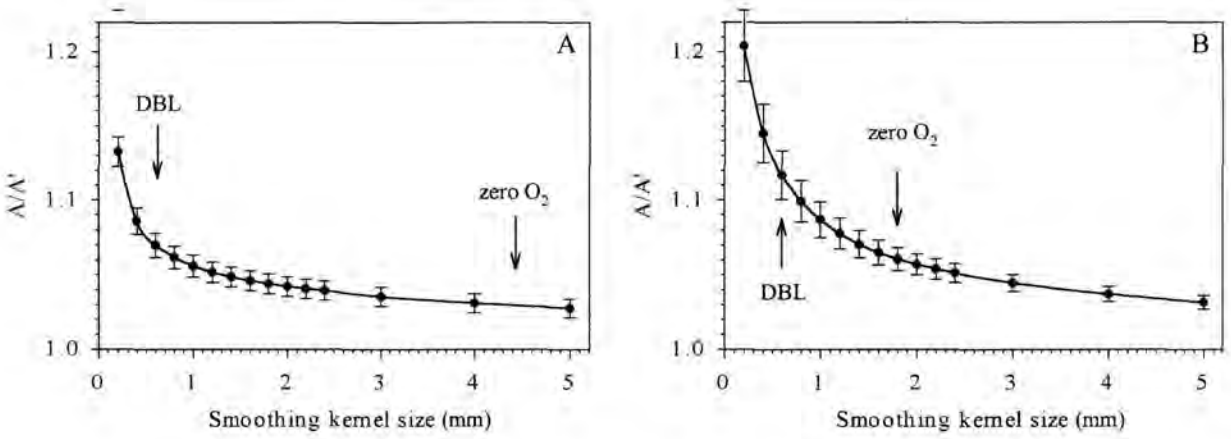

Figure 4: The surface-area calculated after different degrees of smoothing, relative to the projected horizontal area. Figure 4A is from the map form Giglio seen in Figure 2 and 13 similar maps. Figure 4B is from the map form Aarhus seen in Figure 2 and another 17 maps. All error bars are 95% confidence intervals.

DISCUSSION

As seen in Fig. 4, the area increase due to topography is quite moderate in both examples. The discrepancy between a conceptual model accounting only for vertical gradients, and the more complex model taking topography into account, is thereby equally small. This is not caused by exceptionally smooth sediment surfaces at the two sites. But the smoothing effect of molecular diffusion causes the DBL to follow the relief with continuous isolines with mostly small angles relative to horizontal (α). The relation between α and the area increase is not linear. Below about 20° the surface slope has little influence on the surface area, and the areas with angles above 20° are too rare to make a large impact on the average surface area.

Table 1 shows a short compilation of other studies that quantified the difference between vertical diffusive flux and 3D diffusive flux caused by surface topography. The gelatinous systems, like biofilms and photosynthetic mats, reach quite large factors between vertical diffusive flux and 3D diffusive flux. In an extreme example, presented by de Beer and Stoodley (1995), the influence was linked to the vertical sides of clusters and channels in the biofilm structure. But with DBL thickness of just 200 µm the structures were completely submerged in the DBL, which caused the diffusive flux to occur almost perfectly vertical. So even if a marine sediment has a surface as complex as this biofilm, the influence of structures as small as 100 to 300µm would be negligible.

Study	J'/J_z
A biofilm with complex surface structure, where the roughness was submerged in the DBL (de Beer and Stoodley 1995).	1.00
A model benthic community in a laboratory flume, where the topography consisted of annelid faecal-mounts on a more or less flat background (Røy et al. 2002).	1.08
The coastal marine mud, measured in Aarhus Bay (present study)	1.14
The organic-rich near-shore sand littered with seagrass fragments. (present study)	1.21
A gelatinous microbial mat from a hyper-saline environment. The mat was structured by tufts and clusters cyanobacteria and diatoms, with a size scale in the same range as the thickness of the DBL. The original J'/J_z of 1.49 was recalculated by Røy et al. (2002) to 1.3-1.4. Original reference; Jørgensen and Des Marais (1990)	1.3-1.49
A heavily bioturbated sediment from a shallow estuarine lagoon, stabilised by diatoms. The original J'/J_z of 2.5 was calculated according to the procedure of Jørgensen and Des Marais (1990), and therefore probably contain an overestimation (Røy et al. (2002). Recalculating along the same lines as was done for Jørgensen and Des Marais (1990) give a J'/J_z of 1.8. Original reference; Gundersen and Jørgensen (1990).	1.8 – 2.5
A biofilm with complex surface structure, where a 50µm thin DBL wrapped around the surface elements (de Beer and Stoodley 1995).	2-2.5

Table 1

The mat described by Jørgensen and Des Marais (1990) was structured by tufts and clusters of cyanobacteria and diatoms, with size scales of a few mm. The exopolymers in the mat allowed stabile steep structures of a size that could be partly followed by the DBL under high flow-velocities. Under lower flow velocities, the thicker DBL again partly drowned the topography, causing the vertical flux to contain most of the diffusive exchange. Still, the study of Jørgensen and Des Marais (1990) demonstrates that for sediments with large amounts of exopolymers, a large topographical influence is possible. But the sizes of the structures responsible for the enlarged exchange surface are large enough to be easily recognised. The study of Gundersen and Jørgensen (1990) shows just such an example, from a *Chorophium* bed stabilised by diatoms. The studies of Jørgensen and Des Marais (1990) and Gundersen and Jørgensen (1990) were point examples, brought forward to show that horizontal gradients in the DBL *could* be an important factor. Covering less than 1 cm^2 combined, their results were not intended to be extrapolated to the marine environment in general. Given the constraints imposed by the smoothing effect of the DBL, we therefore believe that the range of divergence between J_z and J' found in Aarhus Bay and Giglio is representative for similar marine sediments, in spite the much higher estimates published

previously. Using the range between 12 and 25% as a best current estimate of the error imposed by sediment topography on calculated diffusive fluxes implies that a measured flux should be multiplied by a factor of 1.12 to 1.25. The higher value should only be used on sediments as rough as the sediment seen in Fig 2A.

The exchange surface towards the water column is not the only part of the sediment that is influenced by the surface topography. Underneath the DBL, O_2 penetrates into the sediment forming a thin oxic zone. The average O_2 penetration in fine-grained coastal and estuarine sediments is generally only a few mm (Revsbech et al. 1979; Cai and Sayles 1996). Under diffusive control, the thickness of the oxic zone is mainly determined by the oxygen concentration in the water column and the volume-specific oxygen consumption rate (Glud et al. 2003). Local hot-spots in oxygen consumption rate often associated with faecal mounds are reflected in locally reduced oxygen penetration depth (Glud et al. 1996; Huettel et al. 2003). To decrease the penetration depth by 50%, a four fold increase in rate is necessary, and partly therefore multiple measurements of oxygen penetration depth are often remarkably similar (Fig. 1). Further, the edges of the hot-spot are smoothed by lateral diffusion, causing a gradual abnormality in the zero isoline. The zero isoline is therefore almost parallel to the DBL, even when the activity of the sediment is uneven. This can be seen directly in two-dimensional oxygen distributions from coastal and estuarine sediments (e.g. Glud et al. 1996, Glud et al. 2001). Thus, (Glud et al. 2003) extended the measured A'/A of the DBL to account for the enlargement of the entire oxic zone. From the factor A'/A, Glud et al. (2003) calculated the average angle between vertical microprofiles and the oxic surface layer, in order to assess the overestimation of the thickness of the oxic skin due to oblique penetration of the oxic layer. There is, however, no reason to assume that topographic variation much smaller than the thickness of the oxic layer should be reflected in the O_2 penetration depth. The situation is similar to the smoothing out of smaller variations in isolines around the sediment surface, with the only difference that the isoline now under consideration is the zero-line. To approximate the area of the oxic-anoxic interface, we should therefore smooth with a kernel with the characteristic size of the diffusive distance between the zero isoline and the mixed water column, i.e. the DBL thickness plus the oxygen-penetration (Fig. 2). The area increase of the exchange surface and of the oxic skin are therefore different, as shown in Fig. 4 and Fig. 5.

The small triangles in Fig. 5 illustrate how the oblique penetration of the oxic zone stretches out the vertical scale. The vertical scale should therefore be compressed by $(\delta/\delta') = A'/A$, before profile interpretation. Alone, this compression causes the volume of the oxic

zone to be underestimated. To calculate the correct oxic volume, we must enlarge the area by the same factor that the vertical scale was compressed. This makes sense, as $\delta/\delta' = A'/A$, which is the ratio between the 3-dimensional area and the projected horizontal area. The average surface slope from the Giglio sediment is illustrated by the thick lines at the bottom of Fig. 5. At a first glance, it appears that the topographic influence of such steep slopes must be most significant. But as the influence is related to the relative length of A' and A, the effect is actual moderate.

If the sediment appearance from other locations is comparable to the images in Fig. 2, Fig. 4 can be used to evaluate in which range we should expect to find A'/A for the oxic-anoxic interface. Instead of reading at the left arrow, where A'/A associated with the DBL is found, A'/A for the oxic/anoxic boundary should be read at the actual O_2 penetration depth.

A similar argumentation as for the oxic skin can be applied on other laminated processes controlled by diffusion from the water column. The common principle is that the deeper the respective layer is situated, the smaller is the influence of surface topography.

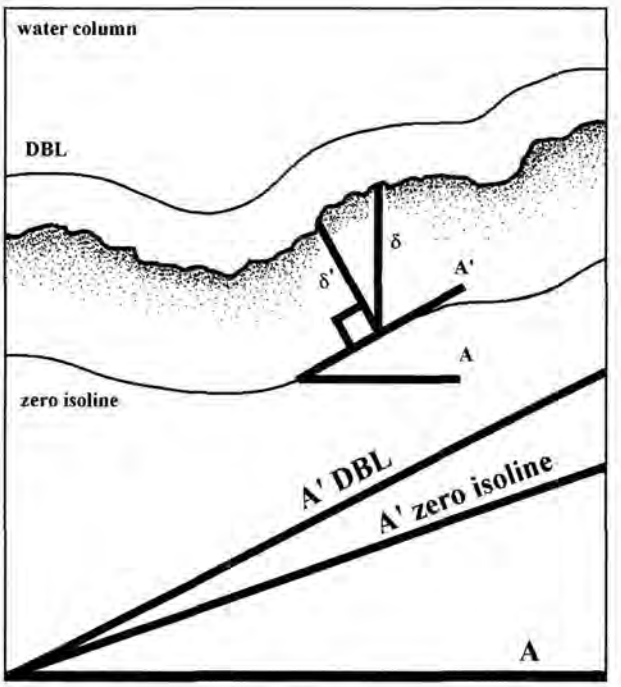

Figure 5. Geometric representation of the relation between the vertical flux and the diffusive exchanges across a sculptured a sediment-water interface. The small triangles demonstrate one point on the sediment surface, while the thick lines at the bottom of the figure represent the calculated average sediment slope for the Giglio sediment. The sediment mapped in Aarhus bay was significantly smoother.

REFERENCES

Aller, R. C. 1980. Quantifying Solute Distributions in the Bioturbated Zone of Marine-Sediments By Defining an Average Micro-Environment. Geochim. Cosmochim. Acta. 44: 1955-1965.

Boudreau, B. P. and B. B. Jørgensen. 2001. The Benthic Boundary Layer: Transport processes and biogeochemistry. Oxford University Press.

Briggs, K. B. 1989. Microtopographical roughness of shallow-water continental shelves. IEEE J. Oceanic Eng. 14: 360-367.

de Beer, D. and P. Stoodley. 1995. Relation between the structure of an aerobic biofilm and transport phenomena. Water Sci. Technol. 32: 11-18.

de Beer, D., P. Stoodley, F. Roe and Z. Lewandowski. 1994. Effects of biofilm structure on oxygen distribution and mass transport. Biotechnol. Bioeng. 43: 1131-1138.

Fenchel, T. 1996. Worm burrows and oxic microniches in marine sediments .1. Spatial and temporal scales. Mar. Biol. 127: 289-295.

Fenchel, T. and C. Bernard. 1995. Mats of colourless sulphur bacteria .1. Major microbial processes. Mar. Ecol. Prog. Ser. 128: 161-170.

Glud, R. N., J. K. Gundersen, H. Røy and B. B. Jørgensen. 2003. Seasonal dynamics of benthic O_2 uptake in a semi enclosed bay: Importance of diffusion and fauna activity. *In press,* Limnol. Oceanogr. (Chapter 5 of this thesis).

Glud, R. N., A. Tengberg, M. Kühl, P. O. J. Hall, I. Klimant and G. Holst. 2001. An *in situ* instrument for planar O_2 optrode measurements at benthic interfaces. Limnol. Oceanogr. 46: 2073-2080.

Glud, R. N., N. B. Ramsing, J. K. Gundersen and I. Klimant. 1996. Planar optrodes - a new tool for fine scale measurements of two-dimensional O_2 distribution in benthic communities. Mar. Ecol. Prog. Ser. 140: 217-226.

Gundersen, J. K. and B. B. Jørgensen. 1990. Microstructure of diffusive boundary layers and the oxygen uptake of the sea floor. Nature. 345: 604-607.

Harper, M. P., W. Davison and W. Tych. 1999. One-dimensional views of three-dimensional sediments. Environ. Sci. Technol. 33: 2611-2616,.

Huettel, M., H. Røy, E. Precht, S. Ehrenhauss. Hydrodynamical impact on biogeochemical processes in aquatic sediments. *In press*, Hydrobiologia.

Jahnke, R. A. 2000. Constraining organic matter cycling with benthic fluxes, p. 302-319. *In* B. P. Boudreau and B. B. Jørgenesen [eds.], The benthic boundary layer: Transport processes and biogeochemistry. Oxford University Press.

Jørgensen, B. B., 1996. Case study – Aarhus Bay, p. 137-154. *In* Jørgensen, B.B., and K. Richardson [eds.], Eutrophication in Coastal Marine Ecosystems. Amer. Geophys. Union.

Jørgensen, B. B. and D. J. Des Marais. 1990. The diffusive boundary layer of sediments: Oxygen microgradients over a microbial mat. Limnol. Oceanogr. 35: 1343-1355.

Jørgensen, B. B. and N. P. Revsbech. 1983. Colorless sulfur bacteria, Beggiatoa spp and Thiovulum spp in O_2 and H_2S microgradients. Appl. Environ. Microbiol. 45: 1261-1270.

Paul, A. Z., E. M. Thorndike, L. G. Sullivan, B. C. Heezen and R. D. Gerard. 1978. Observations of the deep-sea floor from 202 days of time-lapse photography. Nature. 272: 812-814.

Revsbech, N. P. 1989. An oxygen microsensor with a guard cathode. Limnol. Oceanogr. 34: 472-276.

Røy, H., M. Hüttel and B. B. Jørgensen 2002. The role of small-scale sediment topography for oxygen flux across the diffusive boundary layer. Limnol. Oceanogr. 47: 837-847. (Chapter 3 of this thesis).

Swift, S. A., C. D. Hollister and R. S. Chandler. 1985. Close-up stereo photographs of abyssal bedforms on the Nova Scotian continental rise. Mar. Geology. 66: 303-322.

Thamdrup, B., H. Fossing and B. B. Jørgensen. 1994. Manganese, iron, and sulfur cycling in a coastal marine sediment, Aarhus Bay, Denmark. 58: 5115-5129.

Wheatcroft, R. A. 1994. Temporal variation in bed configuration and one-dimensional bottom roughness at the mid-shelf stress site. Cont. Shelf Res. 14: 1167-1190.

Ziebis, W., S. Forster, M. Huettel and B. B. Jørgensen. 1996. Complex burrows of the mud shrimp *Callianassa truncata* and their geochemical impact in the sea-bed. Nature. 382: 619-622.

Seasonal dynamics of benthic O_2 uptake in a semi enclosed bay: Importance of diffusion and fauna activity

Ronnie N. Glud, Jens K. Gundersen, Hans Røy, and Bo Barker Jørgensen

ABSTRACT

The benthic O_2 uptake and the O_2 microdistribution in a coastal sediment of Aarhus Bay, Denmark, were investigated during a seasonal study. Measurements were performed *in situ* by a profiling lander and a flux chamber O_2 lander as well as on recovered sediment cores. The O_2 penetration depth, the diffusive O_2 uptake and the volume specific O_2 consumption rate strongly depended on the seasonal changes in bottom water O_2 concentration and the sedimentation of organic carbon. The *in situ* O_2 penetration depth varied between 0.5 mm in summer and 4.5 mm in winter. The diffusive O_2 uptake varied between 8 and 30 mmol m^{-2} d^{-1}, while the volume specific O_2 consumption rate varied by a factor of 13. The O_2 distribution was very sensitive to environmental controls, and microprofiles obtained in the laboratory tended to overestimate the *in situ* O_2 penetration depths and underestimate the *in situ* diffusive O_2 uptake. Three-dimensional O_2-flux calculations based on *in situ* microtopographic mapping showed that the actual diffusive exchange rate was ~10% higher than the simple one-dimensional, microprofile-derived diffusive O_2 exchange. The total O_2 uptake measured in the laboratory showed less distinct seasonal variation, but on the average it was ~20% higher than the diffusive O_2 uptake. The difference reflected the microtopography of the sediment surface and the contribution from benthic macrofauna. *In situ* total O_2 uptake was generally twice as high as laboratory rates, reflecting a higher fauna related O_2 consumption in the larger enclosures incubated *in situ*. Annually, the *in situ* three-dimensional diffusive O_2 consumption was 6.2 mol O_2 m^{-2}, while the additional benthos mediated O_2 uptake was 3.9 mol O_2 m^{-2}. Thus 40% of the total O_2 uptake was due to faunal activity and respiration. The present study demonstrates the importance of realistic fauna representation during sediment incubations in order to obtain correct benthic mineralization rates.

INTRODUCTION

The oxygen uptake rate of the seafloor is the most widely used measure of benthic mineralization (e.g. Thamdrup 2000). The total O_2 uptake (TOU) is usually quantified from the O_2 disappearance rate in sediment enclosures and the TOU thereby represents an integrated measure of the diffusive, advective and fauna mediated O_2 consumption. The enclosure technique, however, does not provide information on the O_2 penetration depth or the vertical distribution of O_2 consumption rate. The introduction of O_2 microelectrodes in aquatic biology in the early eighties allowed the benthic O_2 dynamics to be studied in more detail (Revsbech et al. 1980)

Early microprofile measurements revealed that the oxic zone extends only a few millimetres into fine-grained coastal and shelf sediments (e.g. Revsbech et al. 1980)
The oxic zone has proved to be very dynamic with an intense heterotrophic and autotrophic O_2 consumption. Furthermore, detailed microsensor studies documented the existence of a 0.1-1.2 mm thick Diffusive Boundary Layer (DBL) (Jørgensen and Revsbech 1985; Archer et al. 1989; Gundersen and Jørgensen 1990; Jørgensen and Des Marais 1990). The main transport mode within the DBL is molecular diffusion and the zone is characterized by linear O_2 concentration gradients (Jørgensen and Revsbech 1985). The diffusive solute transport through the DBL can limit biogeochemical reactions (Boudreau and Guinasso 1982) and benthic O_2 consumption of highly active sediments, (Gundersen & Jørgensen 1990; Jørgensen and Des Marais 1990). The DBL blankets the complex 3D microtopography of the sediment surface and the DBL thickness is controlled by the flow velocity of the overlying water and by the sediment roughness (e.g. Jørgensen and Des Marais 1990)

The ability to resolve linear concentration gradients within the DBL allows the one-dimensional diffusive O_2 uptake (DOU) to be calculated (e.g. Jørgensen and Revsbech 1985). Alternatively, the diffusion-mediated O_2 consumption rate within the sediment can be modelled from the curvature of measured concentration profiles (e.g. Nielsen et al. 1990; Berg et al. 1998). This, however, requires knowledge on the interstitial transport coefficients for O_2 (Iversen and Jørgensen 1993). The two relatively simple approaches assume that the DBL and the sediment-water interface is represented by infinite flat planes (Jørgensen and Des Marais 1990; Gundersen and Jørgensen 1990) On the scale of the DBL, however, the benthic interface is a topographically complex landscape and, consequently, simple one-dimensional diffusion models may not adequately describe the three-dimensional diffusion-flux (Jørgensen and Des Marais 1990; Røy et al. 2002)

Fauna activity further complicates matters as irrigation enhances the ventilation of the sediment and introduces oxygenated water to deeper otherwise anoxic sediment layers (Aller 1988; Kristensen 1988; Fenchel 1996). Fauna activity can thereby strongly enhance the benthic exchange rates. In impermeable sediments without flow-induced advection, the additional fauna-mediated O_2 uptake (FOU) can be calculated as the difference between TOU and DOU (e.g. Archer and Devol 1992; Glud et al. 1994a). This parameter includes both the faunal respiration and the O_2 uptake in the surrounding sediment related to irrigation and other faunal activity. In the present study, we compared three different measuring techniques for quantifying the benthic O_2 consumption rate. Measurements were performed *in situ* and in the laboratory during a seasonal study of a coastal marine sediment. The FOU was quantified and its importance for the total benthic mineralization activity is discussed. Some of the data have previously been published in a report (Gundersen et al. 1995, in Danish), to the Danish Environmental Protection Agency.

MATERIALS AND METHODS

Study site

The semi-enclosed Aarhus Bay is situated in Kattegat on the Baltic Sea – North Sea transition, Denmark. The bay covers an area of 320 km^2 and has an average water depth of 15 m. The present study was carried out in the central part of the bay at "Station 6" (56°09.1'N, 10°19.2'E) with a water depth of 16 m (Thamdrup et al. 1994). The presented data were mostly obtained during 1990-1992 as part of an intense field study focusing on coastal element cycling (Jørgensen 1996). The water column was stratified by a halocline during 75% of the study period (Rasmussen and Jørgensen 1992; Jørgensen 1996). The sediment consists of 20% fine sand, 22% silt, and 55% clay, and the site has a mean net deposition rate of 2.5 g m^{-2} d^{-1} (Pejrup et al. 1996). The upper 4 mm of the sediment has an average porosity of 0.87 ± 0.05 vol/vol (n=34) and an organic matter content of 9.9% ± 0.9% dry weight (n = 34) (Rasmussen and Jørgensen 1992)

Laboratory measurements

The study site was visited 24 times during 1990-1991 by a small research vessel, "Genetica II". On each occasion a series of sediment cores were recovered by a "Haps corer" (Kanneworff and Nicolaisen 1973). Six undisturbed subcores were taken by 25 cm long Plexiglas tubes with an inner diameter of 5.4 cm. Water (approximately 30 L) was subsequently collected 20 cm above the seafloor by a pump positioned on a small tripod that

was lowered from the ship. Temperature and O_2 concentration were determined in surface and bottom water on each occasion. Cores and water samples were transported back to the laboratory in insulated containers within 2 hours after recovery. Upon return, 6 uncapped cores were submerged in an aquarium containing bottom water from the sampling site kept at *in situ* temperature. In order to maintain *in situ* O_2 concentration, the water was continuously flushed with an air/dinitrogen mixture regulated by a digital gasmixer. The rotation of Teflon coated magnets attached to the inner wall of each coreliner ensured a good exchange between the water phase of the cores and the exterior seawater (Rasmussen and Jørgensen 1992). Sediment cores were preincubated in darkness over night prior to measurements

Next day, 2-12 (average of ~7) oxygen microprofiles were measured using Clark type microelectrodes with an internal reference and a guard cathode (Revsbech 1989). The profiles were measured at a depth resolution of 50 µm and always in at least two different sediment cores. Profiles were generally measured in areas unaffected by faunal activity and no significant difference was observed between profiles obtained in different cores on a given date. The microelectrodes had tip diameters of 3-20 µm, 7 stirring effects <2%, and 90% response times of < 2 s (Revsbech 1989; Glud et al. 2000). The sensors were positioned by a motorized micromanipulator and the sensor current was measured by a picoamperemeter connected to an A-D converter, which transferred the signals to a PC (Revsbech and Jørgensen 1986). The microprofiles had two inherent calibration points: The reading in the overlying water with a known O_2 concentration and the constant low reading in the anoxic sediment

After microprofiling, the sediment cores were capped, leaving an internal water height of 8-12 cm. A glass tube with an internal diameter of 5 mm penetrated each lid and allowed the subsequent insertion of an O_2 microelectrode in the overlying water phase. The glass tube was filled with paraffin oil to impede diffusive exchange between the enclosed water volume and the air (Rasmussen and Jørgensen 1992). During incubation, small magnets stirred the overlying water phase in each core. This ensured a DBL-thickness during core incubations and microprofile measurements similar to the *in situ* DBL thickness

In situ O_2 measurements

On each sampling occasion in 1990-1991, O_2 microprofiles were measured *in situ* using a profiling lander (Gundersen and Jørgensen 1990). The central part of the instrument consisted of a movable electronic cylinder equipped with microsensors. For the present study, six O_2 microelectrodes were used with similar measuring characteristics as outlined above. The cylinder was mounted on a tripod that was lowered by wire from the ship. After the instrument had stabilized on the seafloor for one hour, the cylinder was moved downward in increments of 50 µm. At each depth horizon data from all sensors were recorded and transferred via cable to an onboard PC. A video mounted on the tripod allowed visual inspection of the sediment during deployment.

During 1992, laboratory measurements and *in situ* microprofiles were obtained on a more irregular basis, while on 15 occasions *in situ* TOU was measured by a benthic chamber lander (Glud et al. 1995). As the instrument was positioned on the seafloor a central chamber of 896 cm^2 was inserted into the sediment. Video recordings demonstrated that the sediment surface was practically undisturbed during chamber insertion. After one hour the lid closed, leaving an internal water height of approximately 10 cm. During incubation a central impeller mixed the overlying water phase, and two minielectrodes with similar measuring characteristics as outlined above continuously recorded the O_2 concentration of the enclosed water volume. The stirring resulted in a DBL thickness of ~500 µm, which was similar to the DBL in laboratory incubated sediment cores and close to the average DBL thickness measured *in situ* (see below). During incubations ten spring-loaded syringes retrieved water samples at predefined time intervals for subsequent O_2 analysis and sensor calibration along with an onboard reading in anoxic sediment. At the end of the incubation, a scoop closed the chamber from below and, after recovery the exact water height of the water phase was determined. The enclosed sediment was sieved through a 1 mm mesh screen to collect the entire macrofauna community. The fauna was identified and the dry weight was determined after 24h at 70°C, while its organic matter content was determined as loss on ignition after 24h at 550°C

Microtopography mapping

The microtopography of the sediment surface at the study site was determined in December 2001 using an *in situ* version of the optical instrument described by Røy et al. (2002). A line generating laser-diode (Lasiris LAS 670 5 with LAS 20 line) was positioned on a moving sledge at ~15 cm distance to the seafloor. A digital video camera (SONY DX-1000 in

Amphibico underwater house) was fixed on the sledge and recorded the movement of a vertically projected laser line from a 45° angle (Fig. 1). The position of the moving sledge relative to the stationary frame was recorded in the upper corner of the view-field of the camera via a position sensor with an optical output. The instrument was lowered by wire to the seafloor with the video camera continuously recording. After one minute, the translation mechanism was activated, and the sledge translated a horizontal distance of 12 – 15 cm. Recorded images were extracted for every 0.1 mm of translation based on the state of the position sensor. Images of the projected line were used to determine the relative height of the sediment surface. Given the optical dimensions and the 0.1 mm distance between images, the micro-topography was determined with 0.13 x 0.1 mm horizontal resolution while the vertical resolution was better than 20 µm (Røy et al. 2002). From 13 independent scans, 18 topographic maps were extracted each covering ~40 cm^2.

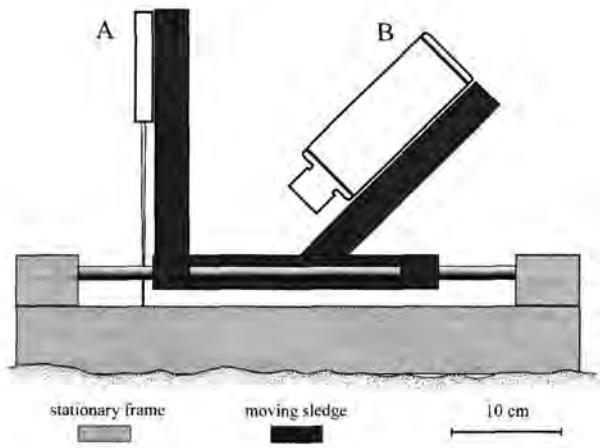

Figure 1. Schematic presentation of the *in situ* instrument used for 3D topographic mapping of the seafloor. A) shows the laser diode module, while B) is the video camera.

Oxygen microprofile calculations

The upper DBL boundary of the measured microprofiles was determined as the intersection between the extrapolated linear O_2 gradient in the DBL and the constant O_2 value in the overlying water (Fig. 2A) (Jørgensen and Revsbech 1985). The thickness of the DBL was estimated from the intersection point and the position of the sediment surface, which typically was identified from a distinct break in the concentration profile (Fig. 2A)

The diffusive O_2 uptake (DOU) of the sediment was calculated from: $DOU = D_0 dC(z)/dz$, where D_0 is the temperature corrected molecular diffusion coefficient of O_2 and C is the O_2 concentration at a given depth, z, with the DBL (Fig. 2A) (Crank 1983). The D_0

was taken from Broecker and Peng (1974) and was temperature corrected as described by Li and Gregory (1974). The average volume specific O_2 consumption rate was calculated by dividing the DOU by the O_2 penetration depth. For whole core incubations the TOU was calculated from the initial linear O_2 decrease in the enclosed water volume (Fig. 2B).

The volume specific O_2 consumption rates were also quantified from the O_2 microprofiles measured within the sediment using a simple manual curve fitting approach and assuming zero order kinetics (Nielsen et al. 1990; Rasmussen and Jørgensen 1992). The measured profiles could always be fitted by one, two or three two-degree polynomials. The depth integrated O_2 consumption rate and the O_2 exchange at the sediment-water interface were subsequently calculated (Rasmussen and Jørgensen, 1992). The DOU was thereby calculated from each microprofile by two independent approaches using either the concentration gradient measured in the DBL or the O_2 distribution measured in the interstitium. For the calculations based on the interstitial data, the sediment diffusion coefficient, Ds, of O_2 was estimated from the sediment porosity, φ, using the relation, $D_s = (1+3(1-\phi))^{-1} D_0$ (Iversen and Jørgensen 1993).

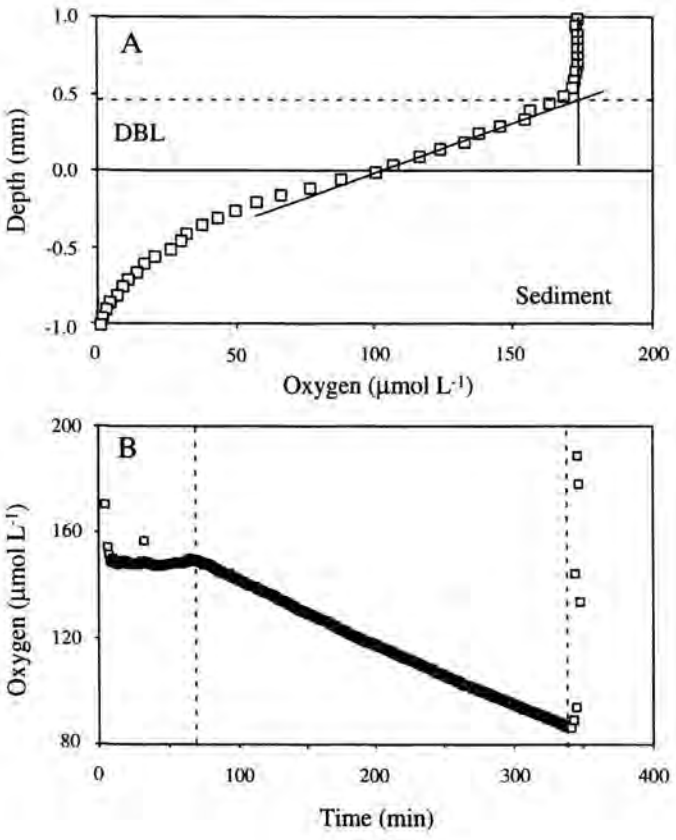

Figure 2. A) A typical O_2 microprofile measured *in situ* during late summer of 1990. The solid horizontal line indicates the estimated position of the sediment surface, while the broken line indicates the estimated position of the upper DBL boundary. The slope of the concentration gradient within the DBL is shown. B) The readings of an O_2 mini electrode during deployment of the benthic chamber lander in the summer of 1992. The time axis shows minutes after lander deployment. The left vertical broken line indicates the time when the chamber lid was closed, while the right line indicates the time of chamber recovery.

RESULTS

The temperature of the bottom water varied throughout the year between 14.0°C in September and 1.5°C in February, while the temperature range of the surface water was from 16.2°C to 1.5°C. During autumn and winter there was no temperature difference between surface and bottom water. In spring and early summer the halocline was stabilized by a temperature difference between the two water masses (Fig. 3A) The pycnocline was mostly situated between 8 and 12 m water depth but varied considerably as a result of wind-induced seiching (Jørgensen 1996). The O_2 concentration in the surface water varied between 234 and 381 µmol L^{-1} but was always close to air-saturation (90-110%). Light penetration was limited by the relatively high phytoplankton biomass and we never observed net O_2 production at the seafloor. Consequently, periods with stratification resulted in O_2 depletion of the bottom water. Minimum O_2 concentration of 55-70 µmol L^{-1} (18-25% air-saturation) were reached during summer and early autumn (Fig. 3B). Generally, the pattern in bottom water temperatures and O_2 concentrations from 1990-1991 were reproduced in 1992 (Fig. 3).

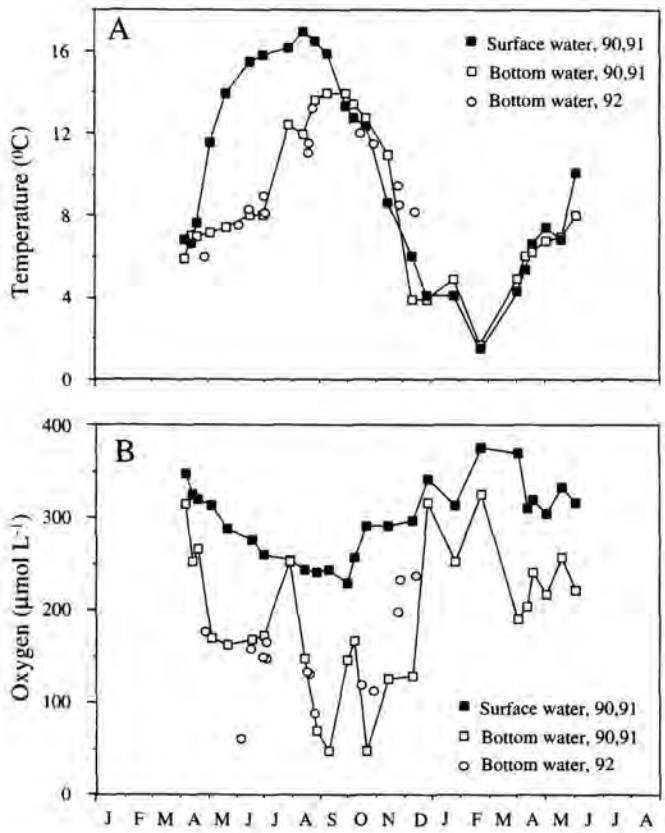

Figure 3. A) Temperature of surface water and bottom water during 1990-1991 and of the bottom water in 1992. B) O_2 concentration in the surface water and the bottom water during 1990-1991 and of the bottom water in 1992.

The laboratory and the *in situ* determined O_2 penetration depths varied on a seasonal basis (Fig. 4). Both data sets revealed maximum penetration depths of ~4.5 mm during winter while minimum values of ~0.8 mm were obtained in early autumn (Fig. 4). The ~6 fold variation in O_2 penetration depth correlated well with the O_2 concentration of the bottom water (Fig. 3 and 4). Oxygen depletion in the bottom water immediately resulted in a narrowing of the oxic zone. Thus, a decrease in O_2 bottom water concentration from 260 to 75 µmol L^{-1} in August 1990 was followed by a decrease in O_2 penetration from 2.2 to 0.8 mm (Fig. 3 and 4). The few measurements of O_2 penetration performed in 1992 reproduced the data of 1990 with a single exception that coincided with a distinct depletion in bottom water O_2 concentration in the beginning of June 1992 (Fig. 3 and 4).

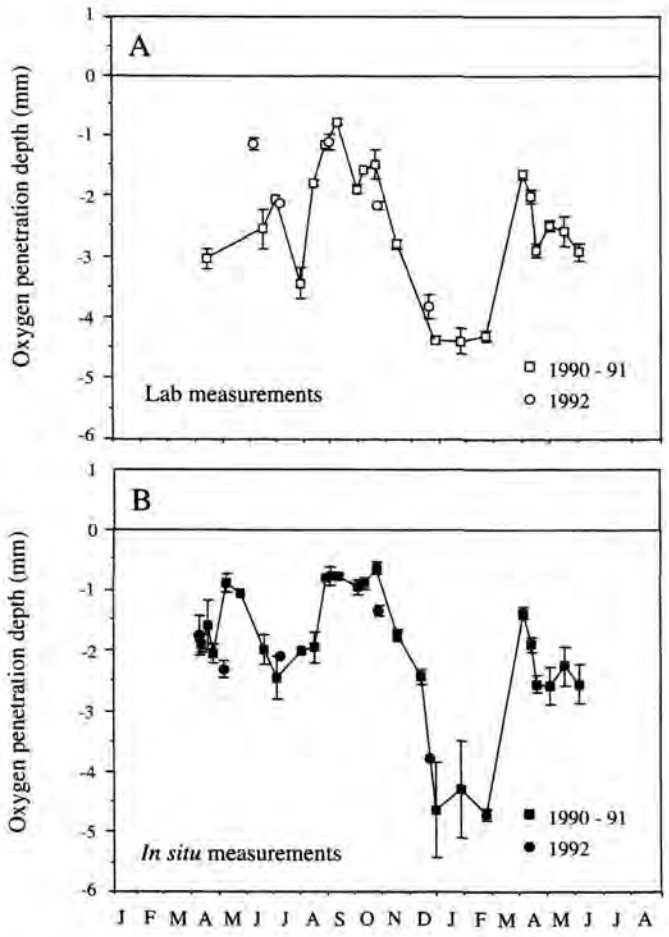

Figure 4. A) O_2 penetration depths measured in the laboratory during 1990-1991 and 1992. B) O_2 penetration depths measures *in situ* during 1990-1991 and 1992.

Along with the bottom water O_2 the input of organic carbon clearly affected the interfacial O_2 dynamics. In early September the O_2 concentration of the bottom water was 53 µmol L^{-1} and the O_2 penetration depth was only 0.78 ± 0.04 mm. The major part of the volume specific O_2 consumption as modeled from the curvature of the O_2 concentration profiles was associated with the oxic-anoxic interface presumably due to intensified oxidation of reduced solutes diffusing up from the anaerobic degradation below (Fig. 5A).

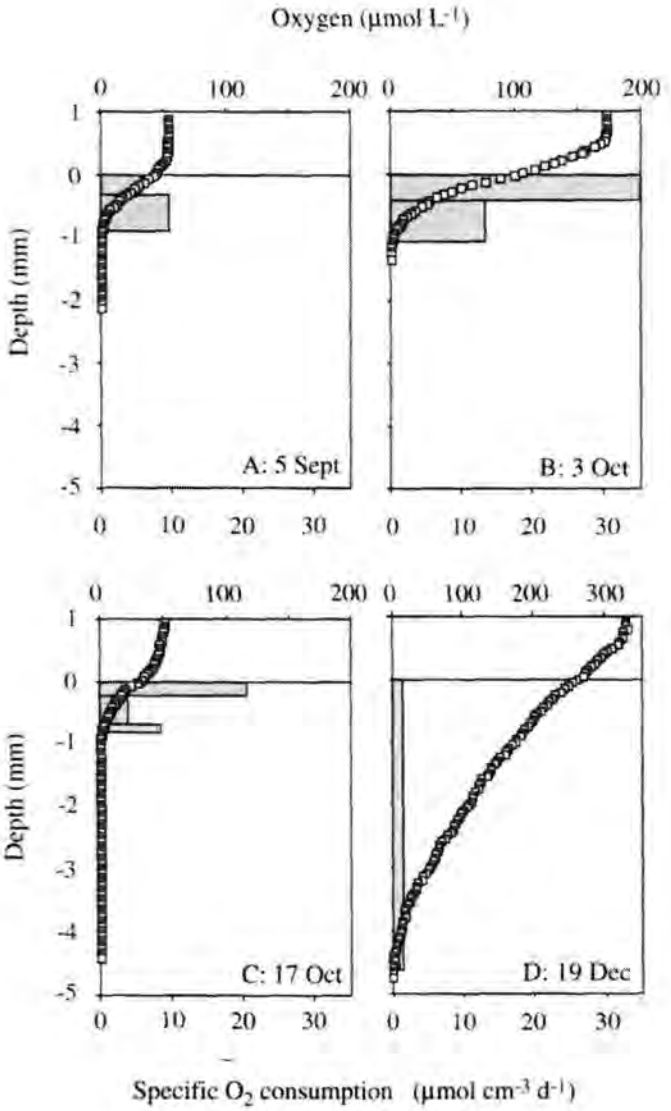

Figure 5. Typical O_2 microprofiles measured *in situ* on four different occasions during 1990. The horizontal line indicates the estimated position of the sediment surface. Grey boxes represent the volume specific O_2 consumption rates modelled from the curvature of the O_2 profiles.

By mid-September a bloom of dinoflagellates *(Ceratium* spp.) was deposited on the sediment surface and shortly after wind-induced seiching resulted in elevated O_2 concentration in the bottom water. The two events led to an intensified O_2 consumption at the sediment-water interface, which was suddenly enriched with labile organic material, and resulted in an increased O_2 penetration depth (Fig. 5B). Subsequently, the ongoing mineralization resulted in declining O_2 concentration of the bottom water and a decrease in the O_2 penetration depth (Fig. 5C). The volume specific O_2 consumption calculated from profiles measured on 17th October reflected intensified activity at the sediment surface and at the oxic-anoxic interface below. During winter, low sedimentation rates and high bottom water O_2 concentration resulted in a deep oxic zone with a low, depth-independent volume specific O_2 consumption rate (Fig. 5D).

The diffusive O_2 uptake calculated from the *in situ* DBL profiles showed two seasonal maxima (Fig. 6A), coinciding with distinct sedimentation events in April and in October 1990 (Valeur et al. 1995; Pejrup et al 1996). The following spring bloom in April 1991 was less distinct but also caused an elevated DOU (Fig. 6A). The summer and winter were characterized by relatively low O_2 consumption rates, presumably due to limiting O_2 concentrations in summer and low organic sedimentations rates in winter. The seasonal pattern was recognized also in the DOU determined in recovered sediment cores yet the temporal dynamics were less distinct (Fig. 6B). The O_2 consumption modeled from interstitial *in situ* O_2 microprofiles revealed a similar seasonal pattern as the *in situ* DBL measurements (Fig. 6C). On a yearly basis (from May 1990 to May 1991) the *in situ* DOU was 5.5 mol m^{-2} yr^{-1}, while the laboratory determined DOU was 5.1 mol m^{-2}. The depth integrated volume specific O_2 consumption of the *in situ* microprofiles revealed a yearly O_2 consumption rate of only 4.2 mol m^{-2} yr^{-1}. Generally, data from 1992 followed the pattern of 1990 (Fig. 6).

The moderate seasonality in DOU actually covers much more intense dynamics in the aerobic benthic activity. The average volume specific activity, as calculated from the ratio between the *in situ* DOU and O_2 penetration depth, varied by a factor of ~13 (Fig 7). The previously resolved activity peaks becomes more distinct and reflects the availability of electron donors in the oxic zone, either as organic carbon or inorganic products of the anaerobic degradation.

By far the most microprofiles reflected a smoothly declining O_2 concentration within the sediment (Fig. 5). However, on a few occasions measurements directly indicated that fauna activity was of importance for the benthic O_2 exchange. The *in situ* microprofile of Fig. 8 clearly reflects a rhythmic irrigation of a burrowed polychaete affecting the distribution at the sediment water interface. Apparently, the microelectrode passed along the vertically oriented burrow in which the polychaete pumped O_2 down to otherwise anoxic sediment (Fig. 8).

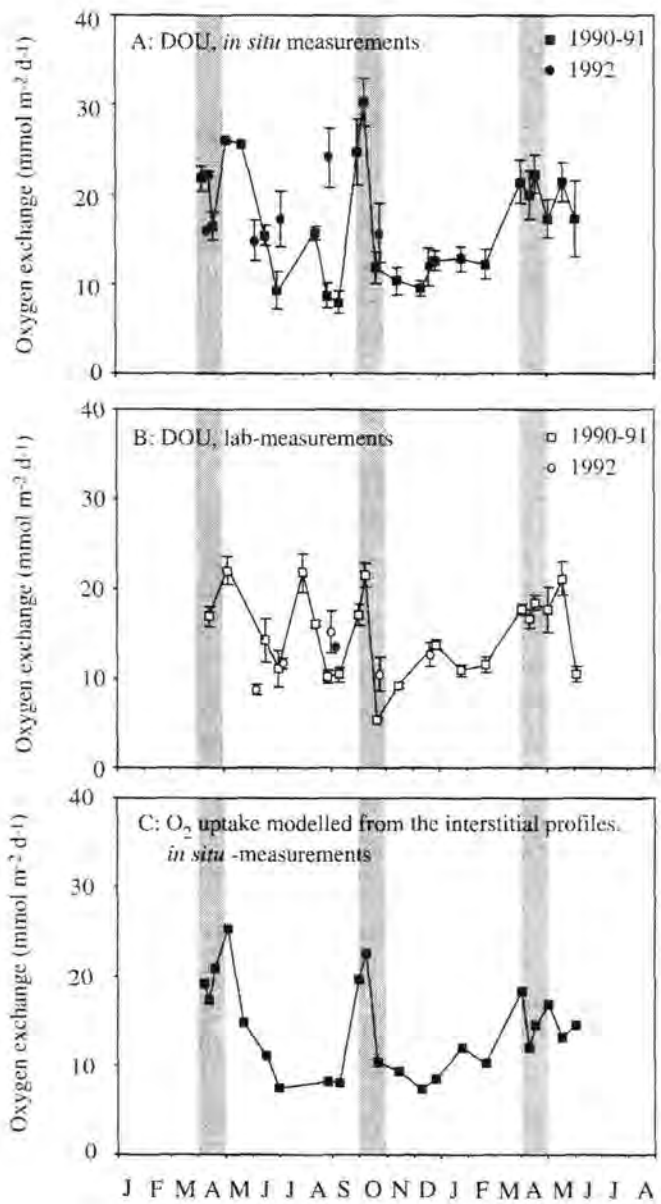

Figure 6. A) *In situ* DOU calculated from O_2 gradients measured within the DBL during 1990-1991. B) Laboratory DOU calculated from O_2 gradients measured within the DBL during 1990-1991. C) Area O_2 consumption rates modelled from the curvature of the average interstitial O_2 microprofiles measured *in situ* during 1990-1991. Circles of each panel represent measurements performed during 1992. The shaded areas represent periods of intensified sedimentation as deduced from Valeur et al. (1995).

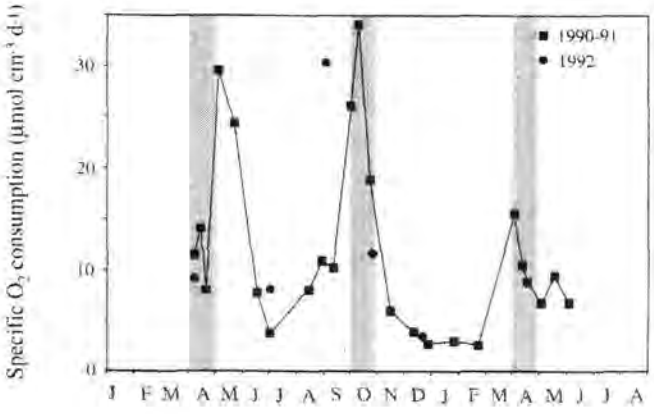

Figure 7. Average volume specified O_2 consumption rates within the oxic sediment calculated from the DOU and the O_2 penetration depth of *in situ* profiles measured during 1990-1991 (black squares) and in 1992 (black circles). The shaded areas represent periods of intensified sedimentation as deduced from Valeur et al. (1995).

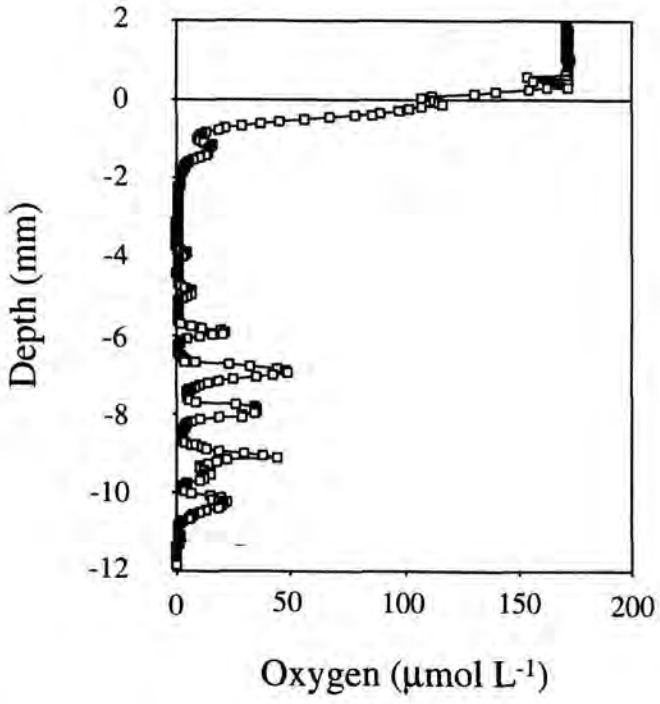

Figure 8. An *in situ* O_2 microprofile measured in the vicinity of an actively ventilated polychaete burrow. The horizontal line indicates the estimated position of the sediment surface.

The total O_2 uptake measured in recovered sediment cores was in general higher than the microelectrode-derived O_2 uptake rates (Fig. 9A). There was no distinct seasonal pattern in the laboratory determined TOU, although the values tended to reach a minimum during winter (Fig. 9A). The average TOU for 1990-1991 was 18.7 mmol m^{-2} d^{-1}, and the integrated yearly TOU was 6.5 mol m^{-2} yr^{-1}. The corresponding values obtained the following year were 14.8 mmol m^{-2} d^{-1} and 5.1 mol m^{-2} yr^{-1}, respectively. The somewhat lower rates during 1992 were mainly caused by the O_2 depletion event primo June that presumably repressed the TOU (Fig. 9A). The *in situ* determined TOU during 1992 also showed minimal values during winter (Fig. 9B), but the absolute rates were significantly higher than in laboratory incubations. On nine events, the TOU was measured simultaneously *in situ* and in the laboratory, and on the average the *in situ* rates were higher by a factor of 2.0 ± 0.6. There was, however, no clear relation between the recovered macrofauna biomass and the *in situ* TOU (see tables in annex). The annual TOU as measured *in situ* was 10,1 mol m^{-2} yr^{-1}. The yearly benthic O_2 uptake determined by different techniques thereby varied between 4.2 and 10.1 mol m^{-2} yr^{-1} for the period of 1990-1992 (Table 1).

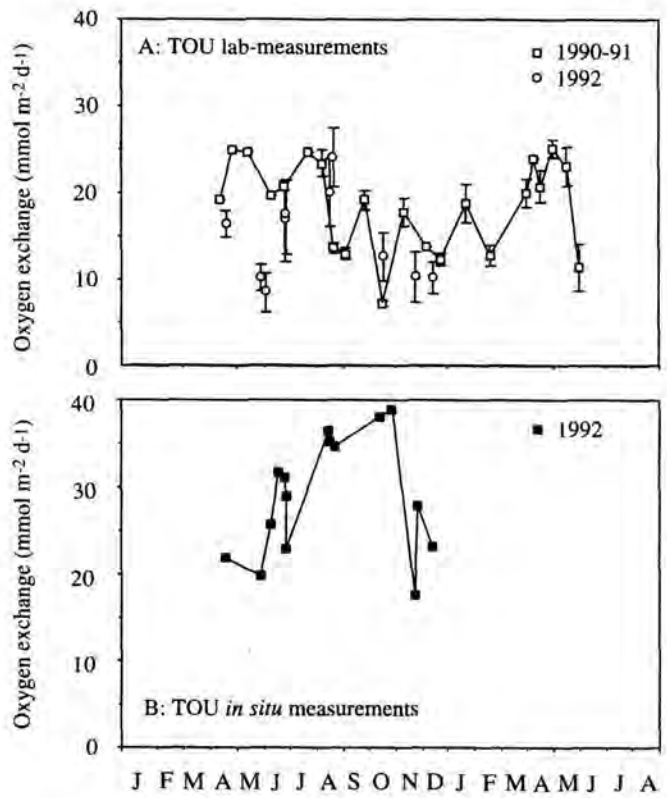

Figure 9. A) TOU measured in the laboratory in recovered sediment cores during 1990-1991 and 1992. B) *In situ* TOU measured during 1992.

Table 1 Annual benthic oxygen uptake rates in Aarhus Bay (mol $m^{-2} yr^{-1}$).

	1990/1991 (May-May)	1992 (Jan-Jan)
DOU - measured in the lab	5.1 (5.7)	-
TOU - measured in the lab	6.5	5.1
DOU - measured *in situ*	5.5 (6.2)	-
O_2 consumption – modeled *in situ*	4.2	-
TOU- measured *in situ*	-	10.1

Numbers in parenthesis represent values accounting for a 3D diffusive interface (see text).

Two characteristic examples of the benthic microtopography at the investigated site are presented as shaded reliefs in Fig. 10. Most structures can be recognized as biogenic structures such as fecal mounds and gastropod tracks (Fig. 10A, 10B). The typical vertical distance between maximal and minimal altitude in the scans was ~5 mm. The 3D sediment-water interface area as estimated by matrix smoothing of the original scans (Røy et al. 2992) was on the average 106% ± 1% of the horizontal plane area. Apart from the fact that the area across which diffusion takes place is larger than the plane horizontal area, the 3D topographic structure of the interface also means that a vertically aligned microelectrode will approach the sediment surface at an angle (Jørgensen and Des Marais, 1992). The average angle between the horizontal plane and the sediment surface was calculated by simple trigonometry to be 19.37° (cf. Jørgensen and Des Marais, 1992). Due to the 3D structure of the sediment-water interface, the DOU calculated from the vertically obtained microprofiles will underestimate the actual diffusive O_2 uptake rate. The ratio between the 3D and the 1D diffusive O_2 uptake equals (A'/A) x (δ/δ'), where A'/A represents the ratio between the area of the slanted sediment surface and the area of the horizontal plane, while (A/A') is the ratio between the actual DBL thickness perpendicular to the slanted sediment surface and the measured DBL thickness (for details see Jørgensen and Des Marais, 1990; Røy et al 2002). Accounting for the average DBL thickness measured *in situ* (451 µm), the ratio between the 3D and 1D diffusive O_2 uptake varied between 1.0 and 1.9 for the two selected horizontal transects (Fig. 10E and 10F). The average difference between 3D and 1D DOU based on all the performed scans was a factor of 1.12 ± 0.01.

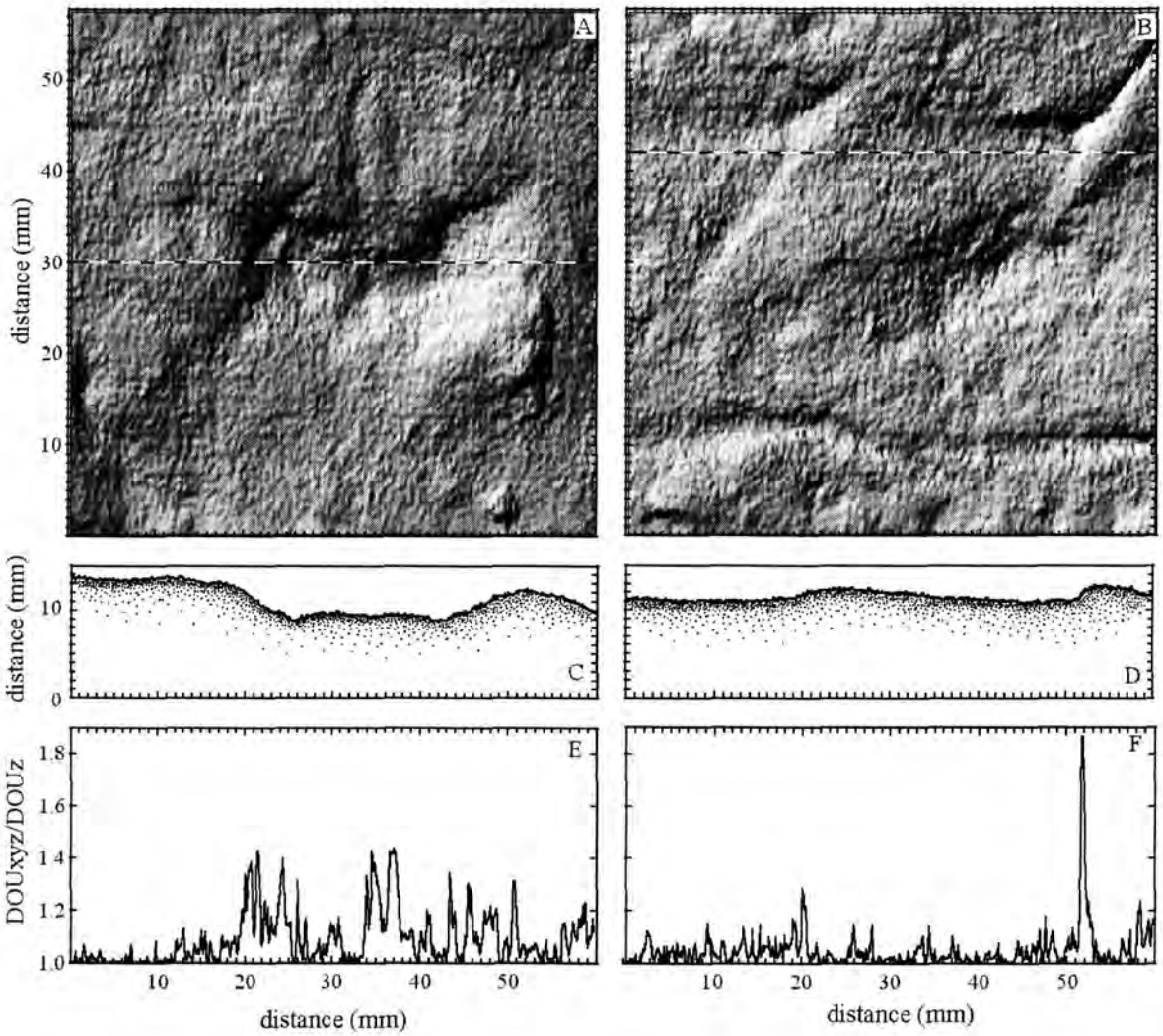

Figure 10. A, B) Examples of 30 cm^2 sediment topography presented as shaded reliefs. C, D) Extracted topographic profiles. The lines in A and B represent the positions of the extracted profiles presented in C and D,. E, F) The relation between the diffusive flux along the vertical axis as measured with microelectrodes and the true 3D diffusive flux taking into account all spatial dimensions. The ratio has been calculated along the transects shown in A, C and B, D.

DISCUSSION

In situ versus laboratory determined O_2 uptake

Microprofile measurements performed at water depths >1000 m have demonstrated that core recovery affects the interstitial O_2 distribution (Glud et al. 1994a; Glud et al. 1999; Sauter et al. 2001). Temperature and pressure induced artifacts lead to elevated DOU and underestimated O_2 penetration depths. For coastal environments with low O_2 penetration depth, transient temperature induced disturbances are quickly reequilibrated when *in situ* conditions are re-established in the laboratory, and *in situ* and laboratory obtained microprofiles generally show good agreement (Glud et al. 1998; 1999). There are, however,

few comparative studies of *in situ* determined microprofiles from coastal environments. In the present study, laboratory determined DOU underestimated the *in situ* rates while the O_2 penetration depth was generally overestimated (Fig. 11).

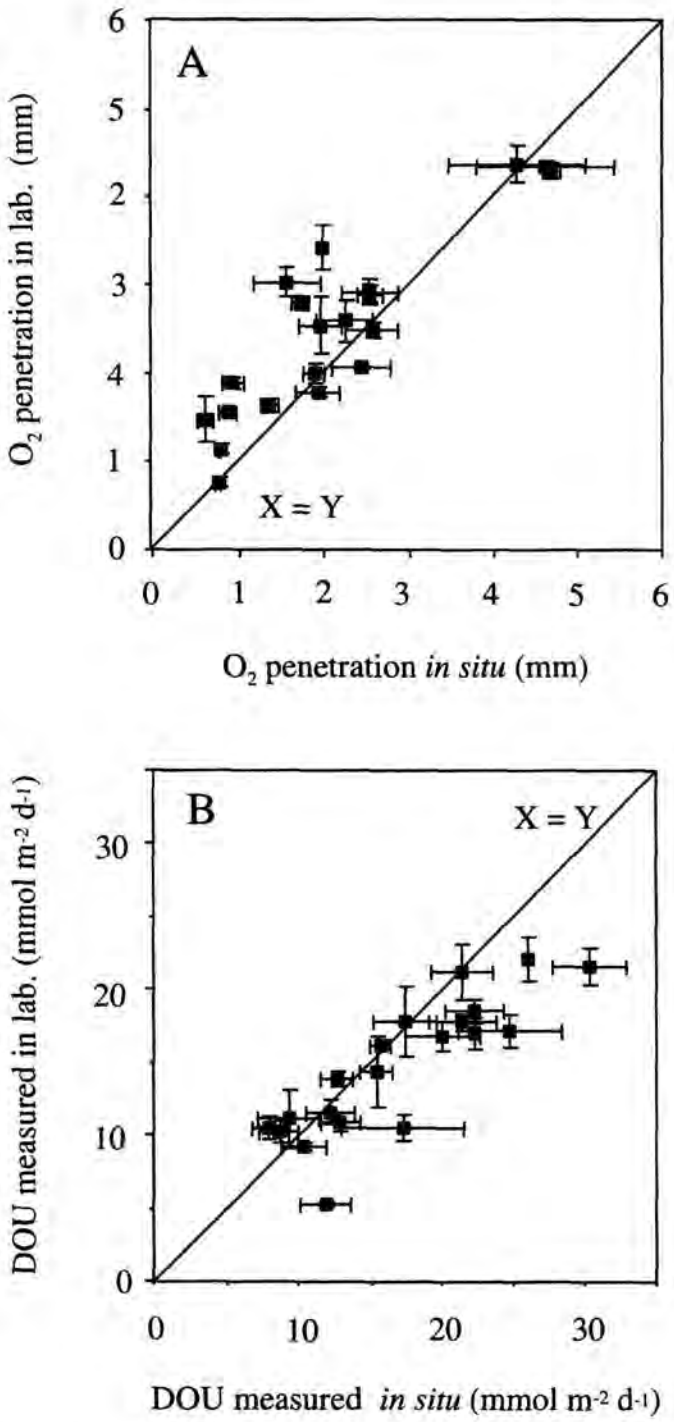

Figure 11. A) O_2 penetration depths measured in the laboratory compared to the corresponding values measured *in situ*. B) DOU measured in the laboratory compared to the corresponding values measured *in situ*. The line X=Y is included in both panels.

The effect was most pronounced in highly active sediment with shallow O_2 penetration depths, where the interfacial O_2 dynamics were most sensitive to changes in the environmental controls (Fig. 11). Even though cores were taken to re-establish at *in situ* conditions in the laboratory, small differences in temperature or O_2 concentration cannot be excluded, and irreversible disturbances during core recovery could have affected the laboratory measurements. Differences in DBL thickness can probably be neglected (see below). We have no general explanation for the observed difference. However, our data underline the importance of performing benthic exchange measurements under *in situ* conditions, or preferentially *in situ.*

In situ and laboratory TOU measured in parallel clearly differed. On the average *in situ* rates were 2.0 ± 0.6 (n=9) times higher than laboratory determined rates. The discrepancy was due to an exclusion of larger fauna specimens in the relatively small sediment cores used for the laboratory incubations. By selecting undisturbed sediment cores, larger infauna tends to be excluded since animals and their burrows have been disturbed, destroyed, or blocked during core insertion. Furthermore, successfully recovered specimens may be inhibited in their pumping and respiration activity as a result of the mechanical disturbance associated with core recovery. In general, large sediment enclosures are to be preferred in order to obtain reliable total benthic exchange rates. The *in situ* determined TOU represents only single deployments and the statistical liability of the measurements cannot be directly assessed. However, *in situ* incubations performed on subsequent days resulted in similar TOU (and FOU) values (Fig. 9B), indicating that single deployments actually represent the fauna related O_2 uptake well. A recent computer study simulating multiple chamber insertions on a virtual seafloor inhabited by user-defined macrofauna communities concluded that single deployments with the applied chamber would quantify the actual TOU of the macrofauna-inhabited sediment in Aarhus Bay during summer with a relative error of 9% (Glud & Blackburn 2002). This precision is in the same range as the standard deviations of our DOU measurements (Fig. 6). We therefore argue that the *in situ* TOU is the most correct measure of the actual benthic O_2 consumption rate in the present study.

Importance of the DBL for the DOU

The DBL thickness determined on the basis of *in situ* microprofiles varied between 299 and 706 µm, with an average value of 451 µm (n=98). The corresponding range for the laboratory measurements was 313-590 µm and the average was 457 µm (n=138). The *in situ*

DBL conditions were, thus, closely reproduced by the laboratory set-up. The available data on *in situ* determined DBL thicknesses are limited but the present values are in the lower range of previously presented values derived from *in situ* microprofiles (Archer et al. 1989; Glud et al 1994a; Glud et al 1998; Jørgensen 2001; Wenzhöfer et al. 2001). Most of these values are, however, obtained at significantly larger water depths where a lower mean flow velocity can be expected. A microsensor derived DBL thickness generally underestimates the actual DBL thickness, as microelectrodes have been shown to perturb the DBL resulting in a 25-45% compression of the DBL thickness right below the sensor tip (Glud et al. 1994b). Therefore, the microprofile-derived DBL thickness should be regarded as minimum value.

The mean diffusion time, t_{DBL}, for O_2 molecules to cross the DBL can be estimated as $t_{DBL} = \pi(\delta_{DBL})^2 / 4\ D_0$, where δ_{DBL} is the DBL-thickness and D_0 is the temperature corrected molecular diffusion coefficient of O_2 (Steen-Knudsen 2002). Whether the transport time through the DBL limits the benthic O_2 consumption rate depends on the mean lifetime of an O_2 molecule within the sediment. During winter, the O_2 availability was high, the activity was low and, consequently, the oxic zone was relatively deep as shown in Fig. 5D. The volume specific O_2 consumption rate was depth independent, and only 16% of the decrease in benthic O_2 concentration occurred within the DBL. The amount of O_2 dissolved in the porewater could sustain the benthic O_2 consumption for 41 min, while the average transport time for an O_2 molecule across the 656 µm thick DBL was 4.7 min. The O_2 flux was therefore mainly regulated by the consumption within the sediment, and changes in the DBL thickness would only affect the DOU marginally.

During early October, 45% of the O_2 decline occurred in the DBL (Fig. 5B), the entire interstitial O_2 pool would only sustain the O_2 consumption for 1.6 min, and the DBL passage for an O_2 molecule on the average took 2.1 min. A reduction in the DBL thickness could therefore potentially have stimulated the O_2 uptake during this period.

However, the volume specific O_2 consumption was not depth independent (Fig. 5B), and a significant fraction of the O_2 consumption was probably related to the oxidation of solutes from anaerobic degradation (e.g. NH^{4+}, Fe^{2+}) as indicated by the high activity at the oxic-anoxic interface. In this case a more detailed modeling of the mobility of reduced constituents is required to quantitatively evaluate the importance of DBL impedance for DOU or for the O_2 penetration depth (Jørgensen and Boudreau 2001).

Microtophography and diffusive flux

Based on the microtopographic mapping, the difference between a 3D and a 1D DOU calculation was a factor of 1.12 ± 0.01. In other words, 10.7 ± 1.0% of the total diffusive flux was not accounted for by the simple one-dimensional microprofile approach. The annual TOU measured in the laboratory was 22% higher than the corresponding DOU (Table 1). About half of this difference can now be ascribed to the simplified approach of performing a one-dimensional calculation on a truly three-dimensional interface.

A topographically structured oxic zone blankets the anoxic sediment, and vertical oxygen-profiles penetrate this oxic skin at an angle and thereby overestimate the O_2 penetration depth. The average factor by which the actual O_2 penetration depth is overestimated by a vertical measurement can be calculated by simple trigonometry to be l/cos (19.37) or 1.06 (Jørgensen and Des Marais 1990; Røy et al. 2002). The 6% overestimation by the vertical approach cannot fully explain the observed difference between the DOU and the depth integrated O_2 consumption as derived from the interstitial microprofiles (Table 1). We used the average porosity of the upper 4 mm to assess the tortuosity corrected diffusive coefficient of the interstitium (see materials and methods). In reality the porosity can be expected to decrease with sediment depth and our simplification could have biased the calculated depth distribution of the volume specific O_2 consumption rates. However, again this cannot explain the observed discrepancy between the two independent measures of the diffusive mediated O_2 uptake. A number of studies have documented that interstitial meiofauna activity can lead to enhanced dispersal and solute transport (Aller and Aller 1992; Glud and Fenchel 1999; Rysgaard et al. 2000). Such activity can increase the solute transport coefficients within the sediment and for the given study a 30% higher effective diffusion coefficient of the interstitium would lead to identical DOU and modelled depth integrated O_2 consumption rates. We propose that this is the main cause for the observed difference between the two microprofile-based approaches for determination of the O_2 uptake.

Importance for fauna for the benthic O_2 uptake

The difference between TOU and DOU quantified in sediment cores during the present study ranged between 0.8 and 8.7 mmol m^{-2} d^{-1}, with an average value of 4.0 ± 3.1 mmol m^{-2} d^{-1}. Accounting for the topographic effect on the DOU, this only leaves an annual FOU of 0.79 mol m^{-2} yr^{-1} in the recovered sediment cores. The corresponding *in situ* value for FOU was, however, 5 times higher, 3.94 mol m^{-2} yr^{-1} or ~40% of the measured TOU (Fig. 12).

Recovered undisturbed sediment cores selected for laboratory incubation clearly undersampled the *in situ* density of macrofauna especially for the larger specimens. The few cores that contained an active macrofauna specimen on a given day indeed revealed an elevated TOU. However, on a seasonal scale there was no clear relation between the biomass of the enclosed fauna during a given incubation and the measured TOU or calculated FOU (see Web Appendix 1 and 2 at the end of the chapter). The reason is presumably that fauna biomass poorly reflects the fauna mediated O_2 uptake of a diverse benthic community undergoing seasonal changes in temperature and bottom water O_2 concentration. To what extent a given biomass stimulates the benthic O_2 consumption rate naturally depends on functional characteristics of the fauna (deposit feeding, filter feeding, irrigation patterns etc.), but to what extent a given activity affects the benthic O_2 uptake also depends on the redox state of the sediment, the O_2 penetration depth, the O_2 concentration of the bottom water and the temperature. The *in situ* TOU (or the FOU) quantified during a seasonal study does therefore not necessarily correlate well to enclosed biomass.

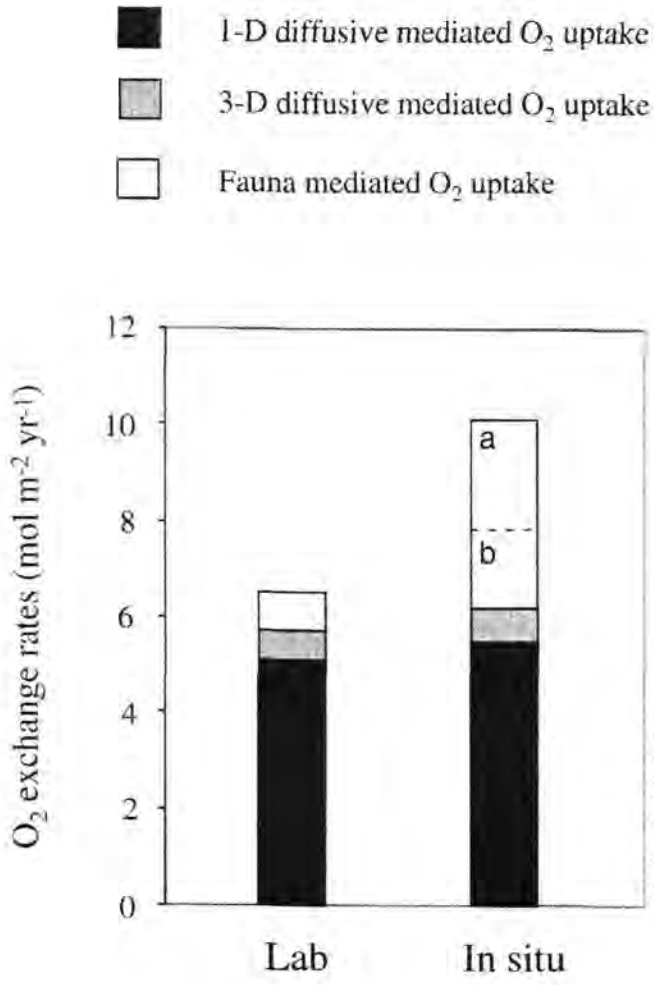

Figure 12. The various components of the TOU measured in the laboratory and *in situ*. The broken line divides the *in situ* FOU into a) the enhanced benthic O_2 consumption caused by animal activity (e.g. irrigation) and b) the calculated maximum macrofauna respiration.

The sediment recovered from the 15 *in situ* incubations with the chamber lander contained ~25 species of macrofauna, with an average density of 2800 ± 700 m^{-2} and a dry weight of 89.5 ± 30.0 g m^{-2} (including shell weight). Both in abundance and biomass, small specimens of bivalves (*Abra alba, Mysella bidendata, Corbula gibba,* and *Macoma calcarea)* were dominant, while polychaetes (e.g. *Terrebelides stroemi, Nephtys* sp. and *Pectinaria* sp.) and echinoderms (e.g. *Ophiura albida* and *Echinocardium cordatum*) were encountered less frequently. These observations were supported by survey data obtained by the local county, that quantifies the abundance and biomass of each taxonomic group at the investigated site on a monthly basis (Technical Report 1998, County of Aarhus – www.aaa.dk). Using their values for the 9 dominant species (accounting for ~80% of the total abundance) at the investigated site during 1996 and the empirical relation between biomass and metabolic rate for marine invertebrates as established by Gerlach et al. (1985) the annual O_2 consumption of the benthic fauna was calculated to be ~1.64 mol m^{-2}. This estimate must be taken as a maxiumum since the applied relation is based on a temperature of 20°C. There is no simple way to recalculate to the correct *in situ* temperature (Banse 1982; Gerlach 1985). The calculated fauna respiration thus accounts for a maximum of ~40% of the annual FOU. The remainder is ascribed to stimulated microbial activity, especially along burrows and funnels of irrigating specimens. These calculations document that the fauna is indeed important for the benthic O_2 uptake in the studied sediment, but that the fauna respiration itself is the minor part of the total fauna-related O_2 consumption (Fig. 12). In environments rich in benthic fauna, *in situ* incubations by relatively large chambers are thus required in order to obtain realistic estimates of the benthic O_2 consumption rate.

Importance of benthic aerobic mineralization in Aarhus Bay

The annual net photosynthesis during 1991 in Aarhus Bay amounted to 21.8 mol C m^{-2} yr^{-1}, while the measured planktonic respiration was 14.8 mol C m^{-2} yr^{-1} (Jørgensen 1996). This leaves 7.0 mol C m^{-2} yr^{-1} for the entire benthic community, not accounting for lateral import or export. Sediment trap measurements performed during the same period concluded that the annual net deposition at the seafloor was somewhat higher, 9.9 mol C m^{-2} yr^{-1} (Valeur et al. 1995), while determination of the sediment accumulation rate showed that 2.1 mol C m^{-2} yr^{-1} was buried below the bioturbated horizon (Jørgensen, 1996). The difference, 7.8 mol C m^{-2} yr^{-1}, should thus be available for the benthic community.

As argued above, the *in situ* TOU represents our best estimate of the integrated benthic activity, and by assuming an RQ (respiratory quotient) of 1.00 the annual benthic

mineralization rate during 1992 was 10.1 mol C m^{-2} yr^{-1}. This is close to the net deposition rate and corresponds to ~46% of the net primary production in the area. Taken together with the distinct temporal pattern in sedimentation and DOU, this strongly indicates a tight pelagic-benthic coupling at the investigated site

The anaerobic degradation in the sediment of Aarhus Bay is dominated by sulfate reduction. Accounting for the upper 16 cm of the sediment the sulfate reduction during 1990-1991 was responsible for a carbon mineralization of 4.5 mol C yr^{-1}, while iron reduction accounted for 1.3 mol C yr^{-1} (Thamdrup et al. 1994). Manganese reduction was without quantitative importance (Thamdrup 2000), while denitrification amounted to 0.15 mol C yr^{-1} (Jørgensen 1996). Assuming a complete aerobic oxidation of the reduced sulfur and iron on an annual scale, the O_2 consumption required for H_2S and Fe(II) oxidation was equivalent to 5.8 mol yr^{-1} or 57% of the total O_2 uptake. The aerobic degradation of organic carbon accounted for 4.2 mol C m^{-2} yr^{-1} (10.1- (4.5+1.3+0.15)) or 42% of the total benthic mineralization. This is relatively high compared to previously presented studies on shelf and costal sediments where the aerobic mineralization generally is estimated to be in the range of 5-25% of the total benthic mineralization (Thamdrup 2000). However, as shown in the present study, the FOU can be significant and in many instances it may be poorly represented by traditional incubation techniques. Consequently, the relative contribution of the aerobic mineralization may be underestimated correspondingly.

ACKNOWLEDGEMENT

We thank "Skipper-Hans" for many joyful hours at sea, Fritz Hansen for skilful technical assistance, and Lars B. Pedersen and Anni Glud for producing the numerous electrodes used during this study. The study received financial support from the Danish Environmental Foundation and the Max Planck Society – the support is gratefully acknowledged. We thank Bent Sømod for providing the fauna data collected by the County of Aarhus, Denmark. Two anonymous reviewers are thanked for constructive criticism that helped improving the manuscript.

REFERENCES

Aller, R.C. 1998. Benthic fauna and biogeochemical processes in marine sediments: The role of burrow structures. P. 301-338. *In* Blackburn, T.H., and J. Sørensen (eds), Nitrogen cycling in coastal waters. Wiley & Sons.

Aller, R.C., and J.Y. Aller 1992. Meiofauna and solute transport in marine muds. Limnol. Oceanogr .37: 1018-1033.

Archer, D., S. Emerson, and C.R. Smith. 1989. Direct measurements of the diffusive sublayer at the deep seafloor using microelectrodes. Nature 340: 623-626.

Archer, D., and A. Devol. 1992. Benthic oxygen fluxes on the Washington shelf and slope: A comparison of *in situ* microelectrode and chamber flux measurements. Limnol. Oceanogr. 37: 614-629.

Banse, K. 1982. Mass-scaled rates of respiration and intrinsic growth in very small invertebrates. Mar. Ecol. Prog. Ser 9: 281-297.

Berg, P., N. Risgaard-Petersen, and S. Rysgaard. 1998. Interpretations of measured concentrations profiles in sediment porewater. Limnol. Oceanogr. 81: 289-303.

Boudreau, B.P., and N.L.Jr. Guinasso. 1982. The influence of a diffusive sublayer on accretion, dissolution, and diagenesis at the seafloor, p. 115-145. *In* Fanning K.A., and F.T. Manheim (eds), The dynamic environment of the ocean seafloor. Lexington Books.

Boudreau, B.P., 1988. Mass-transport constraints on the growth of discodial ferromanganese nodules. Amr. J. Science 288: 777-797.

Bouldin, D.R. 1968. Models for describing the diffusion of oxygen and other mobile constituents across the mud-water interface. J. Ecol. 56: 77-87. 22

Broecker, W.S., and T.H. Peng. 1974. Gas exchange rates between air and sea. Tellus 26: 21-35.

Crank, J. 1983. The mathematics of diffusion. Clarendon Press. Oxford. Fenchel, T. 1996. Worm burrows and oxic microniches in marine sediments. I. Spatial and temporal scales. Mar. Biol. 127: 289-295.

Gerlach, S.A., A. Hahn, and M. Schrage. 1985.Size spectra of benthic biomass and metabolism. Mar. Ecol. Prog. Ser. 26: 161-173.

Glud, R.N., J.K. Gundersen, B.B. Jørgensen, N.P. Revsbech, and H.D. Schulz, 1994a. Diffusive and total oxygen uptake of deep-sea sediments in the eastern South Atlantic Ocean: *In situ* and laboratory measurements. Deep Sea Res. 41: 1767-1788.

Glud, R.N., J.K. Gundersen, N.P. Revsbech, and B.B. Jørgensen. 1994b. Effects on the diffusive boundary layer imposed by microelectrodes. Limnol. Oceanogr. 39: 462-467.

Glud, R.N., J.K. Gundersen, N.P. Revsbech, B.B. Jørgensen, and M. Huettel. 1995. Calibration and performance of the stirred flux chamber from the benthic lander, Elinor. Deep Sea Res. 42: 1029-1042.

Glud, R.N., O. Holby, F. Hoffman, and D.E. Canfield. 1998. Benthic mineralization and exchange in Arctic sediments (Svalbard, Norway). Mar. Ecol. Prog. Ser. 173: 237-251.

Glud, R.N., J.K. Gundersen, and O. Holby. 1999. Benthic *in situ* respiration in the upwelling area off central Chile. Mar. Ecol. Prog. Ser. 186: 9-18.

Glud, R.N., and T. Fenchel. 1999. The importance of ciliates for interstitial solute transport in benthic communities. Mar. Ecol. Prog. Ser. 186: 87-93. 23

Glud, R.N., J.K. Gundersen, and N.B. Ramsing. 2000. Electrochemical and optical oxygen microsensors for *in situ* measurements, p. 19-72. In Buffle J., and G. Horvai (eds), *in situ* monitoring of aquatic systems: Chemical analysis and speciation. Wiley & Sons.

Glud, R.N., and N. Blackburn. 2002. The effects of chamber size on *in situ* benthic oxygen uptake measurements: A simulation study. Ophelia 56: 23-31.

Gundersen, J.K., and B.B. Jørgensen. 1990. Microstructure of diffusive boundary layers and the oxygen uptake of the sea floor. Nature 345: 604-607.

Gundersen, J.K., R.N. Glud and B.B. Jørgensen. 1995. Havbundens iltomsætning. Havforskning fra Miljøstyrelsen 57, 155 pp Miljøstyrelsen, Copenhagen.

Iversen, N., and B.B. Jørgensen. 1993. Diffusion coefficients of sulfate and methane in marine sediments: Influence of porosity. Geochim. Cosmochim. Acta 57: 571-578.

Jørgensen, B.B., and N.P Revsbech. 1985. Diffusive boundary layers and the oxygen uptake of sediments and detritus. Limnol. Oceanogr. 30: 111-122.

Jørgensen, B.B., and D.J. Des Marais. 1990. The diffusive boundary layer of sediments: Oxygen microgradients over a microbial mat. Limnol. Oceanogr. 35: 1343-1355.

Jørgensen, B.B., 1996. Case study – Aarhus Bay, p. 137-154. *In* Jørgensen, B.B., and K. Richardson (eds), Eutrophication in Coastal Marine Ecosystems. Amer. Geophys. Union.

Jørgensen, B.B., and B.P. Boudreau. 2001. Diagenesis and sediment-water exchange, pp. 211- 238. In Boudreau, B.P., and B.B. Jørgensen (eds).The benthic boundary layer. Oxford Univ. Press. 24

Jørgensen, B.B., 2001. Life in the diffusive boundary layer, pp. 348-373. In Bodreau, B.P., and B.B. Jørgensen (eds).The benthic boundary layer. Oxford. Univ. Press. Kanneworff, E., and W. Nicolaisen. 1973. The Haps, a frame supported bottom corer. Ophelia 10: 109-116.

Kristensen, E. 1988. Benthic fauna and biogeochemical processes in marine sediments: Microbial activity and fluxes, p. 275-299. *In* Blackburn, T.H., and J. Sørensen (eds). Nitrogen cycling in coastal waters. Wiley & Sons.

Li, Y.H., and S. Gregory. 1974. Diffusion of ions in sea-water and in deep-sea sediments. Geochim. Cosmochim. Acta 38: 703-714.

Nielsen, L.P., P.C. Christensen, N.P. Revsbech, and J. Sørensen. 1990. Denitrification and oxygen respiration in biofilms studied with a microsensor for nitrous oxide and oxygen. Microb. Ecol. 19: 63-72.

Pejrup, M., J. Valeur, and A. Jensen. 1996. Vertical fluxes of particulate matter in Aarhus Bight, Denmark. Cont .Shelf. Res. 16: 1047-1064.

Rasmussen, H., and B.B. Jørgensen, 1992. Microelectrode studies of seasonal oxygen uptake in a coastal sediment: role of molecular diffusion. Mar. Ecol. Prog .Ser. 81: 289-303.

Revsbech, N. P., J. Sørensen, T.H. Blackburn, and J.P. Lomholt. 1980. Distribution of oxygen in marine sediments measured with a microelectrode. Limnol. Ocenogr. 25: 403-411.

Revsbech, N. P., and B.B. Jørgensen. 1983. Photosynthesis of benthic microflora measured with high spatial resolution by the oxygen microprofile method: Capabilities and limitations of the method. Limnol. Oceanogr. 28: 749-756. 25

Revsbech, N. P., and B.B. Jørgensen. 1986. Microelectrodes and their use in microbial ecology, p. 293-352. *In*, Marshall K.C. (ed), Advances in Microbial Ecology.

Revsbech, N. P., 1989. An oxygen microelectrode with a guard cathode. Limnol. Oceanogr. 34: 474-478.

Rysgaard, S.P., P.B. Christensen, M.V. Sørensen. P. Funch, and P. Berg. 2000. Marine meiofauna and nitrogen mineralization in sandy and soft sediments of Disko Bay, West Greenland. Aqua. Microb. Ecol. 21: 59-71.

Røy, H., M. Huettel, and B.B. Jørgensen. 2002. The role of small-scale sediment topography for oxygen flux across the diffusive boundary layer. Linmol. Oceanogr. 47: 837-847.

Sauter, E.J., M. Schlüter, and E. Suess. 2001. Organic carbon flux and remineralization in surface sediments from the northern North Atlantic derived from porewater oxygen microprofiles. Deep-Sea Res. 48: 529-553.

Sten-Knudsen. 2002. Biological membranes: Theory of transport, potentials and electrical impulses, pp 671. Cambridge University Press, Cambridge.

Thamdrup, B., H. Fossing, and B.B. Jørgensen. 1994. Manganese, iron, and sulphur cycling in a coastal marine sediment, Aarhus Bay, Denmark. Geochim. Cosmochim. Acta 58: 5115-5129.

Thamdrup, B., 2000. Microbial manganese and iron reduction in aquatic sediments. Adv. Microb. Ecol. 16: 41-84.

Thamdrup, B., and D.E. Canfield. 2000. Benthic respiration in aquatic sediments. P. 86-103. *In* Sala, O.E.R., R.B. Jackson, H.A. Mooney, and R.W. Horwarth (eds). Methods in Ecosystem Science Springer, New York. 26

Valeur, J.R., A. Jensen, and M. Pejrup. 1995. Turbidity, particle fluxes and mineralization of carbon and nitrogen in a shallow coastal area. Mar. Freshwater Res. 16: 409-418.

Wenzhöfer, F, M. Adler, O. Kohls, C. Hansen, B. Strotmann, S. Boehme, and H.D. Schulz. 2001b. Calcite dissolution driven by benthic mineralization in the deep-sea: *In situ* measurements of Ca2+, pH, pCO2. Geochim. Cosmochim. Acta 65: 2677-2690.

Web Appendix 1. Data presented in figure 3B, 4A, 4B, 6A, 6B, 9A, for details see text.

Day*	O_2 concentration (μmol L^{-1})	DOU lab (mmol m^{-2} d^{-1})	OP** lab (mm)	TOU lab (mmol m^{-2} d^{-1})	DOU *in situ* (mmol m^{-2} d^{-1})	OP** *in situ* (mm)
96, 90-91	320	-	-	-	21.8 ± 1.4	-1.89 ± 0.15
102, 90-91	258	16.9 ± 1.1	-3.02 ± 0.17	-	22.3 ± 0.3	-1.58 ± 0.40
109, 90-91	271	-	-	19.3 ± 1.5	16.4 ± 1.6	-2.05 ± 0.16
123, 90-91	175	22.0 ± 1.5	-	25.1 ± 0.7	26.1 ± 0.0	-0.88 ± 0.15
140, 90-91	169	-	-	24.8 ± 0.7	25.6 ± 0.0	-1.05
166, 90-91	174	14.3 ± 2.4	-2.53 ± 0.32	19.7 ± 3.6	15.4 ± 1.1	-1.98 ± 0.24
180, 90-91	178	11.1 ± 2.0	-2.05	20.8 ± 0.5	9.3 ± 2.1	-2.45 ± 0.35
207, 90-91	259	21.8 ± 2.1	-3.42 ± 0.26	24.8 ±	-	-2.00
223, 90-91	154	16.1 ± 0.3	-1.78 ± 0.05	23.4 ± 2.6	15.7 ± 0.7	-1.95 ± 0.26
236, 90-91	76	10.2 ± 0.8	-1.14 ± 0.05	13.7 ± 0.6	8.7 ± 1.4	-0.80
249, 90-91	53	10.5 ± 0.8	-0.76 ± 0.06	13.0 ± 0.7	8.0 ± 1.2	-0.78 ± 0.04
270, 90-91	152	17.1 ± 1.2	-1.88 ± 0.07	19.2 ± 1.1	24.8 ± 3.6	-0.95 ± 0.12
277, 90-91	172	21.5 ± 1.3	-1.55	-	30.3 ±2.6	-0.89 ± 0.10
290, 90-91	53	5.4 ± 0.1	-1.47 ± 0.25	7.2 ± 0.3	11.9 ± 1.7	-0.63 ± 0.10
314, 90-91	131	9.2 ± 0.3	-2.78 ± 0.08	17.8 ± 1.6	10.4 ± 1.5	-1.75 ± 0.10
340, 90-91	135	-	-	13.8 ± 0.5	9.5 ± 0.9	-2.43 ± 0.12
355, 90-91	322	13.8 ± 0.5	-4.35 ± 0.06	12.4 ± 0.8	12.7 ± 1.1	-4.63 ± 0.80
384, 90-91	259	10.9 ± 0.7	-4.37 ± 0.21	18.8 ± 2.2	12.9 ± 1.4	-4.29 ± 0.80
411, 90-91	330	11.6 ± 0.8	-4.29 ± 0.09	12.8 ± 1.2	12.2 ± 1.7	-4.70 ± 0.10
451, 90-91	197	17.7 ± 0.6	-1.63 ± 0.08	20.1 ±1.6	21.5 ± 2.4	-1.38 ± 0.10
460, 90-91	210	16.8 ± 1.1	-1.99 ± 0.11	24.0 ± 0.4	20.0 ± 2.7	-1.90 ± 0.12
467, 90-91	246	18.5 ± 0.8	-2.88 ± 0.10	20.8 ± 1.9	22.3 ± 2.1	-2.55 ± 0.14
481, 90-91	223	17.7 ± 2.4	-2.48 ± 0.09	25.1 ± 1.0	17.4 ± 2.2	-2.58 ± 0.30
497, 90-91	262	21.2 ± 1.9	-2.58 ± 0.24	23.1 ± 1.0	21.4 ±2.2	-2.26 ± 0.32
512, 90-91	228	10.6 ± 0.9	-2.91 ± 0.15	23.1 ± 2.2	17.3 ± 4.3	-2.55 ± 0.32
664, 90-91	174	-	-	11.4 ± 2.8	16.2 ± 5.3	-1.76 ± 0.30
154, 1992	66	8.8 ± 0.6	-1.13 ± 0.10	10.2 ± 1.5	14.9 ± 2.3	-2.32 ± 0.13
160, 1992	66	-	-	8.5 ± 2.3	-	-
181, 1992	171	-	-	16.8 ± 4.7	-	-
183, 1992	172	11.7 ± 0.6	-2.10 ± 0.04	17.2 ± 4.2	17.3 ± 3.1	-2.10
231, 1992	95	-	-	20.1 ± 3.9	-	-
239, 1992	95	15.2 ± 2.3	-1.09 ± 0.13	24.1 ± 3.4	24.1 ± 3.3	-0.80 ± 0.20
299, 1992	118	10.6 ± 1.9	-2.15 ± 0.06	12.7 ± 2.8	15.7 ± 3.3	-1.35 ± 0.09
327, 1992	-	-	-	10.3 ± 3.0	-	-
348, 1992	244	12.8 ± 1.3	-3.8 ± 0.20	10.2 ±1.8	11.9 ± 2.1	-3.78 ± 0.03

*Day 1 represents 1 January 1990, until 31 December 1991 after which days are renumbered from 1 again to align to the figures presented above.

** OP means O_2 penetration depth

Web appendix 2. Total O_2 uptake rates measured *in situ* (see Fig 9) and the dry weight of the enclosed macrofauna for details see text.

Day*	TOU (mmol m^{-2} d^{-1})	Dry weight of fauna (g m^{-2})
116	21.9	57.6
154	19.8	82.1
165	25.8	102.2
174	31.8	114.2
181	31.2	69.2
182	28.9	121.2
183	22.9	57.6
230	36.5	131.3
231	35.3	47.0
237	34.7	104.2
286	38.0	102.5
301	39.0	72.9
327	17.7	86.6
329	28.0	69.3
347	23.2	125.0

* Day 1 represents 1 January 1992

Oxygen uptake by aquatic sediments measured with a new non-invasive eddy correlation technique

Peter Berg, Hans Røy, Felix Janssen, Volker Meyer, Bo Barker Jørgensen, Markus Hüttel, Dirk de Beer

ABSTRACT

This paper presents a new non-intrusive technique for measuring sediment O_2 uptake, which in its concept differs fundamentally from other methods used today. In almost all natural aquatic environments, the vertical transport of O_2 through the water column towards the sediment surface is facilitated by turbulent mixing. The new technique relies on measuring two turbulent quantities simultaneously and at the same point in the water above the sediment: the fluctuating vertical velocity using an Acoustic Doppler Velocimeter and the fluctuating O_2 concentration using an O_2 microelectrode. From these two quantities, which typically are measured 10-50 cm above the sediment surface for a period of 10-20 min and at a frequency of 15-25 Hz, the vertical flux of O_2 towards the sediment surface is derived. Based on measurements performed under realistic field conditions and comparisons with *in situ* flux chamber measurements, we believe that the new technique is the optimal approach for determining O_2 uptake by sediments. The technique is superior to conventional methods as measurements are done under true *in situ* conditions without any disturbance of the sediment. Furthermore, the technique can be used for bio-irrigated or highly porous sediments, such as sands, where traditional methods often fail. While this paper only focuses on O_2 uptake by sediments, the technique can also be applied to other solutes that can be measured at sufficiently high temporal resolution.

INTRODUCTION

Consumption of O_2 in aquatic sediments is attributed to two types of reactions: aerobic decomposition of organic matter and oxidation of reduced products of anaerobic decay, including NH_4^+, Mn^{2+}, Fe^{2+}, H_2S, FeS, and FeS_2. Sediment O_2 uptake provides valuable information on these reactions and is a frequently measured parameter in biogeochemical studies of aquatic sediments. At the same time, it is a parameter that is often difficult to measure accurately with the methods available today.

Oxygen uptake by sediments is affected strongly by the transport processes responsible for the movement of O_2 from the overlying water down through the sediment. These transport processes include molecular diffusion, bioturbation (the diffusion-like transport caused by movements of fauna), bio-irrigation (the pumping activity of tube-dwelling animals) and current- or wave-driven advection. Recent studies have shown that bioturbation is often a significant transport process comparable in strength to molecular diffusion (Aller and Aller 1992; Forster et al. 1995; Berg et al. 2001). Likewise, bio-irrigation can be a dominant transport process in sediments densely populated by tube-dwelling animals (Aller 1983; Pelegri et al. 1994; Wang and Van Cappellen, 1996). Other transport processes also can stimulate O_2 uptake by sediments. Currents over an uneven bottom or wave action on more shallow sites can induce a significant advective transport, either through the interstitial pores in more permeable sediments such as sand, or through tubes and borrows created by fauna (Rutgers van der Loeff 1981; Savant et al. 1987; Thibodeaux and Boyle 1987; Shum 1992; Webster 1992; Webster and Tayler 1992). In some sediments, this advection is the dominant transport process and enhances O_2 uptake many-fold relative to uptake dominated by molecular diffusion (Forster et al. 1996; Lohse et al. 1996).

The two commonly used methods for determining O_2 uptake by sediments are laboratory measurements in recovered sediment cores kept in a controlled environment as close to the *in situ* conditions as possible (e.g., Rasmussen and Jørgensen 1992) and measurements with *in situ* chambers which isolate a fraction of the sediment surface and bottom water from the surroundings (e.g., Jahnke and Christiansen 1989). In both cases, the sediment O_2 uptake is determined by measuring O_2 depletion in the overlying water over time. Typically, sediment cores have a diameter of 5-10 cm while chambers cover a larger area of the sediment surface, for example 30 x 30 cm (Glud et al. 1998 and 1999).

One problem with these methods is that they may affect active transport processes that influence O_2 uptake in the undisturbed sediment. While a good representation of *in situ* molecular diffusion and also *in situ* bioturbation caused by smaller animals (meiofauna) can be obtained in sediment cores, this method tends to underestimate the effects of bioturbation and bio-irrigation caused by larger animals (macrofauna). Studies comparing O_2 uptake measured in cores and *in situ* chambers for the same sediment have found O_2 uptake to be several fold lower in cores. The difference was explained as a result of more realistic representation of irrigating macrofauna in the larger chambers (Glud et al. 1998, 1999 and 2003). When measurements are made in both sediment cores and *in situ* chambers the

overlying water is kept fully mixed by stirring. This induced rotational flow differs from naturally occurring flow patterns over the sediment surface and represents another problem of these conventional methods. For example, representative O_2 uptake generally can not be measured in cores or in *in situ* chambers where advective transport processes within the sediment are created by current or wave action (Huettel and Webster 2001; Reimers et al. 2001). In addition to these shortcomings, sediment core and *in situ* chamber measurements are difficult to perform when objects such as rocks, mussels, epifauna, and macroalgae are abundant either on the sediment surface or in the upper sediment layer. Under such circumstances it is difficult not to disturb the sediment considerably when cores are collected or when the *in situ* chambers are deployed.

In this paper we present a new non-intrusive technique for measuring O_2 uptake by aquatic sediments. In almost all natural environments, O_2 taken up such sediments is transported down through the water column by turbulent motions. The technique relies on measuring the turbulent fluctuations of the vertical velocity and the corresponding O_2 concentration, simultaneously and at the same point above the sediment surface. If such measurements are done with an adequate temporal resolution to capture these fluctuations and for a period long enough to obtain a statistically sound representation of their variations, then the vertical flux of O_2 can be derived. If possible to perform from a technical point of view, such measurements obviously do not suffer from the same shortcomings as sediment core and *in situ* chamber measurements because O_2 uptake is determined under true *in situ* conditions and without any disturbance of the sediment. This technique has been used for several decades to determine land-atmosphere exchanges of CO_2, moisture, and energy in the atmospheric boundary layer (e.g., Wyngaard 1989) and is commonly referred to as flux determination or measurement by eddy correlation. The latter term is adopted here. Despite the clear advantages of the technique, it has only been used a few times in aquatic environments to determine fluxes of energy, for example between water and sea ice (Fukuchi et al. 1997, Shirasawa et al. 1997). The obvious reason is that other than for temperature, it is difficult to construct a sensor that can measure scalar properties such as O_2 concentration in water at a well-defined point and with a sufficiently fast response to capture all turbulent fluctuations. However, as documented below, we have been able to make these measurements with O_2 microelectrodes specially constructed to have a fast response. The fluctuating vertical velocity is measured using a standard instrument, an Acoustic Doppler Velocimeter, referred to as the ADV below, which is commercially available. The ADV gives the full 3D turbulent velocity field, and is widely used in aquatic

environments to study processes such as the transport of particles in the shear layer over sediment surfaces. While this paper only focuses on O_2 uptake by sediments, the technique can also be applied to other solutes that can be measured at sufficiently high temporal resolution.

THEORY

Fig. 1 shows an example of a depth profile of the O_2 concentration in a marine muddy sediment and the overlying water, measured *in situ* with a microelectrode. The O_2 is consumed in the upper 1.5 mm of the sediment and the smoothness of the profile suggests that the important mechanisms for the vertical transport of O_2 in the sediment are molecular diffusion and possibly bioturbation caused by meiofauna. In the water column, where the two possible transport mechanisms are molecular diffusion and advection, no concentration gradients are visible 0.7 mm, or more, above the sediment surface. This reflects a shift in the dominant transport process from molecular diffusion within the diffusive boundary layer to advection above the layer. It is also evident that this advective transport of O_2 results exclusively from turbulent motions since there was no continuous flow pointing toward the sediment at this site. The characteristic variation of the turbulence is that the O_2 concentration is higher when the vertical velocity is pointing toward the sediment and lower

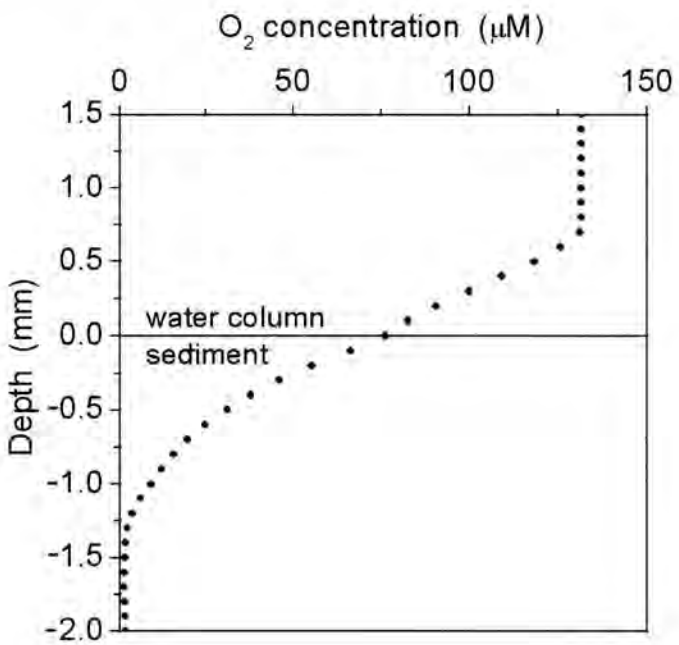

Figure 1. Depth profile of the O_2 concentration measured *in situ* with a microelectrode in a marine muddy sediment and the overlying water.

when the velocity is pointing upward. Over time this gives rise to a net transport of O_2 toward the sediment. An example of this pattern is shown in Fig. 2 from some of our measurements with high temporal resolution of the vertical velocity and the connected O_2 concentration.

The mathematical expression for the vertical O_2 flux in any position in the water column, at any point in time and as the result of advection and molecular diffusion is

$$Flux = UC - D\frac{dC}{dx} \tag{1}$$

where U is the vertical velocity, C is the O_2 concentration, D is the molecular diffusivity of O_2 in water, and x is the depth coordinate (e.g., Berner 1980 or Boudreau 1997).

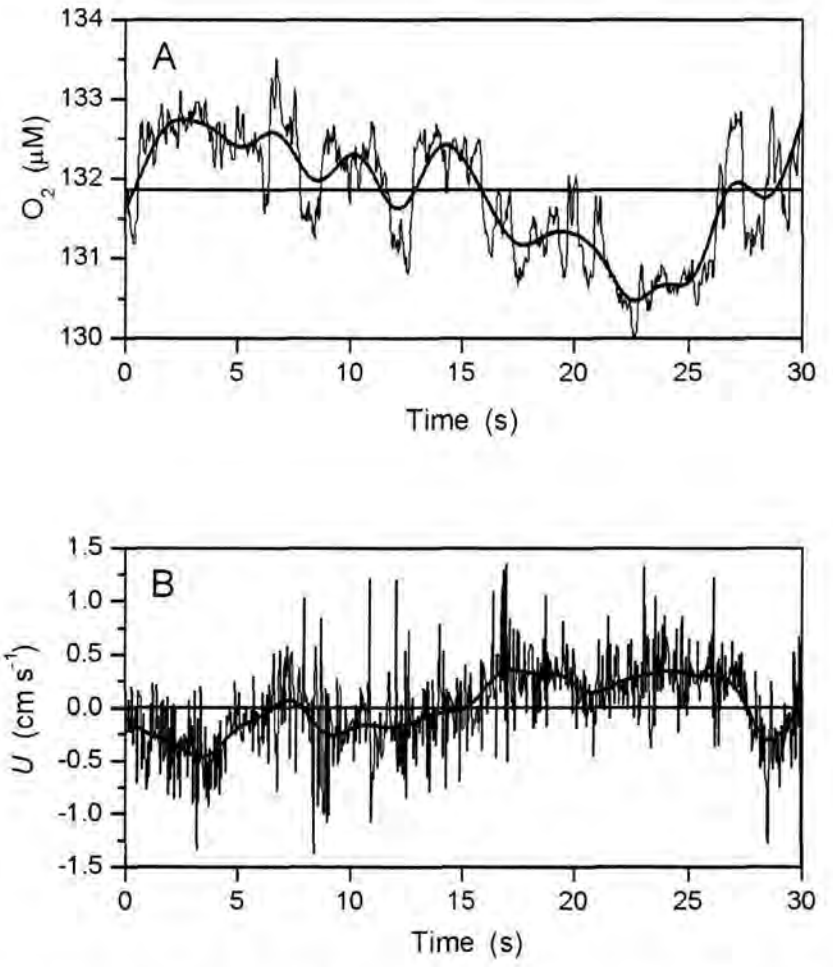

Figure 1. A time series of the fluctuating O_2 concentration (A, thin lines) and the connected vertical velocity (B, thin lines). Negative velocity values indicate a flow towards the sediment surface. The data were measured 15 cm above a sediment surface at a frequency of 25 Hz. The mean values for the time series are also shown (horizontal lines) as are the smoothing of the O_2 concentration and vertical velocity (thick lines).

In the water column above the diffusive boundary layer, turbulent mixing is the dominant vertical transport in almost all natural aquatic environments. Even when density stratifications caused by temperature or salinity differences are present and vertical concentration gradients are evident, molecular diffusion is usually insignificant relative to turbulent mixing. For that reason, the diffusive term in Eq. (1) can be neglected. Furthermore, it is a common practice when dealing with turbulent advections to separate both instantaneous values of U and C into two components equal to $\overline{u}+u'$ and $\overline{c}+c'$ where $\overline{u}$ is the mean vertical velocity, u' is the vertical turbulent fluctuating velocity, $\overline{c}$ is the mean concentration, and c' is the turbulent fluctuating concentration (e.g., Stanišić 1985). It should be noted that there are no simplifications hidden in these separations. The separations are now substituted into Eq. (1), which is then averaged over a period of time significantly longer than the time scale of the turbulent fluctuations, in which case both averages of u' and c' becomes equal to zero. It is finally assumed that that the mean vertical velocity is equal to zero ($\overline{u}=0$). Unless there is a continuous flow into or out of the sediment, which is a rare situation, $\overline{u}$ is by nature equal to zero. With these assumptions Eq. (1) gives the following expression for the vertical O_2 flux averaged over time

$$\overline{Flux}=\overline{u'c'} \tag{2}$$

where the bars symbolize the averaging (e.g., Stanišić 1985). Equation (2) has been used for decades to determine fluxes by eddy correlation in the atmospheric boundary layer (e.g., Wyngaard 1989). In such applications of Eq. (2), where time series of u' ($u'_1, u'_2, u'_3, \cdots u'_N$) and c' ($c'_1, c'_2, c'_3, \cdots c'_N$) are extracted from measurements, the flux is simply calculated as the average of the sum $u'_1c'_1+u'_2c'_2+u'_3c'_3+\cdots+u'_Nc'_N$.

When measuring U in the water column under stationary conditions, where no changes in size or direction of the current occur, $\overline{u}$ can be defined as the mean of all U, $\overline{U}$. Since it is difficult to position the ADV so that the U is measured exactly perpendicular to the sediment surface, which in turn may not be completely even and well-defined, $\overline{U}$ is likely to have some small value and a correction must be made for Eq. (2) to be valid. The correction can be made either by rotating the measured 3D velocity field (U, V, W, where V and W are to two horizontal velocity components) so $\overline{U}$ equals zero, or if $\overline{U}$ is only slightly off from zero, simply by subtracting $\overline{U}$ from each individual U value. In the latter case, u' becomes equal to $U-\overline{U}$ and the average of all u' will consequently always equal zero as

assumed in the derivation of Eq. (1). If non-stationary conditions are present, the correction must vary in time and u' can, for example, be calculated from the running average of U. A challenging aspect of this more advanced correction, as discussed in detail below, is to determine how many adjacent data points to include in the running averaging. If too few points are included, some of the larger scale turbulent fluctuations are filtered out, and if too many points are included, non-turbulent motions may affect the flux calculation. The isolation of c′ from the measured O_2 concentration, C, is done along the same lines.

Analysis of our measurements have shown that u' can often be calculated as $U-\overline{U}$, while c′ in most situations technically should involve running averaging since non-turbulent variations in C occur, presumably caused by a slow drift in the O_2 microelectrode calibration. However, one can show that the running averaging can be avoided if these variations happen on a time scale significantly larger that the scale of the turbulent fluctuations. In such situations C can be used directly in the flux calculation and Eq. 2 simplifies to

$$\overline{Flux} = \overline{u'C} \tag{3}$$

Equation 3 represents the simplest way to determine sediment O_2 uptake from measured time series of U and C.

If both u' and c′ are extracted from the measured data, other advantages exist. Both Eq. (2) and (3) include an integration in the time domain. This integration can also be performed in the frequency domain after Fast Fourier Transformation of the time series of u' and c′. More specifically, one can show that the vertical O_2 flux can also be expressed as the integral over the frequency of the one-sided cospectrum of $u'c'$

$$\overline{Flux} = \int_0^\infty \mathrm{Co}_{u'c'}(f)\,df \tag{4}$$

where f is the frequency (e.g., Priestley 1992). The cospectrum of $u'c'$ itself offers immediate information on the frequencies of the turbulent eddies that are responsible for the vertical O_2 transport. As shown below, this is a valuable approach to evaluate if the O_2 microelectrode responds fast enough to capture all turbulent fluctuations facilitating the vertical transport of O_2.

METHODS

Instrument

The ADV is a commercially available instrument manufactured by companies such as Nortek AS, Norway and SonTek/YSI Inc, USA. The ADV measures the 3D velocity field in a small cylindrical volume, approximately 1.5 cm long and 0.6 cm in diameter, located on the ADV's center line 10 cm from the base of the three sensors, as marked on Fig. 3. The velocities are determined with a resolution in time as fine as 25 Hz and in the velocity ranges from ± 3 to ± 250 cm s^{-1}. The ADV measurements are largely unaffected by water quality (O'Riordan et al. 1996; Yang et al. 1996). However, the speed of sound in water is correlated to temperature and salinity, and these parameters must be known in order to obtain the most accurate determination of the 3D velocity field.

Figure 3. The Acoustic Doppler Velocimeter and the O_2 microelectrode mounted on a rack. The position of the Acoustic Doppler Velocimeter's measuring volume and the tip of the O_2 microelectrode are marked with an arrow.

The O_2 microelectrode is of the Clark-type (Revsbech 1989) and was constructed to have a short response time by using a thin silicon membrane and a compact tip architecture. The sensor has a 10 μm tip diameter and a 0.2 s response time for a 90% response to concentration changes. To maximize signal to noise ratios, sensitivity and signal speed, the cable connections between sensor and pico-ampere meter were kept as short as possible. This was achieved by using a customized submersible pico-ampere meter where the sensor was inserted directly in the amplifier housing. Since seawater acts as shielding, this pico-ampere meter can resolve significantly smaller fluctuations *in situ* than under normal laboratory conditions.

Both the ADV and the O_2 microelectrode were mounted on a rack constructed for initial tests of the technique (Fig. 3). The tip of the microelectrode was located immediately next to the border of the ADV's measuring volume. The rack was designed so that the position of the measuring volume and the tip of the microelectrode could be adjusted in the range of 10-55 cm above the sediment surface. Prior to measurements the rack was positioned manually on the sediment surface with the sensors facing up into the current, and the ADV and pico-ampere meter were connected to the surface through independent cables. Data acquisition was controlled above the water surface by an IBM compatible PC, which communicated digitally with the ADV and by analog with the pico-ampere meter. The PC and supporting electronics were powered by batteries and were isolated galvanically from all other electronic devices.

Both the velocity and the O_2 concentration measurements contain some high frequency noise (Fig. 2). The noise from the ADV is purely random, can be assumed to follow a Gaussian distribution, and consequently converges to the value zero when averaged over multiple data points without introducing bias (SonTek/YSI Inc 2001). The electronic circuitry and components behind the O_2 concentration measurements are all well-known and well-described (Tietze and Schenk 1993), and have similar noise characteristics as the ADV. This was confirmed by measurements during which the O_2 microelectrode was replaced with a dummy electrode. These measurements led to the calculation of an O_2 uptake of zero. A similar result was also obtained in other measurements where the O_2 microelectrode and the ADV were positioned apart.

Measurements

The technique was tested under field conditions on three occasions. The first series of measurements was done in the river Wümme near Bremen, Germany, which is approximately 7 m wide, with a water depth of 1 m and a sandy bottom. This site allowed us to keep all equipment not mounted on the rack on land, and also to make easy adjustments of the orientation of the rack and the measuring height above the sediment surface. Additional measurements for comparison of the O_2 uptake in recovered sediment cores or *in situ* chambers were not pursued since these two methods are likely to fail in permeable sands, as described above. At the time of measurement the river current was 13 cm s^{-1}. Three time series were sampled for each of the four measuring heights, 15, 20, 40 and 55 cm, above the sediment surface. Each time series had a duration of 10 min and was sampled at a frequency of 25 Hz to ensure that all concentration changes that could be registered by the O_2 microelectrode were sampled.

The second series of measurements was done in Aarhus Bay, Denmark, a relevant marine environment with respect to future use of the new technique. The sediment was a fine-grained mud and was located at 12 m water depth. At the time of measurement, the current was 2 cm s^{-1} at 15 cm above the sediment surface. Four 10 min time series were sampled 15 cm above the sediment surface at a frequency of 25 Hz. For comparison to the eddy correlation measurements, four *in situ* chambers were deployed. These chambers had an 19 cm inner diameter and were 32 cm tall. The lid on each chamber had a large venting opening that was closed by a stopper after deployment, a sampling port with syringe holder for water samples and a second port for replacement of sampled water. The water inside the chambers was stirred during measurements by a flat rotating disk, 15 cm in diameter and 1 cm in height. Throughout the 3 h incubation, the disks were rotated at a speed of 20 rpm in a position approximately 7 cm above the sediment surface. Prior to measurements the chambers were pushed approximately 20 cm into the sediment enclosing a water volume of approximately 3.4 l. A more accurate estimate of this water volume was calculated from the dilution of 50 ml of a neutrally buoyant sodium bromide solution injected into each chamber. Oxygen concentrations in the chambers were monitored during the incubation with O_2 optodes (Presens) mounted in the lids. In addition, the O_2 concentration in the chambers was determined by Winkler titration of water samples retrieved at the beginning and the end of the incubation. For additional comparison, three depth profiles of the O_2 concentration were measured with microelectrodes in sediment cores collected at the site.

The deployment of the rack holding the ADV and the O_2 microelectrode, the deployment of the *in situ* chambers and the collection of sediment cores were done by divers.

The third and last series of measurements were done in the sound, Limfjorden, Denmark. The sediment was a fine-grained mud and was located at 8 m water depth. At the time of measurement, directional changes in the current were observed and its strength varied between 1.5-4 cm s^{-1} at 40 cm above the sediment surface. Six 10 min time series were sampled 40 cm above the sediment surface at a frequency of 25 Hz. For comparison to the eddy correlation measurements, six *in situ* chambers were deployed and operated as described for the Aarhus Bay site.

RESULTS AND DISCUSSION

The results of the eddy correlation measurements in the river Wümme are shown in Fig. 4. The sediment O_2 uptake was calculated from Eq. 3 where u' was determined as $U - \overline{U}$. Some aerial variation in uptake was expected since the rates represent an increasing upstream area of the sediment surface as increasing measuring heights were used. However, the mean values of the O_2 uptake were not significantly different (ANOVA, $p > 0.18$), and an overall mean of 210 ± 16 mmol m^{-2} d^{-1} was calculated from the combined data. It is expected that some advective transport in the upper sediment layer was induced at the main current of 13 cm s^{-1} during the eddy correlation measurements, which presumably explains the relatively high O_2 uptake. This high uptake, combined with the relatively small error estimates, is seen as a promising result for the new technique. All potential shortcomings and errors in the eddy correlation measurements, such as the response time of the O_2

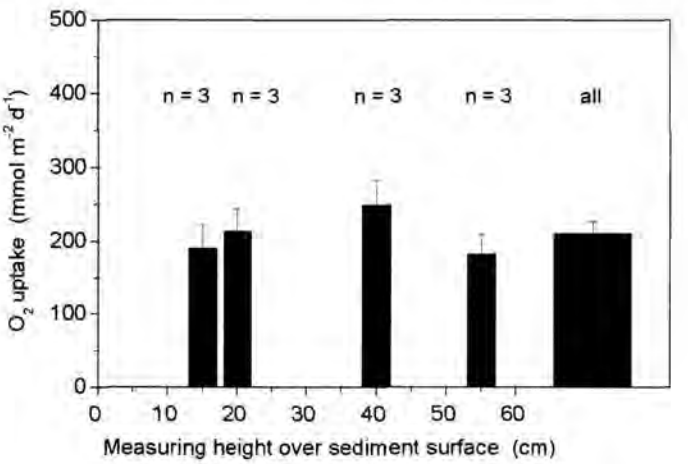

Figure 4. The O_2 uptake by a sandy river sediment (Wümme) determined by the eddy correlation technique (Error bars represent 1 SE).

microelectrode being too slow to capture all important turbulent fluctuations, would lead to an underestimation of the O_2 uptake.

Also for the time series from Aarhus Bay, u' was determined as $U - \overline{U}$ and the sediment O_2 uptake was calculated from Eq. 3. The uptake is shown in Fig. 5 as are the results from the *in situ* chambers and the calculated uptake from the O_2 micro-profiles using the gradients in the diffusive boundary layer. Bio-irrigation is not included in the latter calculation, which may explain the lower estimated O_2 uptake relative to the chamber measurements. The O_2 uptake determined in chambers and by the new technique are different (ANOVA, p = 0.03), and the difference is most likely explained by an underrepresentation of faunal activity, especially the irrigating macro-fauna, in the chambers. Since the current was low when the measurements were made and given the impermeable structure of the muddy sediment, it seems unlikely that advective transport, other than that induced by irrigating fauna, would influence the O_2 uptake in the sediment. The relative standard error estimate of 7% for the O_2 uptake determined by eddy correlation was of the same magnitude as the 10% and 6% standard errors found in the chamber measurements and the flux calculations from micro-profiles.

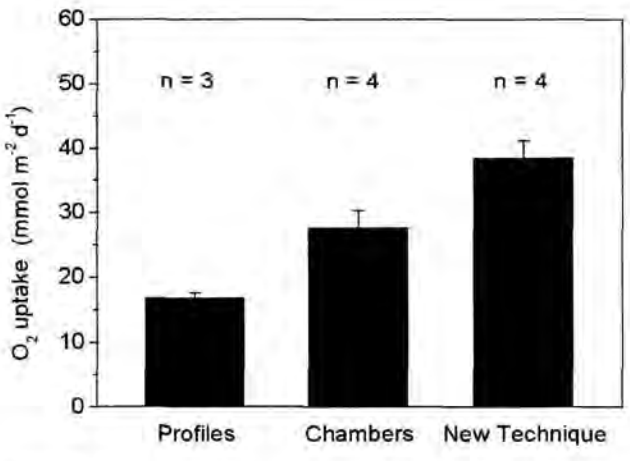

Figure 5.

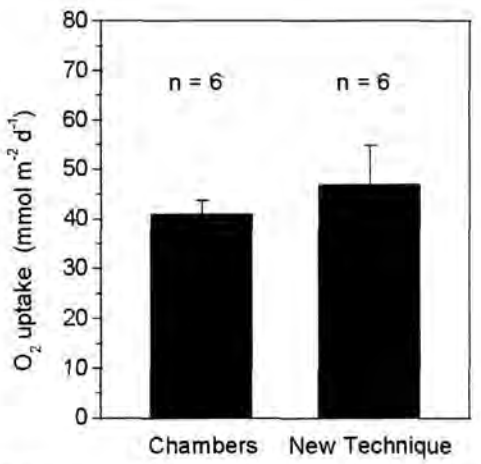

Figure 6.

Figure 5. The O_2 uptake by a muddy marine sediment (Aarhus Bay) determined by O_2 micro-profiles, *in situ* chambers and the eddy correlation technique (Error bars represent 1 SE).

Figure 6. The O_2 uptake by a muddy marine sediment (Limfjorden) determined by *in situ* chambers and the eddy correlation technique (Error bars represent 1 SE).

As the result of the non-stationary current conditions observed during the measurements in Limfjorden, u' was determined from the running average of U before the sediment O_2 uptake was calculated from Eq. 3. The number of adjacent data points used in the running average was found in an analysis as described in detail below. The O_2 uptake is shown in Fig. 6 as are the results from the *in situ* chambers. The two uptake are not different (ANOVA, $p = 0.50$), and have relative standard error estimates of 7% for chamber measurements and 17% for the new technique. The latter standard error is considerably larger than those found when using the technique for the other sites and is probably explained by several factors. First, some natural variation in the uptake was expected with the observed changes in current, both in direction and strength. Second, in order to avoid boundary errors, the first and the last data points in the 10 min time series were used only to calculate the running average of U, and not used directly in the flux calculation. The flux was for that reason calculated from connected values of u' and C only covering a time interval of less than 8 min, which obviously increased the uncertainty of the calculation. A smaller standard error would likely have been found if time series longer than 10 min had been measured at this site.

A further analysis of the eddy correlation measurements requires that the fluctuating component of the O_2 concentration, c', also is known. Data from the Aarhus Bay site was used in the example presented below. Since the measured O_2 concentration generally contained some large scale variations in time, presumably representing a slow drift in the O_2 microelectrode calibration, c' must be determined from the running average of C. The number of adjacent data points, N_r, included in the running average was found by calculating the O_2 uptake repeatedly from Eq. 2 for increasing N_r and observing how the uptake changed. An example for one time series is shown in Fig. 7A. Obviously, if N_r equals 1, all fluctuations in the time series are filtered out, which means that c' equals zero and results in an O_2 uptake of zero. For increasing N_r an increasing number of turbulent fluctuations are included in the calculation, the ones with the highest frequency first. The resulting increase in O_2 uptake levels off and reaches a nearly constant value of 33 mmol m^{-2} d^{-1}. It should be noted that the same O_2 uptake also was calculated for this particular time series by using Eq. 3. The value of N_r chosen from the results shown and used in the further calculations was 3700, which corresponds to an average over 148 s. By knowing both c' and u', the cumulative O_2 uptake for the time series can be calculated, which exhibited a relatively steady increase through time as shown in Fig. 7B. In order to avoid

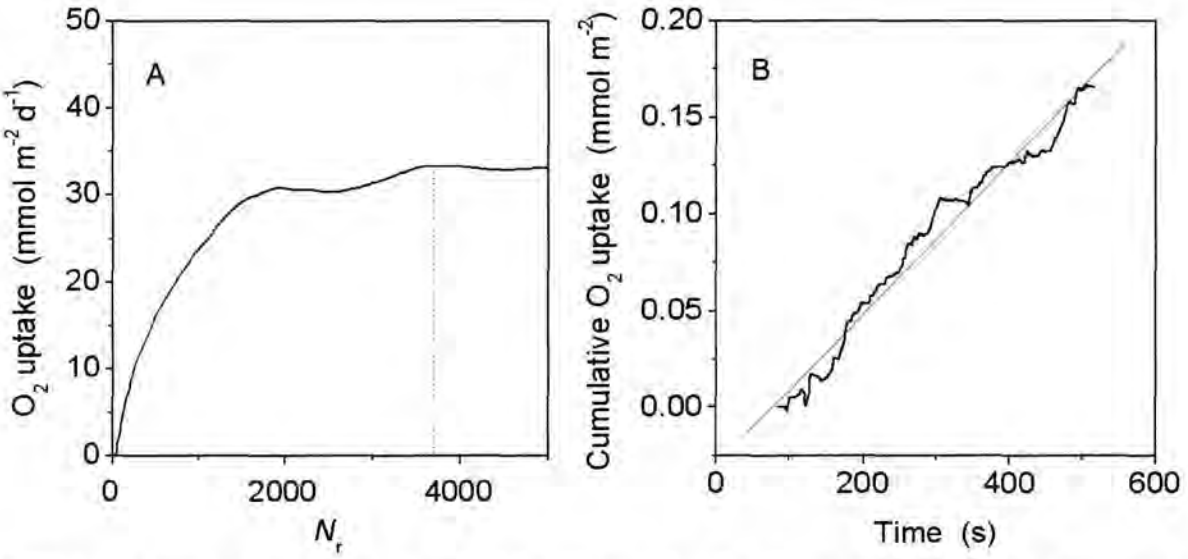

Figure 7. (A) Determination of the number of data points, N_r, that is used in calculation of the running average of C. (B) The cumulative O_2 uptake over time. The thin line represents a linear fit.

boundary errors, the first and the last 1850 data points were used only to calculate the running average of C, and were not used directly in the flux calculation. This represents a disadvantage of the running averaging or other similar averaging methods.

One of our initial concerns in evaluating the new technique was whether the O_2 microelectrode would respond fast enough to capture all turbulent fluctuations responsible for the vertical O_2 transport towards the sediment. Although the high O_2 uptake calculated using the technique suggested that all fluctuations were probably accounted for, we investigated this question further. From Fig. 8A, which shows the same data as Fig. 7A but now on a logarithmic x-axis, it is evident that no contributions to O_2 uptake are calculated for N_r smaller than 40, which corresponds to average over 1.6 s. Although the running averaging is not a sharp-cutting filter, it is reasonable to assume that turbulent eddies with frequencies higher than 1 Hz would be included in the calculation at this value of N_r. It should be emphasized that all measurements were done using O_2 microelectrodes with a 0.2 s response time for a 90% response to concentration chances. With that in mind, these results show that the turbulent transport was facilitated exclusively by fluctuations with frequencies lower than 1 Hz. In addition, this result is supported by a calculation of the one-sided cospectrum of $u'c'$, shown in Fig. 8B, for the same time series. Although longer time series are required to obtain more homogeneous results, no contributions to the O_2 uptake are visible for frequencies higher than 1 Hz. Similar results were obtained in an equivalent

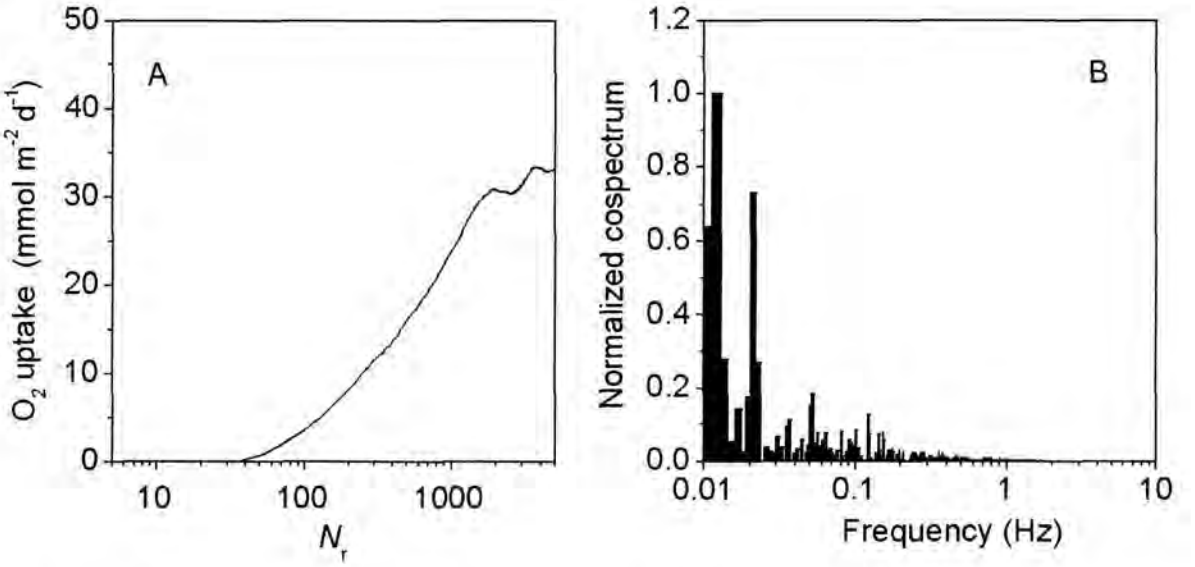

Figure 8. (A) Same data as shown in Fig. 7A, but now on a logarithmic x-axis. (B) The normalized one-sided cospectrum of showing the frequencies of the turbulent eddies that are responsible for the vertical O_2 transport.

analysis of the first series of measurements for the sandy river sediment where current velocity was more than 6 times larger.

The tests of the new technique presented here were conducted under realistic field conditions and resulted in successful determination of O_2 uptake (Fig. 4, 5 and 6). An analysis of the turbulent fluctuations showed that the O_2 microelectrodes responded sufficiently fast to capture all turbulent eddies contributing to the vertical transport of O_2 towards the sediment (Fig. 7 and 8). Based on these results, we conclude that O_2 uptake by aquatic sediments can be determined by the new eddy correlation technique and we believe that the technique may become a standard approach for determining O_2 uptake by sediments in the future. The technique is superior to conventional methods as measurements are done under true *in situ* conditions and without any disturbance of the sediment. In addition, the technique can be used for highly porous sediments, such as sands, where conventional methods often fail. While this paper only focuses on O_2 uptake by sediments, the technique can also be applied to other solutes that can be measured at sufficiently high temporal resolution.

We are currently constructing a new device that can position the ADV and the O_2 microelectrode at a defined height above the sediment surface, turn these instruments in the horizontal plane, lock them into a position facing the current, and perform measurements, all without support from divers. All electronic equipment will be mounted on the device and we anticipate that sampling can be done under most weather conditions down to a water

depth of 200 m. The new device will be used to collect data for various sediments and field conditions including different current velocities and in the presence of density gradients which have the potential for dampening the vertical turbulence.

REFERENCES

Aller RC (1983) The importance of the diffusive permeability of animal burrow linings in determining marine sediment chemistry. J Marine Res 41:299-322

Aller RC, Aller JY (1992) Meiofauna and solute transport in marine muds. Limnol Oceanogr 37:1018-1033

Berg P, Rysgaard S, Funch P, Sejr MK (2001) Effects of bioturbation on solutes and solids in marine sediments. Aquat. Microb. Ecol. 26:81-94

Berner RA (1980) Early diagenesis. A theoretical approach. Princeton University Press, Princeton. N. J.

Boudreau BP (1997) Diagenetic models and their implementation. Springer-Verlag Berlin Heidelberg New York

Forster S, Graf G, Kitlar J, Powilleit M (1995) Effects of bioturbation in oxic and hypoxic conditions: a microcosm experiment with a North Sea sediment community. Mar Ecol Prog Ser 116:153-161

Forster S, Huettel M, Ziebis W (1996) Impact of boundary layer flow velocity on oxygen utilization in coastal sediments. Mar Ecol Prog Ser 143:173-185

Fukuchi M, Legendre L, Hoshiai T (1997) The Canada-Japan SARES project on the first-year ice of Saroma-ko Lagoon (northern Hokkaido Japan) and Resolute Passage (Canada High Arctic). Jour Mar Sys 11:1-8

Glud RN, Gunnersen JK, Holby O (1999) Benthic *in situ* respiration in the upwelling area off central Chile. Mar Ecol Prog Ser 186:9-18

Glud RN, Gunnersen JK, Røy H, Jørgensen BB (2003) Seasonal dynamics of benthic O2 uptake in a semi enclosed bay: Importance of diffusion and fauna activity. Limnol Oceanogr (in press)

Glud RN, Holby O, Hoffmann F, Canfield DE (1998) Benthic mineralization and exchange in Arctic sediments (Svalbard, Norway). Mar Ecol Prog Ser 173:237-251

Huettel and Webster (2001) Porewater flow in permeable sediments – Chapter 7 in The Benthic Boundary Layer (Boudreau BP, Jørgensen BB, Editors). Oxford University Press

Jahnke RA, Christiansen MB (1989) A free-vehicle benthic chamber instrument for sea floor studies. Deep-Sea Res 36:625-637

Lohse L, Epping EHG, Helder W, Vanraaphorst W (1996) Oxygen pore water profiles in continental shelf sediments of the North Sea – turbulent versus molecular diffusion. Mar Ecol Prog Ser 145:63-75

O'Riordan CA, Maldiney MA, Mouchel JM, Poulin M (1996) A new exploration module for the study of particulate matter transport in rivers. Comptes Rendus Acad Sci 322:285-292

Pelegri SP, Nielsen LP, Blackburn TH (1994) Denitrification in estuarine sediment stimulated by the irrigation activity of the amphipod *Corophium volutator*. Mar Ecol Prog Ser 105:285-290

Priestley MB (1992) Spectral analysis and time series. Academic Press. London, San Diego

Rasmussen H, Jørgensen BB (1992) Microelectrode studies of seasonal oxygen uptake in a coastal sediment: role of molecular diffusion. Mar Ecol Prog Ser 81:289-303

Revsbech NP (1989) An oxygen microelectrode with a guard cathode. Limnol Oceanogr 34:474-478

Reimers CE, Jahnke RA, Thomsen L (2001) *In situ* sampling in the benthic boundary layer – Chapter 10 in The Benthic Boundary Layer (Boudreau BP, Jørgensen BB, Editors). Oxford University Press

Rutgers van der Loeff MM (1981) Wave effects on sediment water exchange in a submerged sand bed. Neth Jour Sea Res 15:100-112

Savant SA, Reible DD, Thibodeaux LJ (1987) Convective transport within stable river sediments. Water Resour Res 23:1763-1768

Shirasawa K, Ingram RG, Hudier EJJ (1997) Oceanic heat fluxes under thin sea ice in Saroma-ko Lagoon, Hokkaido Japan. Jour Mar Sys 11:9-19

Shum KT (1992) Wave-induced advective transport below a rippled water-sediment interface. Jour Geophys Res 97:789-808

Stanišić MM (1985) The mathematical theory of turbulence. Springer-Verlag Berlin Heidelberg New York

SonTek/YSI Inc (2001) Acoustic Doppler Velocimeter Principles of Operation. Technical note, September 1

Thibodeaux LJ, Boyle JD (1987) Bedform-generated convective transport in bottom sediments. Nature 325:341-343

Tietze U, Schenk UC (1993) Halbleiter-Schaltungstechnik, Springer-Verlag, Berlin

Wang Y, van Cappellen P (1996) A multicomponent reactive transport model of early diagenesis: Application to redox cycling in coastal marine sediments. Geochim Cosmochim Acta 60:2993-3014

Webster IT (1992) Wave enhancement of solute exchange within empty burrows. Limnol Oceanogr 37:630-643

Webster IT, Tayler JH (1992) Rotational dispersion in porous media due to fluctuating flows. Water Resour Res 28:109-119

Wyngaard JC (1989) Scalar fluxes in the planetary boundary layer – Theory, modeling, and measurement. Boundary-Layer Meteorol 50:49-75

Yang Y, Hirano M, Kimoto D (1996) Experimental studies on turbulent structure of solid-liquid upflow by using ADV. Jpn Soc Civil Eng 40: 819-824

Transport of water and solutes around the symbiont bearing sessile ciliate, *Zoothamnizm niveum*

Hans Røy, Kay C. Vopel, Markus Huettel, Bo Barker Jørgensen, and Jörg Ott

ABSTRACT

The flow field around the marine peritrich ciliate *Zoothamnium niveum* was investigated using particle tracking velocimetry. The animals were collected together with a 9 x 15 cm^2 block of peat on which they were growing. During measurements, the blocks were placed in a flow cell with along-wall flow velocity similar to the environment in which the ciliates live. The feather-shaped colonies of *Z. niveum* generated a unidirectional flow of seawater through the colony, which was not re-circulated. The feeding current was ejected at 0.3 to 0.6 mm s^{-1}. Although the size of the animal suggest that they live partly submerged in the diffusive boundary layer, their feeding currents were closely coupled to the free-flowing water. The surfaces of *Z. niveum* are known to be covered by symbiotic sulfide-oxidising bacteria. Comparing the volume of water filtered with literature values for sulfide turnover suggests that sufficient sulfide could be assimilated at ΣH_2S of 18 µM. Considerations about the diffusive constraints on sulfide flux to the ciliate surface confirmed that sulfide oxidising bacteria could sustain much higher sulfide uptake rates than bacteria on a planar surface, such as microbial mats. The study demonstrate that the filter feeding organelles of *Z. niveum* are preadapted to be prime habitats for sulfide oxidising bacteria, and that the symbiotic consortia of *Z. niveum* are well equipped to exploit co-occurring sulfide and oxygen in the water column.

INTRODUCTION

Symbiotic sulfide oxidation

Symbiotic relations between sulfide oxidising bacteria and invertebrates or protozoa are common in sulfidic environments (review by Cavanaugh 1994). Often obligatory trophic relations have lead to specialised host morphology and physiology, including evolutionary loss of the normal gasthral and intestinal apparatus. Such level of specialisation have occurred several places in the animal kingdom, including gutless nematodes (e.g. Cavanaugh 1983; Dubilier 2001) and mouthless ciliates (Fenchel 1989) as well at the Vestimentiferan tubeworms of the deep-sea hydrothermal vents (Cavanaugh 1981). In other

cases the sulfide oxidising bacteria are present as an external overgrowth or as conglomerates in the host gut, without obvious morphological adaptations of the host (Temara et al. 1993). In such examples, the symbiosis is not necessarily trophic.

The peritrich ciliate *Zoothamnium niveum* is another example of an association between a protozoan and sulfide oxidising bacteria (BauerNebelsick et al. 1996a,b). *Z. niveum* form contractile colonies, living permanently attached to the substrate. The colony shape resembles a feather, which can reach a length of more than 10 mm. The average size is somewhat less impressive between 3 and 5 mm, but still easily visible to the naked eye. The side-branches of the feather carries microzooids (zooid = single animal) in a regular pattern, as well as occasional macrozooids. The surfaces of microzooids and macrozooids, as well as stalk and branches, are covered by a single layer of white bacteria. Only the non-contractile proximal part of the stalk does not carry these bacteria.

The primary feeding strategy of the peritrich ciliates is filter-feeding, and the microzooids of *Z. niveum* possess a fully developed oral ciliature and cytopharynx, similar to *Zoothamnium* species not bearing sulfide oxidising bacteria (BauerNebelsick et al. 1996b). Simultaneous contraction of all zooids, branches and the distal parts of the stalk is characteristic for the *Zoothamnium* genera. For *Z. niveum*, the contraction lasts about 4 ms, during which the animals can reach an average velocity up to 520 mm s^{-1} (Vopel et al. 2002). During the contractions and following slow expansion, the otherwise continuos beating of the cilia is arrested. Macrozooids eventually detaches from the colony to form the dispersion stage (swarmers). Swarmers settle preferentially at spots of low O_2 and high sulfide concentration, but the exact mechanism was not identified. The development from attached swarmer to a functional colony is achieved in about 4 days (Ott et al. 1998).

The type-organisms for the recent redescription of *Z. niveum* (BauerNebelsick et al. 1996b) have been collected on the mangrove islands of the Belizean barrier reef and all recent ecological investigations have been performed on this population. White colonies of *Z. niveum* are found in characteristic "white spots" on undercut sections of peat banks under Red Mangrove (*Rhizophora mangle*). The white colour of the spots is due partly to *Z. niveum* itself, partly to co-occurrence with free-living colourless sulfur bacteria. Typical spots are 5 to 25 mm in diameter, and contain from 9 to 43 *Zoothamnium* colonies (Ott et al. 1998). A particularly conspicuous feature is the occurrence around holes in the peat (Fig 1.). The average lifetime of groups of colonies is given by Ott to be 21 days.

Though the published evidence is mostly only suggestive, *Z. niveum* has been assumed to live in an obligatory symbiosis with sulphide oxidising bacteria. The most

obvious suggestion, that *Z. niveum* is associated with sulphide oxidising bacteria, is the conspicuous white colour of its bacterial coating. In bacteria, such white colour is usually indicative of sulfur globules associated with oxidation of sulfur compounds. Unpublished results associate the symbionts with RuBp-carboxylase/oxygenase, the key carboxylating enzyme in autotrophic microorganisms (reference in BauerNebelsick et al. 1996b). A trophic character of the symbiosis is suggested from observation of bacteria morphotypes in the food vacuoles (BauerNebelsick et al. 1996b), and by poor growth of the ciliates without white symbionts (Ott et al. 1998 ;Vopel et al. 2001). It is observed that *Z. niveum* looses its white colour in about 12 hours, when removed from its natural habitat.

Ott et al. (1998) proposed that *Z. niveum* supply its bacterial symbionts with sulfide through periodic contractions into an anoxic and sulfidic diffusive boundary layer. The high Reynolds number of the contraction should assure that the oxic water in which the colony is normally bathed was shed, while the slow expansion should cause sulfidic water to stick to the colony. Investigations of the physical and chemical microenvironment around the animals, performed by Vopel et al. (2001; 2002), could not confirm this mechanism. Instead, these authors proposed that the currents generated during filter-feeding was supplying the consortia with sulfide.

Sulfide in pore waters

Dissimilatory sulfate reduction is a major pathway for oxidation of organic matter in stagnant marine pore waters. But high rates of sulfide production are not necessarily followed by appreciable H_2S gradients or concentrations in marine sediments. More usually, sulfide is precipitated with iron and then transported to the surface via bioturbation. At the sediment surface, both iron and sulfur are re-oxidised, making a semi-closed cycle. Only when the capacity of this "iron shuttle" is exceeded, free sulfide accumulate and then diffuse along concentration gradients to the areas of re-oxidation or precipitation. The mangrove peat, on which *Z. niveum* grow, does not allow turbation of the structure. Additionally, the carbonaceous reef environment is poor in iron, leading to a low capacity to bind sulfide. Consequently, sulfide reduction drives the peat highly sulfidic.

Hydrogen sulfide in aquatic solution disociates into H_2S, HS^- and S^{2-}. The K_a of H_2S in the order of 10^{-7} signifies that, at normal seawater pH around 8, H_2S and HS^- is present in a ratio of roughly 1:10. The K_a of HS^- is in the order of 10^{-15}, leading to S^{2-} concentration five orders of magnitude below HS^-. The dissociation is a fast chemical reaction and the

species can be considered in steady state for transport considerations. We will adapt the ΣH_2S notation for the sum of H_2S, HS^- and S^{2-}.

Sulfide oxidation in microbial mats

In seawater at pH 8 and 25°C, dissociated hydrogen sulfide reacts spontaneously with molecular oxygen with a half-life around 25 hours. In the chemocline of sulfidic water columns, however, sulfide co-occurs with elevated concentrations of dissolved iron and manganese. As these metals catalyse the reaction, sulfide half-life in these water-bodies is reduced to 2 to 0.3 hour (Zhang and Millero 1994). Still, a low K_m of the sulfide-oxidising enzymes in chemolithoautotrophic bacteria enables these bacteria to compete effectively with the abiotic reaction between oxygen and sulfide (Visser et al. 1997; Zopfi et al. 2001). Though the efficiency of chemolithotrophic growth on sulfide is low, the secondary production from this process allow the formation of dense populations of sulfide oxidising bacteria in habitats where sulfide and oxygen co-occur (e.g. Bernard 1995).

Z. niveum co-occur with dense mats of diatoms and cyanobacteria (Ott et al. 1998). The filamentous sulfur bacteria *Beggiatoa* are often seen near the centre of the white spots, but these bacteria are generally found deeper in the mat structure. The filamentous *Beggiatoa* are motile, and show negative chemotaxia against both O_2 and sulfide. Where O_2 and sulfide diffuse into an overlap, this enables them to align in a dense bacterial plate monopolising the sulfide for their chemoautotrophic metabolism. If the sulfide production decrease, sulfide in the plate is depleted which open up for migration downwards. Simultaneously the O_2 consumption decreases and the O_2 concentration therefore increase from above. As a result, the bacterial plate move towards the sulfide source until the flux of O_2 and sulfide is balanced by the stochiometry of autotrophic growth on sulfide oxidation with O_2 (Nelson 1986). Likewise, an increase in sulfide flux presses the *Beggiatoa* mat towards the surface. Changes in O_2 supply have the exact opposite effect via the same mechanism. A *Beggiatoa* mat can thereby effectively control the gradients of sulfide and O_2, and can deplete both species to below the detection limit of microsensors (1μM) within a layer a few hounded micrometers thick. The absolute upper limit for sulfide oxidation of a *Beggiatoa* mat is set by diffusion through the diffusive boundary layer (DBL). In marine sedimentary environments, this layer has been reported to be between 0.2 and 1.2 mm thick (Jørgensen 2001). For a given O_2 concentration in the water phase, the maximum diffusive O_2 flux through the DBL occurs when the O_2 concentration is depleted to zero at the sediment surface. An accomplishment a *Beggiatoa* mat is practically capable of (Jørgensen

2001). With a DBL thickness of 0.5 mm overlain by air-saturated seawater with an O_2 concentration of 260 µM, the maximum O_2 flux is 1.09 10^{-10} mol cm^{-2} s^{-1}. The corresponding sulfide flux, assuming a stoichiometric ratio of 1: 0.58 (Nelson 1986), is 0.63 10^{-10} mol cm^{-2} s^{-1}.

The fact that the sulfide concentration at mat surfaces is below the detection level of microsensors does not imply that no sulfide is diffusing out of mats. But the maximum gradient across the DBL is if the ΣH_2S concentration at the mat surface is at the detection level (1µM $H_2S \approx$ 12 µM ΣH_2S) and the ΣH_2S concentration in the water column is zero. The resulting maximum flux across a 0.5 mm thick DBL is in the order of 4 10^{-13} mol cm^{-2} s^{-1}

At the limiting O_2 flux, the *Beggiatoa* have moved on top of the sediment. If the balance between O_2 and sulfide supply is shifted further towards sulfide, the diffusive system of the *Beggiatoa* mat brakes down. Black holes appear in the mat, and sulfide is released. Often the veils formed by *Thiovulum* to overcome an unfavourable oxygen/sulfide supply rates is then observed (Fenchel and Glud 1998).

In case mats contain diatoms or cyanobacteria, the mat will have an internal source of oxygen. The colourless sulfur bacteria will then be found deeper in the mat structure, and without the constraints of O_2 flux through the DBL (Jørgensen and Des Marais 1986). The result is a more effective retainment of sulfide inside the microbial mat than in aphotic mats. An even more effective capacity to block sulfide inside the mat is when near-IR light penetrate to below the zone made oxic by oxygenic photosynthesis at the mat surface. In this case, purple sulphur bacteria can deplete sulfide even before it meets molecular oxygen (Jørgensen and Des Marais 1986).

Incentive and objectives of the current study

Sulfide is formed in the porewater of the peat, where molecular diffusion is the dominant transport process. *Z. niveum*, however, being equipped with a filter-feeding apparatus and protruding into the water column, live in an advection dominated environment. Thus both diffusive and advective mechanisms must be considered when resolving the pathway of sulfide from the source in the peat to the bacteria on the surfaces of *Z. niveum*. The flow around *Z. niveum* on mangrove peat is extremely complex, as the feeding currents of the ciliates is superimposed on a unsteady boundary-layer flow past the rough peat surface. The periodic contractions further ad complexity. A detailed study of the flow microenvironment of the ciliates under natural conditions might be a key to understanding the ciliate's physico-

chemical environment, and thereby gain insight in the symbiosis. The aim of the present study was to resolve the flow patterns around the ciliates, and thereby to identify possible sources and pathways for the sulfide utilised by the ectosymbiotic bacteria.

MATERIAL AND METHODS

Field work

Experimental work was conducted on Carrie Bow Cay, Belize, in April 2002, at the field station operated by the Caribbean Coral Reef Ecosystem program of the National Museum of Natural History (Washington DC, USA). Fieldwork was done at the northern end of the calm tidal channel on Twin Cays, primarily the area locally known as Batfish Point. Detailed description of Twin Cays and the tidal channels can be found in Rützler and Macintyre (1982) and Ott et al. (1998).

Observations, *in situ* imaging and ciliate collection were performed while SCUBA diving along undercut peat-banks of the tidal channel. Each day, one spot with several to many white *Z. niveum* was chosen for laboratory investigation. Before the spot and surrounding peat was cut out and transported to Carrie Bow Cay, flow velocity and direction was recorded from timing of natural particles in the water. At the lab, the peat blocks were trimmed to fit a glass flow-cell accommodating a 90 by 150-mm peat block, 45 mm thick. The blocks were inserted in the flow-cell with the ciliates in the same orientation with respect to the current direction as they were found in the field, and the unidirectional flow was adjusted to the measured field velocity. During the entire procedure of collecting and handling, peat and ciliates were never exposed to air.

Laboratory flow cell

The 50 mm overlying water column of the flow cell was re-circulated through an external aerated container holding 7 litre of seawater. Before flowing over the peat, water was passed through 50 mm of coarse filter-foam to dissipate turbulence generated by the in-flowing water jet. A similar arrangement in the outflow served to de-couple the flow over the peat from the outflow. Before measurements, the entire system was allowed to reach equilibrium with respect to oxygen-concentration and temperature. The steady values reached after one to two hours were within the natural variations observed in the habitat.

Figure 1. White spot around a 1 cm wide conduit into the peat wall. Several *Z. niveum* colonies can be seen around the hole. The image has been recorded *in situ*.

Particle Tracking Velocimetry

The supporting framework of the flow-cell was build into one rigid unit together with mounts for a fully digital, progressive scan, interline-transfer CCD camera (PCO SensiCam). The camera was fitted with a video microscope (Navitar), allowing a 2 × 1.5 mm field to be imaged from a 90 mm distance. The supporting frame also carried a line-generating laser-diode module (Lasiris LAS-670-30) used for illumination. Both camera and laser were mounted on micromanipulators, allowing delicate control of illuminated and imaged areas.

The water in the experimental system was spiked with 10μm neutrally buoyant hollow glass spheres, resulting in turbidity similar to the water at Batfish Point. Ciliates close to the centre of the flow-cell were illuminated with a vertical laser curtain parallel to the main flow and imaged by the CCD camera. By varying line-generator, focus and distance to the laser, the thickness of the light sheet could be adjusted down to 0.1 mm. Laser illumination was limited to the time of CCD exposure to prevent local heating of the peat surface.

Image sequences was recorded with 10 frames s^{-1}. Each frame was exposed in 4 pulses, controlled via the electronic shutter in the camera. The 1 ms long sub-exposures were separated by 2 ms intervals, distributing the exposure time over 10 ms. The multiple exposure was not visible in images of particles in the background flow and feeding currents. These currents were resolved by multi-frame Particle Tracking Velocimetry (PTV). By switching back and forth between 3 consecutive images, corresponding particles were identified. The displacement of one particle from the first to the third image generated one velocity vector. Thus, the velocity fields were integrated over 200 ms. Each velocity field typically contained 500 to 1000 independent vectors. Streak lines were calculated from the vector fields using the software package Tecplot (Amtec Engineering).

Within 0.1 s after a *Z. niveum* contraction, the water-velocities in the wake of the contracting animal were high enough to separate particles between sub-exposures. The velocity in these areas was evaluated by measuring displacement of particles between the first and the last sub-exposure in a single frame. Thus, the velocities behind the contracting animals were integrated over 9 ms.

Peat description

After measurements, the peat blocks were dissected and 18 mm cores were taken across the top 40 mm. Permeability was then calculated from percolation under a constant head of 1500 Pa (Klute and Dirksen 1986).

RESULTS

The peat structure was clogged with carbonate clay in spots, but generally the peat structure was porous and open. The permeability of the open peat was $4.6\ 10^{-12}\ m^{-2}$ (SE $1.9\ 10^{-12}$, n = 15) corresponding to the permeability of a fine marine sand (Huettel and Gust 1992). All white spots examined were formed around the mouth of a channel into the peat. These channels apparently form when fleshy roots from the Red Mangrove die and decay. Left is the root bark, lining an open conduit going at least 5 cm into the peat. The diameters of the holes were between 5 and 10 mm, but the opening was not always visible on the surface due to a fluffy overgrowth by mangrove rootlets and microbial mat. White *Z. nivum* grew attached to the exposed edges of the bark and to the peat within a distance of a few mm of the channel opening. White sulphur bacteria were often found together with *Z. niveum*, but the ciliates were not generally found attached to areas covered by such mats.

Z. niveum colonies *in situ* were observed to contract at a frequency of 1.7 minute $^{-1}$ (133 contractions observed over 77.66 minutes, distributed on 24 different colonies). Similar frequencies were observed in the laboratory. Dependency of contraction frequency on concentration of suspended sediment in the water column was tested in the laboratory, but no significant trend could be found. The time between contraction and restarting of cilliary motion was from 2 to 5 seconds. Thus, the animals spend 90 % of the time erect in the water with beating cilia.

Flow velocity along the peat walls during the study period was between 5 and 20 mm s^{-1}, measured 1 to 3 cm from the peat surface. The average velocity was mimicked in the laboratory by adjusting the flow velocity in the flow-cell accordingly. The velocities encountered by the ciliates on the peat surface were determined by the interaction between the main flow and the local topography. An example can be seen in Fig 2, were the flow is visualised by isolines of absolute velocity. As for all other graphs in this manuscript, the main flow was from left to right. White *Zoothamnium* grew attached to both top and sides of the hill in the centre of Fig. 2, which contained the empty bark of a dead mangrove root. Most individuals were found in the dead-water on the sides of the hill.

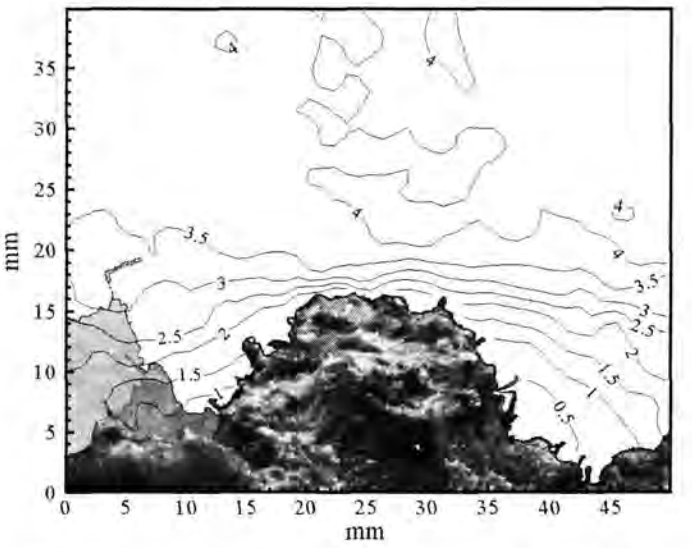

Figure 2. Background flow along the rough peat surface. The flow, coming from the left, is visualised with isolines of equal absolute velocity. Note that these lines do not contain information about the flow direction. The *Zoothamnium* colony on the lee side of the hill, at 35, 10 mm, can be seen close up in Fig. 3.

Flow patterns during feeding

Whereas very young colonies appeared perfectly stiff, animals larger than about 1 mm were flexible enough to curve downstream by even slight currents. The colonies were most often oriented so that the concave side faced towards the substrate. During feeding, a unidirectional current passes through the colony from the convex side towards the concave side (Fig 3 AB).

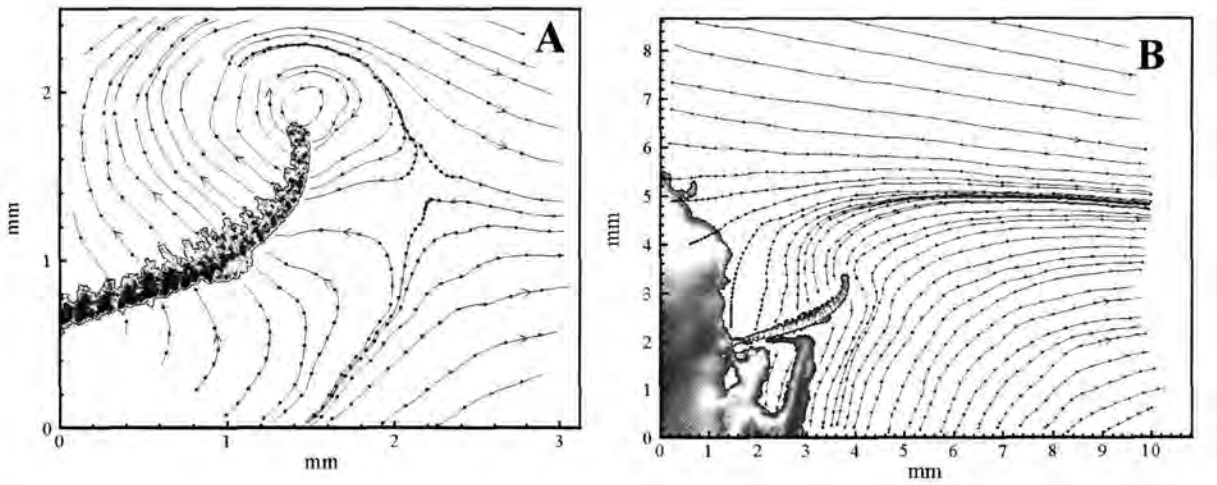

Figure 3. A) Flow field around the outer half of a feeding Zoothamnium niveum. The dots on the streak-lines corresponds to the water-displacement during 1 s. The streak lines show the direction of the momentary flow. As the pattern was quasi stable, suspended particles in the water roughly followed these lines. Where the flow is diverging, as in the area around x=2mm y=1 mm, the flow in the depicted plane is replenished by an out-of-plane component. B) Overview of the area seen in A.

This water is presumably the feeding current, and is ejected in a narrow band along the centreline of the colony. The velocity of the ejected water was always in the range between 0.3 and 0.6 mm s^{-1}, irrespectively of colony size and background flow. The Reynolds number, based on the length of the ejected jet, was 1 for a 2.5 mm long animal. The diverging streak-lines and low flow velocities on the up-stream side of the colony in Fig. 3 suggest that the in-flowing feeding current come from a broader fan than the exiting jet is leaving in. The ejected feeding current did not re-enter the colony (e.g. Fig. 3AB), but was picked up by the background flow and carried away. Friction with the feeding current drives a toroidal secondary flow at the rim of the colony. The plane of measurement in Fig. 3A intersects the structure at the tip of the colony. The cross-section of the secondary flow along the edges of the colony seen in Fig. 3A was similar to the re-circulating vortex seen at the tip of the colony, but moving in a plane out of the paper. So, the complete secondary flow was wrapped along the entire perimeter of the colony. The streak-lines in Fig. 3A could imply that the feeding current is re-circulated in the distal 0.3 mm of the colony, but that this was not the case could be seen by following single particles ejected at the tip, until they left the laser sheet in the right side of the measuring area. Colonies larger than 4 mm were too flexible to keep the straight posture seen in Fig. 3. In these long colonies twists and loops occurred, even though animals often repeated contractions until a stretched-out position was found. The longer colonies also often had side branches. In the resulting complex interactions, the water was often seen to move from one colony's flow system to the next.

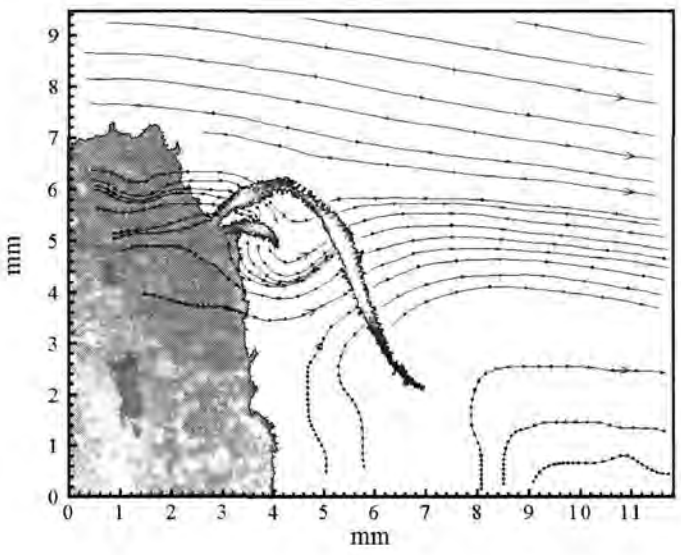

Figure 4. Complex interactions between feeding currents of two *Zoothamnium niveum* colonies. The dots on the streak-lines corresponds to the water-displacement during 1 s.

An example can be seen in Fig. 4. Here, water passes through the zooids at the base of a large colony and is directly picked up by a smaller colony. The ejected water from the smaller colony is then sucked through the large colony again, as the large colony now take in water at the other side due to a 180° twist. *In situ*, larger animals were seen to bend back and forth by oscillating water motions, which must have changed the orientation of the feeding currents continuously.

Z. niveum colonies are about 0.5 mm wide. An average length 4 mm long animal typically has active microzooids over ¾ of its length. Multiplying the 3 by 0.5 mm cross-sectional area with the velocity of the ejected current suggests that a maximum of about 0.75 mm^3 of water pass through the colony each second. With a 0.1 mm thick light sheet, particles in the expelled feeding current all had approximately the same velocity. However, particles dimly illuminated by scattered light along the light sheet often travelled slower, suggesting that the high ejection-velocity was not found throughout the width of the animal. If only the 0.1 mm thick zone where the velocities are consistent are considered as the feeding current, the water passed through the colony amount to 0.15 $mm^3\ s^{-1}$. As a best estimate of the colony filtering rate we will use average, i.e. 0.45 $mm^3\ s^{-1}$. This corresponds to a volume specific clearing rate of the individual microzooids in the order of $10^4\ h^{-1}$.

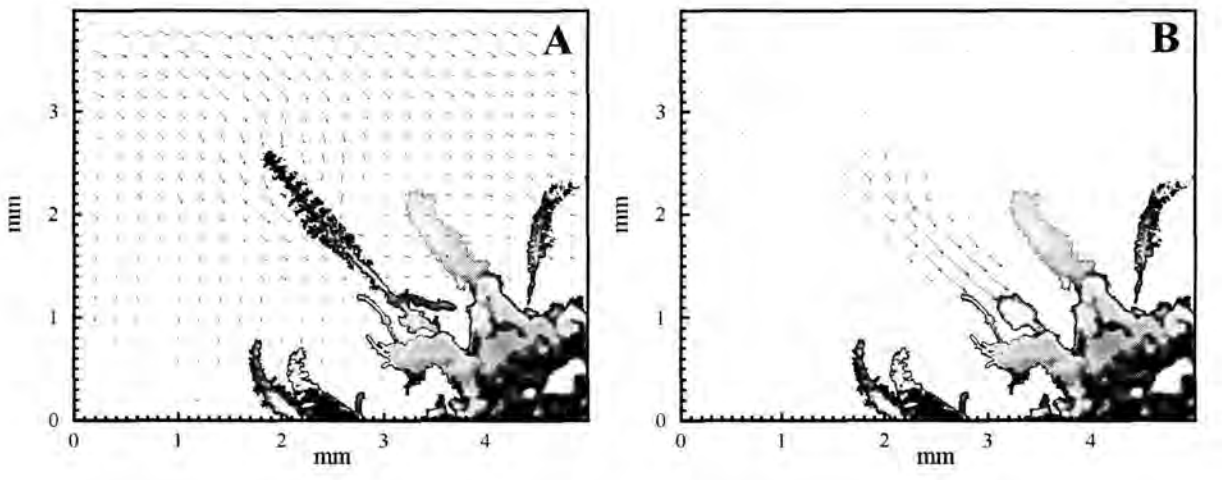

Figure 5. A) Flow field around a feeding *Z. niveum* immediately before a contraction. Several non-contracting colonies are also seen. The vectors correspond to the water displacement during 0.25 s
B) The flow field around a *Z. niveum* within 100 ms after a contraction. The vectors correspond to the water displacement during 0.025 s, one tenth of the vector length in A. The field of view is the same as seen in figure 4, which was recorded 0.1 s before. The contracted animal can be seen at x=3.5mm, y=1mm.

Flow patterns during ciliate contractions

The violent contractions were to fast to resolve with the camera used, but the fluid motions initiated by the contractions could be followed. Fig. 5A shows the momentary flow field around a 2 mm tall feeding colony. The length of the vectors corresponds to the water displacement during 0.25 s. The ejected feeding current can not be seen, as it passes into the depicted plane. The colony was bending slightly away from the camera, so that the base of the animal was in the laser sheet, but the tip of the animal behind it. A part of the secondary toroidal flow along the colony edges can therefore be seen as converging vectors around the animal. 0.1 s later (Fig. 5B) the animal had contracted, leaving a swash of water in its wake. To resolve this water motion, the vector scale has been decreased one order of magnitude relative to Fig 5A. The length of the vectors now represents the water displacement during 0.025 s, which dwarf the vectors of the background flow. The maximum velocity in Fig 5B is about 13 mm s^{-1}, but velocities in excess of 30 mm s^{-1} were observed. The water motion in the swash decayed to almost standstill over the following ~ 0.7 seconds, after which it was intersected by the extending animal. The rising animal dragged water upwards with it. But as the swash had replenished the water around the contracted animal with water from above, the water carried upwards was not primarily water from the peat surface. During extension, the animal unfolded from the base and upwards. The zooids on each branch resumed cilliary pumping when the erect position in the water was found, which immediately expelled the water in the pathway of the feeding current by replacing it with fresh water from the water column. Larger organisms contracted in a motion like a whiplash, transporting much more water towards the peat surface than average and small colonies.

DISCUSSION

Sulfur budget of Zoothamnium niveum

The velocity of the ejected feeding current is in perfect agreement with the range expected for membranelle generated flow velocities (Fenchel 1986). We can use the filtered volume calculated from the velocity of the feeding current for further calculations on the constraints on solute transport to *Z. niveum*. To do this, it is necessary to know the solute demand of the colonies.

Ott et al. (1998) measured the oxygen flux to freshly collected *Z. niveum* in non-sulfidic medium to be 460 nL O_2 mm^{-2} of ciliate surface per hour. The flux decreased to 140 nL O_2 mm^{-2} over 20 hours, after which it remained stable. The time span over which the

flux decreased correspond to the time it takes *Z. niveum* to loose its white colour when removed from its natural environment. We therefore assume that the difference between the initial flux and the stable flux can be attributed to oxidation of the sulfur globules in the symbionts. This assumption is supported by the observation by Ott et al. (1998), that the high flux could be re-established through incubation in sulfidic medium. As calculated from the difference between initial and stable flux, the oxygen flux going to sulfur oxidation is $3.97\ 10^{-10}$ mol $cm^{-2}\ s^{-1}$.

The oxidation of 2 molecules of elemental sulfur to sulfuric acid requires 3 molecules of O_2. By applying this stoichiometric relation to the O_2 flux, we get the initial rate of sulfur oxidation: $2.64\ 10^{-10}$ mol $cm^{-2}\ s^{-1}$. As the elemental sulfur only acts as an intermediate storage compound, the oxidation of S^0 must be coupled 1:1 to uptake and partial oxidation of ΣH_2S during normal growth conditions. One molecule of O_2 is required to oxidise two molecules of hydrogen sulfide to elemental sulfur, and this amount must be added to the $3.97\ 10^{-10}$ mol O_2 $cm^{-2}\ s^{-1}$, raising the O_2 flux required for sulfur oxidation to $6.61\ 10^{-10}$ mol $cm^{-2}\ s^{-1}$. During chemoautotropic growth, a part of the electrons assimilated from hydrogen sulfide are channelled into carbon fixation and are thereby not reflected in the O_2 budget. In *Beggiatoa*, this amount to 20% of the electrons used for energy conservation. Applying the same growth efficiency on the symbionts on *Z. niveum*, we must ad 20% to the ΣH_2S flux calculated form O_2 flux. Summing up, the bacteria on the surfaces of the *Z. niveum* of which Ott et al. (1998) measured the O_2 consumption must have sustained a ΣH_2S flux of $3.19\ 10^{-10}$ mol $cm^{-2}\ s^{-1}$ and an O_2 flux of $6.61\ 10^{-10}$ mol $cm^{-2}\ s^{-1}$ to be in steady state with respect to stored elemental sulfur

We will consider a 4 mm tall *Z. niveum* colony with 50 side-branches carrying a total of 500 microzooids as a standard animal. According to the dimensions given by BauerNebelsick et al. (1996b), the surface area of such a colony is about $2.5\ 10^{-2}$ cm^2. Consequently, the single animal is consuming in the order of $7.97\ 10^{-12}$ mol $\Sigma H_2S\ s^{-1}$. If this sulfide is taken up from the $4.5\ 10^{-4}$ cm^3 of water filtered per second by such a colony, the filtered water must contain at least 18 μM of ΣH_2S.

The white spots of 1 cm^2 typically contained 26 individual colonies (Ott et al. 1998) and the total sulfide oxidation of all *Z. niveum* within one spot thus $2.07\ 10^{-10}$ mol sulfide s^{-1}. Seen per area, the flux needed to sustain the 26 standard *Z. niveum* in the white spot is in the range where sulfide oxidation in a *Beggiatoa* mat is limited by O_2 diffusion through the DBL.

Sulfide assimilation by Zoothamnium niveum

As no sulfide is produced in the fully oxic water where *Z. niveum* lives, the source of the sulfide must be inside the peat on which it grows. We will therefore consider the diffusive and advective pathways that can possibly link *Z. niveum* with this source. The peat constituting the walls of the tidal channels is porous, and the interaction between surface topography and boundary layer flow is bound to generate differential pressures on the wall surfaces. The permeability of the peat of 4.2 10^{-12} m^{-2} is in the range where solute transfer in marine sediments change from diffusion to advection due to such pressure differences (Huettel and Gust 1992). The flow velocities in the tidal channel were, however, lower than what is typical above sandy marine sediments. Further, the measured permeability was integrated across 35 to 40 mm. The peat surface was covered with a dense microbial mat, and was obviously less permeable than the underlying matrix. Predictions about interfacial e fluid exchange based on the integrated permeability are thereby likely to overestimate such processes. Though advective processes can not be excluded, they were not likely to the key factor for mass transfer in the peat. Advevtive processes also fail to explain the patchy distribution of *Z. niveum* colonies, as patches are not generally found on protrusions of the peat (Ott et al. 1998). Consequently, hydrogen sulfide flux from the peat matrix towards the water must be by molecular diffusion.

The surfaces of the peat walls are draped by dense mats of diatoms and cyanobacteria (Ott et al. 1998). Whitish stains of sulfur bacteria in the mat surface could be found, but were not common on the sections of the peat wall investigated. To supply *Z. niveum* with sulfide through the peat surface, this H_2S must escape this microbial mat. Feeding currents, secondary flows and contractions of the ciliates caused mixing of water between the animals in addition to the turbulence associated with flowing water. The water between the colonies was thereby well mixed with the water column, and the microbial mat at the base of *Z. niveum* colonies should be at least as effectively supplied with oxygen as a mat without *Z. niveum*. A microbial mat does not depend on the presence of gradients in the DBL, and the disturbance of the DBL will only relieve constraints on sulfide oxidation. No evidence of the microbial mats being overwhelmed by the hydrogen sulfide flux, such as floating Beggiatoa mats or veils, were observed. As calculated above, the *Z. niveum* colonies in an average white spot requires 2.07 10^{-10} mol sulfide cm^{-2} of base area s^{-1}, which is more than two orders of magnitude above the maximum flux expected to escape a functional mat. Supply via diffusion through the peat matrix from below is therefore questionable.

Ott et al. (1998) suggested that the swarmers (dispersion stage) of *Z. niveum* preferentially settle where the microbial mat leak hydrogen sulfide due to a disturbance. However, many bacteria of sulfureta are motile and perform chemotaxic responses enabling them to close damages in mats fast and effective. Thar (2002) observed that an unknown bacterial species formed veils on sulfidic sand in 2-3 days following a massive disturbance. Within about one week, these whitish-translucent veils were replaced by a *Beggiatoa* mat, with an intermediate stage of *Thiovulum* dominance. A similar sequence resulting in a closed *Beggiatoa* mat within about one week has been observed by Bernard (1995). It is therefore also questionable that a simple wound should supply sulfide to *Z. niveun* over the average lifetime of the white spots of 21 days. Still, a local sulfide source might play a role during initial settling. The attached swarmer has a diameter around 100μm, and will be completely submerged in the DBL. This position will be favourable for intercepting sulfide escaping from the mat. The attached swarmers develop into young colonies over a period of 4 days. During this period, at least two factors involved in sulfide uptake change: Succession of the mat would decrease the amount of sulfide escaping a wound, and the parts of the colony carrying the ectosymbionts will grow into the mixed water column. Both processes will detach the animal from sulfide diffusing from below.

One way of explaining the continued growth on sulfide oxidation as the colony grows away from the peat surface, is the mechanism proposed by (Ott et al. 1998). As seen in Fig. 5B, the rapid contraction of a *Z. niveum* colony generates a swash of water towards the base area of the ciliate. This confirms the observations of Vopel et al. (2001), that a contraction is followed by an increase in oxygen concentration at the base of the colony. Due to the high Reynolds number, the fluid motion initiated by the contraction persists for a while after the driving force has vanished. As a result, the water surrounding the contracted colony is fully oxic water directly from the water column. During the following slower extension, most of the water that follows the colony back up has therefore spend less than one second at peat surface. The model proposed by Ott et al. (1998) suggested that more water should adhere to the colony when extending than during contraction. In this respect our measurements show the exact opposite condition. Considering basic hydrodynamic principles, this was expected: The drag on objects moved through a fluid at high velocities is proportional to the velocity squared. Therefore more water will actually be transported inwards via the fast contraction then will be drawn back out with the slow expansion of the *Z. niveum* colonies. Once back in the mixed water column, the resumption of ciliary pumping ejects the water from the colony. Thereby, the exposure to water from close to the

peat surface is limited. Therefore the contractions can not have a role in solute assimilation via the mechanism proposed by Ott et al. (1998).

On several occasions, it was observed that tracer-particles caught in mucus on the colony surface were shed by contractions. This confirms the suggestion of Vopel et al. (2002), that the primary role of the contractions is in cleaning of the filtering apparatus rather than in the solute uptake. Vopel et al. (2002) also suggested that bacteria shed during contractions due to shear and surface deformation could subsequently be filtered from the water by the ciliates. This is possible, as in the water in the path of the contracting animal ended up around the contracted animal at the peat surface. When the animal unfolded, this water followed the animal upwards due to viscous forces and filled the extending colony.

With diffusive supply of sulfide from below reduced to a secondary role, other possible pathways must be considered. The only alternative to diffusive supply through the peat and microbial mat is supply via the water column. Inside the bark conduits, around which the white spots form, the mass transfer constraints differ drastically from on the outer surfaces of the peat wall. The restriction on water exchange and the effectiveness of radial diffusion from the sulfidic peat to the conduit does not allow the sulfide flux to be countered by an equivalent O_2 flux. Consequently, mats were never observed on the conduit walls, and we can assume that the water deep in the conduits is sulfidic. Via molecular and turbulent diffusion, this sulfidic water will mix into the water at the mouth of the conduits, creating a halo of oxic water with small amounts of H_2S. Turbulent mixing and advective transport will be controlling the concentration and distribution of sulfide in the halo, as these mechanisms will remove solutes much faster than the slow abiotic reaction between sulfide and O_2. Turbulent diffusion is an extremely efficient transport mechanism in the open water. Thus, microsensors with a detection level of one µM can not resolve any vertical gradient 2 to 3 mm above a mat surface, even though a flux of 1.09 10^{-10} mol cm^{-2} s^{-1} has been shown to be passing through (Jørgensen 2001). We should therefore expect that the sulfide concentration to drop very fast with increasing distance from the conduit opening. This is consistent with the sharp limits of the white spots.

We have shown that a concentration of about 18 µM ΣH_2S in the feeding current would contain enough sulfide to supply the ectosymbionts. Still, the bacteria would have to extract the sulfide from the water. The dynamics of water motion over the surfaces of a ciliate is drastically different than water moving over a two-dimensional surface like a microbial mat. At the ciliate surface, the water motion is drawn from the surface via the

cilliary motion, while the flow is retarded by friction with the water away from the animal. In effect, a boundary layer turned inside out. Thus, the surface of the ciliates comes in direct contact with water carrying solutes at the concentration of the bulk water. In case of *Z. niveum* only the oral surface is ciliated. Some build-up of boundary layer and depletion of solutes are therefore to be expected on areas away from the ciliary apparatus. Using Fick's first law of diffusion solved for a cylindrical system, we can calculate across which average diffusive distance the ΣH_2S flux of 3.19 10^{-10} mol cm^{-2} of ciliate surface s^{-1} can be sustained with a concentration difference of 1.8 10^{-8} mol cm^3. With a diffusion coefficient for ΣH_2S of 2.23 10^{-5} cm^{-2} s^{-1}, the maximum diffusive distance is 2.1 10^{-3} cm or 20 µm (see Crank 1975 for details). This is about the distance between microzooids (BauerNebelsick et al. 1996b). As the microzooids force water over their surface, the diffusive distance between the feeding current and the ciliate surface can hardly be longer than the inter-zooid distance. So considerations about mass transfer inside the feeding colony confirm that low concentrations of sulfide can be exploited effectively by the bacteria on the surfaces of *Z. niveum* due to the feeding current. Bacteria on mat would have to assimilate sulfide from the water through a 0.2 to 1.2 mm thick planar DBL (Boudreau and Jørgensen 2001), which places a much harder constrain on the sulfide flux.

We must acknowledge the surfaces of *Z. niveum* as prime habitats for sulfide oxidising bacteria, when sulfide and oxygen coexist in the water around the animals. Seeing the consortia of *Z. niveum* with its ectosymbionts as specialised in acquiring low concentrations of sulfide from the water column agree well with its occurrence on stones and vertical rocks adjacent to decomposing seagrass in the Mediterranean. Diffusive supply from below is hard to imagine when the substrate is stone, and the exploitation of stagnant sulfidic boundary layer on stones in the swash-zone even harder. But when thick layers of seagrass are decomposing in a wave-swept environment, it is likely that small amounts of H_2S are present in the water column. It is interesting to note that the larger the ciliate colony grows, the better it will come in contact with the water column. Any influence the bacteria have that increases the size of the ciliate colony will thereby be beneficial to bacteria living from solutes from the water column. This set a likely scenario for the evolution of a trophic symbiosis, as well as giving a possible explanation for the large size of the *Z. niveum* relative to other ciliates. The feature that makes the surfaces of *Z. niveum* a lucrative habitat for sulfide oxidising bacteria is the feeding current. So rather than being a special case, exploiting sharp crossing gradients of sulfide and O_2, *Zoothamnium niveum* is more likely functionally equivalent to metazoans carrying symbionts in filtering organs.

REFERENCES

BauerNebelsick, M., C. F. Bardele and J. A. Ott. 1996a. Electron microscopic studies on Zoothamnium niveum (Hemprich&Ehrenberg, 1831) Ehrenberg 1838 (Oligohymenophora, Peritrichida), a ciliate with ectosymbiotic, chemoautotrophic bacteria. Eur. J. Protistol. 32: 202-215.

BauerNebelsick, M., C. F. Bardele and J. A. Ott. 1996b. Redescription of Zoothamnium niveum (Hemprich & Ehrenberg, 1831) Ehrenberg, 1838 (Oligohymenophora, Peritrichida), a ciliate with ectosymbiotic, chemoautotrophic bacteria. Eur. J. Protistol. 32: 18-30.

Bernard, C. F. T. 1995. Mats of colourless sulphur bacteria .2. Structure, composition of biota and successional patterns. Mar. Ecol. Prog. Ser. 128: 171-179.

Boudreau, B. P. and B. B. Jørgensen. 2001. The Benthic Boundary Layer: Transport processes and biogeochemistry. Oxford University Press.

Cavanaugh, C., S. l. Gardiner, M. l. Jones, H. Jannasch and J. Waterbury. 1981. Prokaryotic Cells in the Hydrothermal Vent Tube Worm Riftia- Pachyptila Jones - Possible Chemoautotrophic Symbionts. Science. 213: 340-342.

Cavanaugh, C. M. 1983. Symbiotic Chemoautotrophic Bacteria in Marine-Invertebrates From Sulfide-Rich Habitats. Nature. 302: 58-61.

Cavanaugh, C. M. 1994. Microbial Symbiosis - Patterns of Diversity in the Marine-Environment. Am. Zool. 34: 79-89.

Crank, J. 1975. The mathematics of diffusion. Oxford University Press.

Dubilier, N., C. Mulders, T. Ferdelman, D. de Beer, A. Pernthaler, M. Klein, M. Wagner, C. Erseus, F. Thiermann, J. Krieger, et al. 2001. Endosymbiotic sulphate-reducing and sulphide-oxidizing bacteria in an oligochaete worm. Nature. 411: 298-302.

Fenchel, T. 1986. Protozoan filter feeding. Prog Protistol. 1: 65-113.

Fenchel, T. and R. N. Glud. 1998. Veil Architecture in a Sulphide-Oxidizing Bacterium Enhances Countercurrent Flux. 394: 367-369.

Fenchel, T. F. B. 1989. Kentrophoros - a Mouthless Ciliate With a Symbiotic Kitchen Garden. Ophelia. 30: 75-93.

Huettel, M. and G. Gust. 1992. Solute Release Mechanisms From Confined Sediment Cores In Stirred Benthic Chambers and Flume Flows. Mar. Ecol. Prog. Ser. 82: 187-197.

Jørgensen, B. B. 2001. Life in the diffusive boundary layer, p. 348-373. In B. P. Boudreau and B. B. Jørgenesen [eds.], The benthic boundary layer: Transport processes and biogeochemistry. Oxford University Press.

Jørgensen, B. B. and D. J. Des Marais. 1986. Competition for sulfide among colorless and purple sulfur bacteria in cyanobacterial mats. FEMS Microbiol. Ecol. 38: 179-186.

Klute, A. and C. Dirksen. 1986. Hydraulic conductivity and diffusivity: laboratory methods, p. *In* A. Klute [eds.], Methods of soil analysis - part 1 - physical and mineralogical methods. American Society of Agronomy.

Nelson, D. C., J. B. B. and R. N. P. 1986. Growth-Pattern and Yield of a Chemoautotrophic *Beggiatoa* Sp in Oxygen-Sulfide Microgradients. Appl. Environ. Microbiol. 52: 225-233.

Ott, J. A., B. M. and S. F. 1998. The ecology of a novel symbiosis between a marine peritrich ciliate and chemoautotrophic bacteria. Mar. Ecol.-Pubbl. Stn. Zool. Napoli. 19: 229-243.

Raffel, M., C. Willert and J. Kompenhans. 1998. Particle image velocimetry. Springer.

Rützler, K. and I. G. Macintyre. 1982. The habitat distribution and community structure of the barrier reef complex at Carrie Bow cay, Belize., p. 9-45. *In* K. Rützler and I. G. Macintyre [eds.], The Atlantic Barrier Reef Ecosystems at Carrie Bow Cay, Belize, I: Structure and Communities. Smithsonian Institution Press.

Temara, A., C. de Ridder, J. G. Kuenen and L. A. Robertson. 1993. Sulfide-oxidizing bacteria in the burrowing echinoid Echinocardium cordatum (Echinodermata). Mar. Biol. 115: 179-185.

Thar, R. K. M. 2002. Conspicuous veils formed by vibrioid bacteria on sulfidic marine sediment. Appl. Environ. Microbiol. 68: 6310-6320.

Visser, J. M., L. A. Robertson, H. W. VanVerseveld and J. G. Kuenen. 1997. A novel membrane-bound flavocytochrome c sulfide dehydrogenase from the colourless sulfur bacterium Thiobacillus sp. W5. Arch. Microbiol. 167: 295-301.

Vopel, K., M. Pohn, A. Sorgo and J. Ott. 2001. Ciliate-generated advective seawater transport supplies chemoautotrophic ectosymbionts. Mar. Ecol.-Prog. Ser. 210: 93-99.

Vopel, K., C. H. Reick, G. Arlt, M. Pohn and J. A. Ott. 2002. Flow microenvironment of two marine peritrich ciliates with ectobiotic chemoautotrophic bacteria. Aquat. Microb. Ecol. 29: 19-28.

Zhang, J. Z. and F. J. Millero. 1994. Kinetics of oxidation of hydrogen sulfide in natural waters, p. 393-409. *In* C. N. Alpers and D. W. Blowes [eds.], Environmental Geochemistry of sulfide oxidation. Am. Chem. Soc.

Zopfi, J., T. G. Ferdelman, B. B. Jørgensen, A. Teske and B. Thamdrup. 2001. Influence of water column dynamics on sulfide oxidation and other major biogeochemical processes in the chemocline of Mariager Fjord (Denmark). Mar. Chem. 74: 29-51.

Thesis conclusions

The first manuscript dealt with O_2 concentration fluctuations within the diffusive boundary layer (DBL). These fluctuations are a natural property of the DBL and should not be mistaken for simple measurement noise. They are generated in the transition zone between the DBL and the mixed water column, and carried downwards via molecular diffusion. The erratic behaviour of the O_2 concentration in the DBL derives from a co-ordinated movement of the entire gradient. To get an impression of the conditions in the DBL, imagine that the profile is hinged about 1 mm into the sediment, with the upper part gently rocking back and forth. As the only transport mechanism responsible for the fluctuations in the lowest part of the DBL is molecular diffusion, a static DBL will impose the same impedance to diffusive exchange as a DBL with concentration fluctuations, given that the average thickness is the same. The time-scale of the concentration fluctuations imposes the possibility that microprofiles can be measured on a background of changing O_2 concentrations. We therefore advise researchers to integrate over relative long intervals, when O_2 concentrations are measured in the DBL.

The time-scale of the observed O_2 concentration fluctuations exclude an origin from single eddies. Eddies of an appropriate time scale would have been larger than the experimental systems in which the fluctuations were observed. A more likely explanation is an influence of coherent motions in the flow, which contain the right time-scale.

The second and third manuscript focused on how topography influences the O_2 flux through the DBL via exchange-area increase and horizontal gradients. The key factor was the relation between vertical diffusive flux, as measured from microprofiles, and three-dimensional diffusive flux ($J`/J_z$). It was shown that $J`/J_z$ could be calculated from topographic data alone. Two marine locations were investigated through mapping of the mictotopography *in situ*. The ratio between vertical diffusive flux and the full three-dimensional diffusive flux was 1.12 and 1.25. The low impact was linked to the smooth nature of the exchange surface, defined through the isolines of O_2 at the sediment water interface. The DBL follows the sediment relief with continuous isolines, but without responding to small roughness elements on the surface. The isolines also cut off corners around larger topographic elements, which reduced the angle between the isolines and the general sediment plane. The relation between the surface angle and J'/J_z is not linear. At

angles below about 20° the surface slope has little influence on the surface area. The result is that even a rough sediment surface can be modelled quite well as a flat plate in respect to the diffusive flux.

The J′/Jz ratio of 1.25 was measured on a sediment with sea- grass debris on the surface and intense sculpturing by fish and invertebrates. We therefore propose the ratio 1.12 as the best current estimate of the ratio between microsensor derived diffusive fluxes three-dimensional diffusive flux for muddy sediments.

The first three manuscripts represent the core of this thesis. Their conclusions leave the DBL basically as it was described almost 20 years ago. The step forward is that it is explained why a static model considering the sediment water interface as a flat plane with only vertical gradients can be used to describe sculptured sediment surfaces overlain by a dynamic diffusive boundary layer. The key is the effectiveness of molecular diffusion across short distances. Diffusion effectively levels out all heterogeneity in solute distribution that is not maintained by effective sinks and sources. This effect links the O_2 concentration across the entire DBL, even when temporal variations are induced. The gradient carrying the average diffusive flux across the sediment water interface is driven by consumption in the sediment. This gradient is therefore largely preserved during the fluctuations. We also find fast solute redistribution behind the smooth and continuous isolines. If an isoline is bend, the flux must be either converging to, or diverging from the point of curvature. This effect will work against the preservation of the bend in the isoline. It is the same diffusion effect that causes one-dimensional microprofiles to be smooth and continuous.

The fourth paper described the seasonal cycle of O_2 flux to an estuarine sediment, with special emphasis on comparison of *in situ* and laboratory measurements. Only a small part of the difference between the measured diffusive O_2 uptake and total O_2 uptake could be explained by microtopography. Microprofiles measured in the laboratory were in good agreement with *in situ* data, whereas core incubations in the laboratory underestimated the O_2 flux due to underrepresentation of irrigation by larger invertebrates. In environments rich in benthic fauna, *in situ* incubations with relatively large chambers are therefore required in order to obtain realistic estimates of the benthic O_2 consumption rate. Most of our current information on O_2 uptake is based on core incubations. Consequently, the relative contribution of aerobic mineralisation may be underestimated. In addition to the direct

conclusions, the data set probably represents the most complete investigation of seasonal O_2 uptake dynamics ever published.

In the fifth manuscript a novel technique for measuring solute fluxes in aquatic environments was presented. In its simplest form, the flux is calculated by multiplying point measurements of vertical flow velocity and concentration of the solute of interest. The main challenge was not the mathematical details that can be added, but in acquiring simultaneous point measurements of velocity and concentration at a sufficiently high temporal resolution. The technique is superior to conventional methods as measurements are done under true *in situ* conditions and without any disturbance of the sediment. It is therefore an obvious alternative to the large benthic chambers suggested in the preceding manuscript. The technique can also be used for highly porous sediments, such as sands, where chamber-based methods that do not accurately mimic the natural hydrodynamics will fail. While this paper only focused on O_2 uptake by sediments, the technique can also be applied to other solutes that can be measured at sufficiently high temporal resolution.

The sixth manuscript investigated the constraints on sulfide uptake by a colonial ciliate, *Zoothamnium niveum*, which lives permanently attached to mangrove peat. The study demonstrates that the filter feeding organelles of *Z. niveum* are preadapted to be prime habitats for sulfide oxidising bacteria, and that the symbiotic consortia of *Z. niveum* are well equipped to exploit co-occurring sulfide and oxygen in the water where it lives. It is not likely that Z. *niveum* has access to the sulfide diffusing towards the peat surface from below, as several functional groups of bacteria in a microbial mat at the peat surface are utilising sulfide effectively. However, the bacteria on the surfaces of *Z. niveum* can assimilate solutes from the water above the DBL much more effectively than bacteria in a mat, as they are not constrained by the planar DBL of the mat. The feature that makes the surfaces of *Z. niveum* a lucrative habitat for sulfide oxidising bacteria is the feeding current. That makes the consortia of *Z. niveum* and its bacterial overgrowth functionally similar to metazoans carrying symbionts in filtering organs.

Acknowledgements

This Ph.D. project was performed on a stipend from the Danish Research Academy and with support from the Max Planck Society. Niels Peter Revsbech acted as contact person towards the Academy, and his interest and support is greatly appreciated.

The project was supervised by Bo Barker Jørgensen and Markus Hüttel. I can not imagine a better support. Kai-Uwe Hinrichs has agreed to act as referee on the thesis, which is gratefully acknowledged. I also thank my first supervisor ever, Ronnie Glud, for his role in my getting to Bremen in the first place. Whatever this role exactly was...

Throughout my time at the MPI, Gabriele Eickert and Anja Eggers have supplied numerous microsensors and cared for them when they "got ill". The sensors are little pieces of art, and this support has was greatly appreciated. Volker Meyer and Paul Färber assisted with electronics in all thinkable ways. Without the ability to tinker with instruments that they brought me by, this thesis would not have been possible. I am looking forward to working together with the electrode lab and elektro-shop for another period of time.

Friendly support has also been given by a large number of people across the house, including the TA´s of the top; floor Kirsten, Swantje, Gaby and Gaby, Martina and Susanne, the guys in the lander hall; Jens and Axel and the mechanical workshop; Georg, Alfred and Olaf. For scientific discussions, tips and advice I would have to thank most of the staff in the Biogeochemistry and Microsensor groups. Unfortunately too many people to mention here. Under water, André Preisler, Christian and Friederike Wild and Filip Nielsen all served as skilled dive partners.

A special thank you goes to my office consultants on general geology, Eli and Jens. In addition to advice on sedimentology, the credit for every sentence in this thesis without spelling or grammatical errors goes to Eli. Also the constructive comments on the thesis from Eli, Rebecca and Felix were greatly appreciated.

Development of the eddy correlation technique was cosponsored by the National Science Foundation (OCE-0221259) and the Max Planck Society. The hospitality of Christine and Inga, and the attitude of Verner Dam have contributed to the most enjoyable atmosphere around the entire project. Verner is also thanked for his assistance onboard Genetica II.

The work with Zoothamnium niveum was performed under the Caribbean Coral Reef Ecosystems program of the Smithsonian National Museum of Natural History (Washington, DC). I thank Mike Carpenter and Dan Miller for supporting our work at

Carrie Bow Cay, and for making the stay in Belize as enjoyable as it was productive. We also thank Bernd Stickfort for his stubborn efforts in acquiring old zoological literature.

Finally, I thank Mette for allowing me to stay year after year abroad, and apologize for doing so.